AN ABSTRACT OF THE THESIS OF

Nipaka Sukpirom for the degree of Doctor of Philosophy in Chemistry presented on October 15, 2001. Title: Intercalation, Exfoliation, and Nanocomposites of Layered Inorganic Compounds.

Abstract approved:

Redacted for privacy

Michael M. Lerner

The melt intercalation of poly(ethylene oxide) (PEO) between layers of MoO_3 and MPS_3 (M=Mn,Cd) is obtained by heating the ground mixture of PEO and Li_xMoO_3, $K_xMn_{1-x/2}PS_3$, or $K_xCd_{1-x/2}PS_3$. The products are characterized by powder X-ray diffraction (XRD). Below the melting temperature of PEO (66 °C), intercalation rates and yields are low. By heating at 125 °C for 5-30 hours, high intercalation yields are achieved.

Layered titanate compounds are not amenable for melt intercalation. The exfoliation/adsorption method is studied in this thesis. Titanate layers are swollen or exfoliated in aqueous solution by using ultrasound and a swelling agent, tetrabutylammonium hydroxide (TBAOH). The exfoliation/swelling behavior is investigated by particle size distribution analysis and UV-Vis spectrometry. $H_xTi_{2-x/4}\square_{x/4}O_4.yH_2O$ (H-Ti) is exfoliated in TBAOH aqueous solution with the ratio of

TBA ions per protons in titanate (TBA/H) ≥ 0.5 by ultrasonication at 120 W for 30 minutes. $H_2Ti_4O_9.xH_2O$ (H-Ti4) is not exfoliated, but significantly swollen when it is treated by ultrasonication at 180 W for 1 hour in the presence of TBA/H = 5.

The exfoliated H-Ti and swelled H-Ti4 are used as precursors to polymer-containing nanocomposites. Water-soluble polymer, such as PEO, polyvinylpyrrolidone (PVP), and polyethylenimine (PEI) are added to these exfoliation/swelling precursors, and subsequently acidified to pH ~ 1-3. The gels of nanocomposites are obtained immediately. The nanocomposites are characterized by XRD, thermal analyses, elemental analyses, SEM, and FTIR. The data indicate polymer intercalation along with a decreased water content and decreased water interaction with titanate sheet surfaces.

Ultrasound is also studied for the intercalation of long-chain alkylammonium ($C_nH_{2n+1}NH_3^+$, n = 6-18) into H-Ti4. H-Ti4 is ultrasonicated at 180 W for 15 minutes in an aqueous or ethanoic solution of alkylamines. XRD indicates smaller increases of repeating layer distances, as compared to previous reports. This may result from the presence of kinked conformations in the alkylammonium chains.

Intercalation, Exfoliation, and Nanocomposites of Layered Inorganic Compounds

by

Nipaka Sukpirom

A THESIS

Submitted to

Oregon State University

in partial fulfillment of
the requirements for the
degree of

Doctor of Philosophy

Presented October 15, 2001
Commencement June 2002

Doctor of Philosophy thesis of Nipaka Sukpirom presented on October 15, 2001.

APPROVED:

Redacted for privacy

Major Professor, representing Chemistry

Redacted for privacy

Chair of Department of Chemistry

Redacted for privacy

Dean of the Graduate School

I understand that my thesis will become part of the permanent collection of Oregon State University libraries. My signature below authorizes release of my thesis to any reader upon request.

Redacted for privacy

Nipaka Sukpirom, Author

ACKNOWLEDGMENT

The life of graduate students always involves hard work and many problems. In my case, it has also been the best time of my life. I have the following people to thank.

Dr. Michael M. Lerner for his support and guidance in both research and the preparation of this thesis. He has been patient and very helpful.

My graduate committee, Dr. Arthur W. Sleight, Dr. Douglas Keszler, Dr. John Loeser, and Dr. Sherman H. Bloomer, for helpful discussions.

All professors, postdoctorals, and students in the inorganic chemistry division for helpful discussion and sharing instruments.

Dr. Christine Pastorek for her help with spectrometry instruments.

Past and present members of the Lerner groups, Dr. Victor Koch (visiting professor), Dr. Christopher O. Oriakhi, Dr. Sherry Zhang, Ravi Krishnamurthy, Henry Li, Wei Yan, Dr. Hiroyuki Enomoto (visiting professor), and Dr. Lyuba Kabalnova for their ideas, assistance, and friendship.

Ted Hinke has been very helpful for my research. Joey Carson and Carolyn Brumley have comforted me since the day I joined OSU. Dr. Tammy Amos and George Law have been the greatest friends anyone could ask for.

Andrew T. Bauman for his wonderful friendship that I will forever remember.

My mother, Peangjai Sukpirom, and her parents for their love and encouragement. They are my inspiration and my heart.

Department of Chemistry, Chulalongkorn University, Thailand for patiently waiting for the crew to come back. Dr. Aticha Chaisuwan has been giving me advice and confidence.

The National Science Foundation, and the Royal Thai Government for their financial support.

CONTRIBUTION OF AUTHORS

Dr. Michael M. Lerner was involved in the design, analysis, and writing of each manuscript. Dr. Christopher O. Oriakhi gave advises on the melt intercalation research.

TABLE OF CONTENTS

TABLE OF CONTENTS (Continued)

TABLE OF CONTENTS (Continued)

TABLE OF CONTENTS (Continued)

LIST OF FIGURES

LIST OF FIGURES (Continued)

LIST OF FIGURES (Continued)

LIST OF TABLES

INTERCALATION, EXFOLIATION, AND NANOCOMPOSITES OF LAYERED INORGANIC COMPOUNDS

CHAPTER 1

INTRODUCTION

1.1 GENERAL INTRODUCTION

The study of nanocomposites has been an area of scientific interest for almost two decades. As shown in Figure 1.1, the number of publications concerning nanocomposites has dramatically increased over this period.[1] Nanocomposites are materials comprised of two or more components where at least one dimension of one phase is in the nanometer scale.[2] These phases can be inorganic or organic, and amorphous, crystalline, or semicrystalline. The mechanical, electronic, catalytic, magnetic, and optical properties of these materials can be improved, or different, than those obtained from macro- or micro-dimensioned composites. These new properties are often related to confinement, quantum-size effects, and/or interfacial interactions.[3,4]

Nanocomposites can be divided into ordered and disordered forms, as displayed in Figure 1.2. In a disordered system, nanocomposites are often comprised of nanometer-sized filler dispersed in a continuous matrix of the other component. Most often, the fillers are inorganic, while the matrix components are

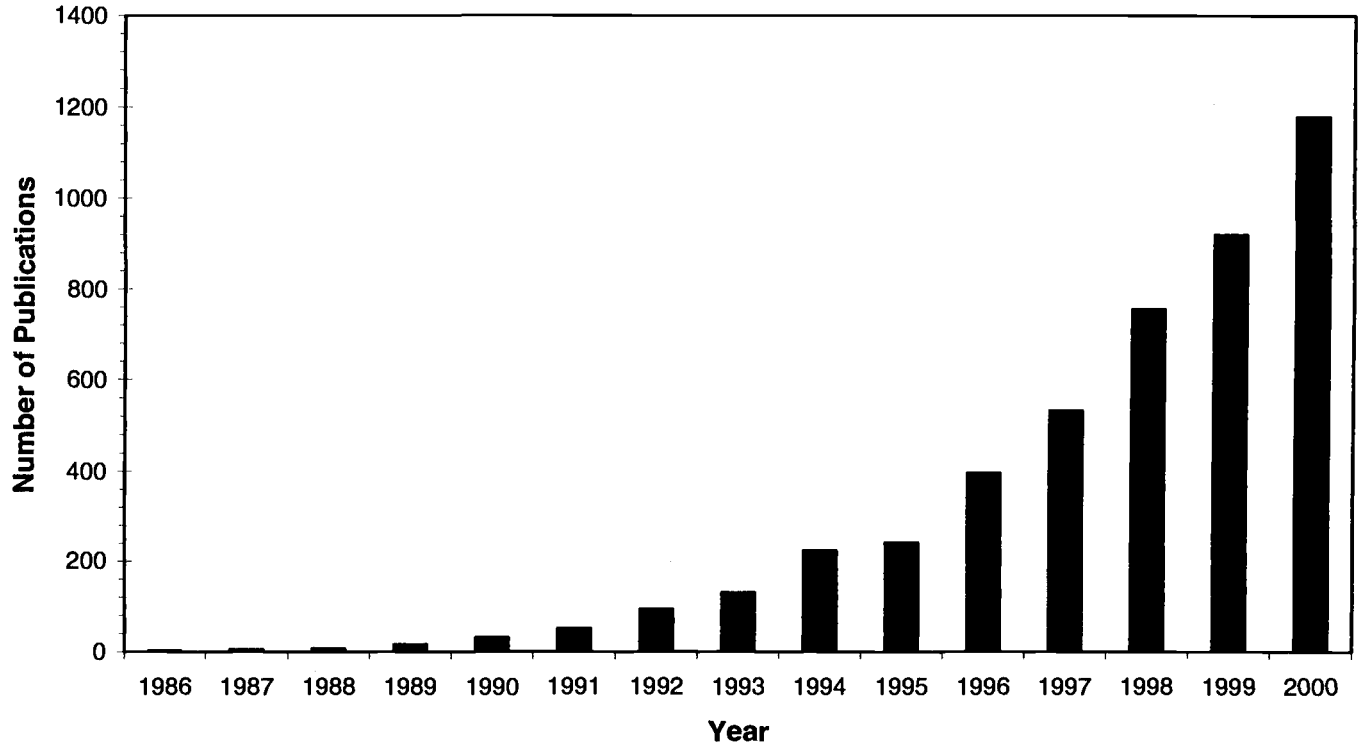

Figure 1.1 The number of publications concerning nanocomposites.

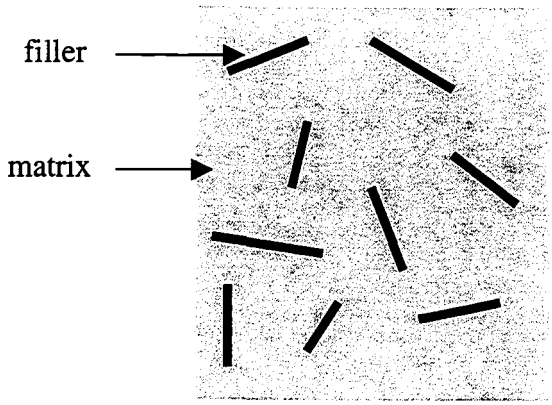

(a) An example of a disordered nanocomposite (plateles dispered in a continuous polymer matrix)

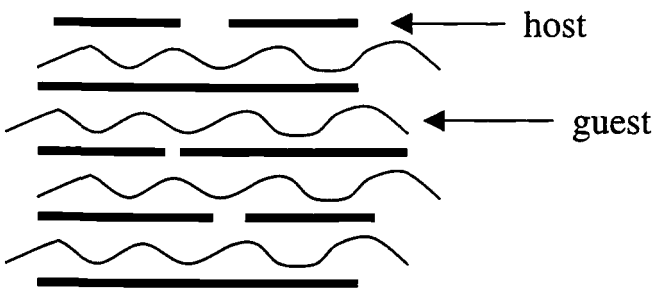

(b) An example of an ordered nanocomposite (polymer intercalated into layer host galleries)

Figure 1.2 The schematic representation of two types of nanocomposites.

polymers. Ordered system usually contains an inorganic host, with guest species inserted into the inorganic framework. Nanocomposites can also be classified by the dimensionality of the inorganic structure: zero-(0-D), one-(1-D), two-(2-D), and three-(3-D) dimensional structures.

1.1.1 Nanocomposites with 0-D inorganic components

In this case, the filler components such as fullerene, and nanoclusters of metal and semiconductors have nanometer scale in all dimensions. Because of the discrete structures, 0-D nanocomposites are nearly always disordered systems. As an example of applications for this class of materials, Ishii et al. and Gonsalves et al. found that resist system nanocomposites containing fullerene have superior etching resistance, pattern contrast, thermal resistance, and mechanical strength in nanolithography, compared to conventional materials.[5-7] Semiconductor-metal nanocomposites provoke significant interest because the electronic properties of each component depends on its size and shape. For examples, Dawson and Kamat found that a gold-capped TiO_2 nanocomposite shows an enhancement in thiocyanate oxidation by more than 40%, compared to using TiO_2. [8]

1.1.2 Nanocomposites with 1-D inorganic components

Materials with one-dimensional structures have chains or tube frameworks, and examples include MX_3 (M=Ti, Zr, Hf, Nb, Ta; X=S, Se), $AFeS_2$ (A=alkali metal), $AMoX_3$ (A=alkali metal, In, Tl; X=S, Se).[3,9] There have been relatively few studies on the inclusion of small ions between inorganic chains. Examples are the inclusion of organic cations between the molybdenum and vanadium phosphates, $(Et_4N)_2[Mo_4O_8(PO_4)_{2/2}(H_{1.5}PO_4)_2].2H_2O$ and $(Me_2NH_2)K_4[V_{10}O_{10}(H_2O)_2(OH)_4(PO_4)_7].4H_2O$.[10,11] However, the recent discovery of carbon nanotubes has inspired an increase in research in this area. Such investigations include the preparation and properties of different nanotube forms. Studies of carbon nanotubes for hydrogen storage and for use as anodes for lithium-ion batteries also show promising results.[12] Some potential applications of carbon nanotubes in organic-inorganic nanocomposites may derive from the strength and elasticity of the filler-based polymer composites.[13]

1.1.3 Nanocomposites with 2-D inorganic components

Two-dimensional materials are comprised of layers with strong intralayer bonding but weak interlayer forces. They have been widely studied as components in both ordered and disordered nanocomposites. Layered materials may contain

neutral, positive-charged, or negative-charged layers, and range from metallic conductors to semiconductors or insulators.[3] Clay materials, such as montmorillonite or hectorite, are the most widely studied hosts in this group because their layers can be easily separated. Compared with raw polycaprolactam (nylon6), a montmorillonite/nylon6 nanocomposite has been shown to provide improved strength, elasticity, and heat resistance. This nanocomposite is now commercially employed in car engine timing belts.[14] Layered surfaces can also be organically modified, so that they become compatible with hydrophobic materials.[15,16] A nanocomposite of poly(etherimides) and an organically modified layered silicate shows improved fire retardancy relative to the pure polymer.[17] Some 2-D nanocomposites will be discussed in detail in a proceeding section.

1.1.4 Nanocomposites with 3-D inorganic components

Three-dimensional structures contain well-defined pores and channels with diameters in nanoscale. Because the 3-D frameworks are rigid, the shapes and sizes of guest species are strictly controlled. Examples are zeolites, β-alumina, pyrochlores, WoO_3, and Mo_6S_8.[3,9] Zeolite are low-dielectric, and highly insulating materials that isolate polymer chains from one another electronically. Conductive polymers such as polypyrrole, polyaniline, polythiophene, and

poly(acrylonitrile) are incorporated inside zeolite structures, making them potential molecular wires.[18-20]

1.2 TWO-DIMENSIONAL HOSTS

Ordered nanocomposites are composed of polymer intercalated into inorganic compounds where the characteristic structures of inorganic layers or frameworks are preserved. The term "intercalation" describes the insertion of a mobile guest species into crystalline host lattice with no or little change of the host structure, though an increase in the gallery dimension occurs. The intercalation can be described by the equation:

$$\text{Host} + x\,\text{Guest} \rightarrow \text{Host}[x\,\text{Guest}] \qquad (1)$$

The interesting properties of ordered nanocomposites result from the confinement of guests within host frameworks, and the high interfacial interaction between different components.

Two-dimensional hosts are especially suited to form ordered nanocomposites. 2-D layered structures allow the access of guests in all direction along the plane. Also, the interaction between layers is generally strong enough that the layered structure is preserved. In contrast, 3-D hosts have rigid structures that admit only guests that are smaller than the pore and channel dimensions. Defects within these channels can also completely block the insertion so that

inhomogeneous nanocomposites are obtained. For 0-D and 1-D hosts, the interaction between the molecules/clusters or chains is very weak after insertion; so that the structures fall apart. [3] Some layered hosts of particular interests are described below.

1.2.1 MoO_3

MoO_3 is monoclinic, but is often described according to a simplified orthorhombic structure with a = 0.3962 nm, b = 1.3858 nm, and c = 0.3696 nm, in which MoO_3 layers are stacked along the b axis.[21,22] In this direction, repeating units are comprised of two MoO_3 layers, so the basal spacing (corresponding to the layer thickness) is 0.69 nm. MoO_3 does not directly react to intercalate organic species. Pre-intercalation with water-solvated alkali cations is accomplished by reduction with $Na_2S_2O_4$, and subsequent ion-exchange with the desired cations at 25 °C. The intercalation of solvated alkali (Li, Na, K, Rb, Cs) and alkaline earth (Mg, Ca, Sr, Ba) cations causes the expansion of basal spacing to 0.95-1.15 nm and 1.32-1.42 nm, respectively. The degree of expansion is not directly related to the charge/size ratio, but corresponds to the layer solvation energy by hydrogen bonds (O-H----O).[23] The insertion of cations, molecules, and polymers between MoO_3 layers has been widely investigated because of the potential application in secondary battery cathodes.

1.2.2 MPS_3(M=Mn,Cd)

MPS_3 (M=Mn,Cd,Fe,Co,Ni,Zn,V) compounds have layered structures. The monoclinic unit cell of MPS_3 extends over one layer and contains two $M_2P_2S_6$ units with the parameters, a = 0.6218 nm, b = 1.0763 nm, c = 0.6867 nm, β=107.58° for $CdPS_3$ and a = 0.6076 nm, b = 1.0524 nm, c = 0.6796 nm, β = 107.35° for $MnPS_3$. Between 10-20% of the M(II) can be substituted by alkali ions at room temperature. The alkali cations, along with solvating ligands, are located in the gallery between MPS_3 layers, resulting in an increased basal spacing. A partially-substituted MPS_3 has been shown to intercalate polymers between layers.[24-26]

1.2.3 $H_xTi_{2-x/4}\square_{x/4}O_4.H_2O$

Protonic layered titanate $H_xTi_{2-x/4}\square_{x/4}O_4.H_2O$ (□ is vacancy, x~0.7), abbreviated as H-Ti, is prepared by the acid-exchange of cesium titanate, $Cs_xTi_{2-x/4}\square_{x/4}O_4$. H-Ti has a body-centered orthorhombic structure that is comprised of lepidocrocite-type layers of linked TiO_6 octahedra and interlayer H_2O molecules and hydronium ions. The unit cell dimension are a = 0.3783 nm, b = 1.8735 nm, and c = 0.2978 nm. Cations can replace protons by ion-exchange and intercalation reactions at ambient temperature.[27] H-Ti exhibits Bronsted acidity to directly intercalate akylamines.[28] The exfoliation of H-Ti has been investigated since

1996.[29] In an aqueous solution of tetrabutylammonium (TBA) ions, protons are ion-exchanged by TBA ions, leading to a large expansion of titanate layers and, at appropriate TBA concentrations, the exfoliation of H-Ti lamella into the aqueous solution.[29,30]

1.2.4 $H_2Ti_4O_9.xH_2O$

Protonic layered tetratitanate $H_2Ti_4O_9.xH_2O$, abbreviated as H-Ti4, is prepared by acid-exchange of $K_2Ti_4O_9$ at elevated temperatures. The $[Ti_4O_9]^{2-}$ layers are comprised of TiO_6 octahedra linked by shared edges and vertices. The monoclinic unit cell contains two layers stacked in the direction of *a* axis in such a way that they shift by *b*/2 with a = 1.9968 nm, b = 0.3746 nm, c = 1.202 nm, and β = 114.01°. Each cell is made from four fomula units of $H_2Ti_4O_9.xH_2O$. Intercalated hydronium ions and hydroxylated protons are both available for reversible ion-exchange.[31,32] H-Ti4 is weaker solid acid than H-Ti; therefore, previous studies on its ion-exchange and intercalation have focused on small cations. A few research groups have reported the intercalation of long-chain alkylammonium ions, and a synthetic strategy has been developed using ion exchange.[33-35] Neither the osmotic swelling nor the intercalation of polymers into H-Ti4 have been previously reported.

1.3 PREPARATION OF ORGANIC-INORGANIC NANOCOMPOSITES

As previously mentioned, the new and improved properties of nanocomposites are derived from the combination of disparate components. For example, the contrast of properties between an elastic polymer and strong, but flexible, clay layers may result in strong materials that are easily processed. Conducting polymeric materials can be orderly arranged within rigid, well-defined channels of insulated host. A broad range of potential combinations remains unexplored, and so maybe a broad range of desirable properties. Therefore, much interest is focused on the preparation and characterization of new organic-inorganic nanocomposites.

Many synthetic problems arise in combining distinctive materials at the nanometer scale. For example, many large organic ions or molecules are hydrophobic, which is not compatible with most charged surfaces. Therefore, synthetic strategies have been, and are being, developed to solve such problems. In the combination of these materials in nanometer scale, there is no single general method for every desired host-guest system. The search for new or improved methods is challenging, and often leads to new types of nanocomposites. There are two widely studied approaches to synthesis organic-inorganic nanocomposites, the sol-gel method and inclusion chemistry. In the sol-gel method, nanocomposites are prepared by polymerization of the inorganic host precursors in the presence of

organic guests. On the other hand, inclusion chemistry involves the intercalation of organic guests into preformed host lattices.

1.3.1 Sol-gel method

Sol-gel chemistry is based on the polymerization of inorganic molecular precursors such as metal alkoxides, $M(OR)_n$. The process involves hydrolysis, condensation of a gel precursor, nucleation, growth of particles, and agglomeration. The polymerization of inorganic precursors in a medium of a soluble organic most often yields disordered nanocomposites. For example, silicon-, titanium-,aluminium-, or zirconium-containg oxopolymers form *in-situ* in a medium containing a soluble polymer such as poly(vinylpyrrolidone), poly(n-butyl acrylate), poly(phosphazine), or poly(N,N-dimethylacrylamide).[36] Ordered nanocomposites are prepared by the insertion of organic species during gelation. Some advantages of the sol-gel approach include: 1) the obtained nanocomposites are very homogeneous, and 2) the mild process allows the functionalization of inorganic surfaces, i.e. using $R'_nM^{+x}(OR)_{x-n}$ as a precursor. However the functionalization is limited by the small number of molecular precursors that have hydrolytically-stable metal-carbon bonds. For example, the hydrolysis and condensation of $RSi(OEt)_3$ produces a layered silicate with –R surface groups because a rather covalent Si-C bond is hydrolytically-stable. However, the more

ionic M-C bonds (M = transition metals) are broken down upon hydrolysis. Finally, these syntheses can involve multiple steps and therefore by rather complicated and have a low yield.[36,37]

1.3.2 Inclusion chemistry

1.3.2.1 Direct intercalation

The direct intercalation, the insertion of extra guests into host lattices without host pretreatment or replacing other guests, can be achieved if the energetics of reaction, generally involving with a redox reaction between host and guest, are greater than the decrease in host lattice.[38] In many cases, the high activation energy for intercalation requires external energy provided at high temperature or high pressure. For example, the direct intercalation of ammonia between layered TaS_2, TiS_2, and ZrS_2 proceeds at room temperature, while elevated temperature is required for the intercalation of pyridine into similar host lattices.[39] High pressure can also be used to increase the rate of insertion of small molecules such as ethanol and methanol into microporous lattices such as zeolites.[40,41] Since the direct intercalation proceeds via a topotatic reaction, there is no report on the incorporation of very large guests such as polymers into layered or microporous hosts. The alternative is intercalation of monomeric precursors, following by *in situ* polymerization within the lattice space. For

example, aniline vapor was diffused into dehydrated channels of aluminosilicate MCM-41, and polyaniline/MCM-41 nanocomposites subsequently obtained by immersion of this precursor into an oxidizing solution.[63]

1.3.2.2 Guest exchange

Generally, the layered structure allows guest-exchange by mass action.[38] Ion-exchange is a common property for charged layer structures. In many cases, especially with large guests, the reaction may take long time or require evaluated temperatures. For example, the ion-exchange of butylammonium ions ($C_4H_9NH_3^+$) for protons in $H_2Ti_4O_9.xH_2O$ is completed in 1 day, whereas the ion-exchange of long-chain alkylammonium ions ($C_nH_{2n+1}NH_3^+$, $n > 6$) requires week- or month-long reactions at elevated temperatures. For some hydrated layers, molecules or polymers can replace water molecules. For example, the melt intercalation of poly(ethylene oxide) into montmorillonite occurs by displacement of solvating water molecules.[43]

1.3.2.3 Swelling/exfoliation and reassembly

One limitation of the methods discussed above is the required diffusion of guest species into the host structure. Instead of using bulk host, which has layer to layer registration, as a starting material for intercalation, layers can be significantly separated (swelling), or completely separated (exfoliation) from one another. Therefore, the guests are allowed to adsorb onto layers directly, without diffusing

into a defined channel or gallery. The host-guest adsorbed layers will often reassemble spontaneously or upon drying. Host layers such as clay materials, MoO_3, MPS_3 (M=Mn,Cd), TiS_2, MoS_2, $V_2O_5.nH_2O$, and $NbSe_2$ can be exfoliated and form nanocomposites with various polymers by this method.[26,44-50] Benefits of this method are that the elimination of diffusion means that the size of guest species is not limited, and the direct surface interaction allows fast reactions. However, some host layers are not easily swelled or exfoliated, and some degrade under required reaction conditions.

1.3.2.4 Application of ultrasound

Ultrasound has a frequency range of 18 kHz to 100 MHz. Ultrasound at 20 kHz (used in this study) does not affect chemical bonding directly, but affects reactions indirectly through the phenomenon of cavitation. Cavitation is the production of microbubbles in a liquid caused by a large pressure drop, like the rapid motion of the propeller blade through the water, and pulls the water molecules apart to create tiny cavities. These bubbles or cavities are created, expanded, and collapsed with the release of intense local energy. In a solid-liquid system, two types of cavitational collapse affect the surface of solids:

(1) The collapse occurs at the surface. Surface defects, entrapped gases, or impurities on the surface cause nucleation and cavitational collapse directly. The localized heating on the surface can lead to fragmentation of solids.

(2) The collapse occurs close to a surface, producing the jet stream of liquid hitting on the surface. This phenomenon can significantly increase mass transport between solution and surface.

Studies on the effects of high intensity ultrasound on inorganic solids, such as ZrS_2, V_2O_5, TaS_2, and MoO_3, show that surface damage, increased surface areas, and increasing particle aggregation are all potential outcomes.[51,52]

The application of ultrasound for the synthesis of organic-inorganic nanocomposites is not entirely new. Chatakonda et al. reported that ultrasound increases the rate of intercalation of organic and organometallic compounds in ZrS_2, TaS_2, and MoO_3 by as much as 200-fold.[53,54] The mechanism does not involve mass transport or swelling/exfoliation behavior, but rather the generation of very small host particles and the increased local temperature. Since the host layers were still in bulk form, the preparation of nanocomposites was still limited by diffusion. Therefore, the rate of intercalation was also limited by guest size, and the intercalation of very large organic species, such as polymers, may not be possible by the use of ultrasonication alone.

A limited number of hosts are readily exfoliated or swell significantly in suitable solvents. As mentioned previously, a swelling agent (TBAOH) has been used successfully with a planar-sheet titanate (H-Ti), although the exfoliation process is slow, and this does not work well with other titanates. The application of ultrasound along with the use of a dispersing agent will be discussed in Chapter 4.

Its application in the synthesis of polymer nanocomposites will be presented in Chapter 3 and 5.

1.4 CHARACTERIZATION OF ORGANIC-INORGANIC NANOCOMPOSITES

Several analytical methods have been used to determine the structures and properties of organic-inorganic nanocomposites. Powder X-ray diffraction (XRD) reveals atomic-scale structural information. Scanning electron microscopy (SEM) and transmission electron microscopy (TEM) show particle morphologies. Thermal analyses and infrared, Raman or UV/Vis spectroscopy are also routinely used. Other methods such as electrochemical analysis, X-ray photoelectron spectrometry, etc. have been used to characterize nanocomposites based on their materials properties. The primary methods used in this thesis are briefly outlined.

1.4.1 XRD

XRD is commonly used to determine the structure of solids. Similar to the diffraction of visible light by a grating of suitably spaced lines, X-rays are diffracted by atom or ions in the regular array of a crystalline solid.[55] The positions of the diffracted beams determine a crystal structure and precise

parameters. The intensities in each direction reveal structure information, and the diffraction peak profiles can indicate the average crystal domain size. XRD patterns in this study were obtained using a Siemens D5000 powder diffractometer, using CuK_α radiation (1.5418 Å), designed for a flat sample surface. The materials dealt with mostly have layered structures, and the platy particles tend to lie flat on the sample holder (the preferred orientation effect). Therefore, the structural information obtained often relates only to the direction perpendicular to the layers. The diffracted peak positions directly provide the repeat distances of layers (basal spacing). Therefore, the change of interlayer distance during an intercalation reaction can be readily obtained.

1.4.2 Thermal analyses

Thermal analyses are used to observe physical and chemical changes as functions of temperature. Thermal gravimetric analysis (TGA) shows the mass of a sample as the temperature increases linearly. The differential scanning calorimetry (DSC) technique indicates where phase changes or chemical reactions absorb (endothermic) or evolve (exothermic) heat. Data from both techniques provide information about water content, organic content, and phase changes. Data obtained also reveal the relative thermal stabilities of nanocomposite components as compared to their bulk phases.[13]

1.4.3 Infrared (IR) Spectrometry

IR spectrometry probes vibrational transitions, which typically have energies in the infrared region. This method is widely useful for analysis and identification of organic materials, inorganic molecules and organometallic compounds.[56] For organic-inorganic nanocomposites, the IR absorption spectrum can be used to confirm the incorporation of the organic component. In addition, peak shifts for organic polymers confined between inorganic host layers can lead to a better understanding of their interaction with host structures. For example, FTIR has shown that the shift in OH-stretching peaks of the kaolinite host to lower wavenumbers depends on the strength of hydrogen-bonding with guest species such as *N*-methylformamide and poly(vinylpyrrolidone).[57]

1.4.4 SEM

SEM is used to capture the micro-scale image of the sample surface. Rather than using visible light as in optical microscopy, electrons are accelerated across high voltages between several hundred to 40,000 V, producing an electron beam with wavelengths at the atomic scale. The surface of a sample is scanned with the electron beam, and the back-scattered beam is collected and displayed on a cathode ray tube.[55,58] Aside from the back-scattered beam, when an electron beam hits a

sample, secondary electrons are produced. Only those electrons near the surface can escape and contribute to the image formation. Therefore, a sloped surface produces more secondary electrons than a flat surface. SEM has a wide range of magnification, usually between about 10x and 100,000x. Although its magnification is not as high as for transmission electron microscopy (TEM), sample preparation is much easier since TEM requires sectioning into a thin form. Therefore, SEM is commonly used for nanocomposite characterization.[58]

1.5 CHARACTERIZATION OF EXFOLIATION AND SWELLING BEHAVIORS

The direct intercalation of large organic species, such as polymers, is not possible for many layered hosts. In such cases, the reactions may be thermodynamically unfavorable, or may require a high activation energy. The exfoliation or dispersion of the host can be one means to allow large guest species to directly adsorb onto the exposed surfaces. This can decrease the activation energy for the overall reaction, and hereby provide a route to new materials. Therefore, it is often important to investigate particle size changes during reactions.

1.5.1 Particle size distribution analyses

The particle size distribution analyzer used in these studies is a Horiba CAPA-700. The principle of analysis is liquid-phase sedimentation by gravity or centrifugation. The measurement is based on the optical transmission method, which uses the Stokes' equation to indicate the relationship between sample absorbance and particle concentration. More details on the method are provided in Chapter 4. The instrument used has a minimum particle size threshold of 100 nm, whereas inorganic hosts are exfoliated into single sheets the dimensions < 1 nm. Although this method cannot identify dispersed particles in all size regions of interest, it is a simple way to determine gross changes in particle sizes. Another useful result is the indication of particle aggregation during processing conditions.

1.5.2 Ultraviolet-Visible (UV/Vis) spectrophotometry

UV/Vis spectrophotometry is based on measuring the absorption of near-UV or visible radiation of materials. Radiation in this region causes electronic transitions at wavelengths characteristic of the molecular structure in a sample.[56] Nanometer-sized semiconductor particles or layers are an intermediate form between molecules and bulk solids. For semiconductor materials, the electronic band structures are due to the confinement of the electron-hole pair in the restricted

space of the semiconductor particles. As the particles get smaller, the band gap is larger, resulting from shifts of the conduction band edge to higher energy and the valence band edge to lower energy. According to the effective-mass equation describing the relative motion of an interacting electron and hole pair,

$$H\Phi = E\Phi \,, \tag{2}$$

where

$$H = \frac{-\hbar^2}{2\mu_{xy}}\left(\frac{\delta^2}{\delta x^2}+\frac{\delta^2}{\delta y^2}\right) - \frac{\hbar^2}{2\mu_z}\frac{\delta^2}{\delta x^2} \tag{3}$$

By neglecting Coulombic terms, the band gap energy is formulated as follows:

$$E = \frac{\hbar^2}{2\mu_{xy}}\left(\frac{n_x^2\pi^2}{L_x^2}+\frac{n_y^2\pi^2}{L_y^2}\right)+\frac{\hbar^2}{2\mu_z}\left(\frac{n_z^2\pi^2}{L_z^2}\right) \tag{4}$$

where x and y are the directions in the layer plane, z is the direction perpendicular to the layer plane, n_i are integers, L_i is the dimension of particle in i direction, and μ_{xy} and μ_z are the reduced effective masses of electron-hole pairs within the layer plane and perpendicular to plane, respectively. Since $L_x \sim L_y >> L_z$ for nano-sized layers, the first term can be neglected. Therefore, the electronic band energy found by UV/Vis is based on the thickness of layered sheet. The smaller the thickness (L_z), the larger the exciton energy (ΔE_g).[54-56] This effect has been observed for several layered semiconductor materials in colloidal or exfoliated state such as

GaS, GaSe, GaTe, PbI_2, and TiO_2 (from hydrolysis of $TiCl_3$ and from exfoliation of $H_xTi_{2-x/4}\square_{1/4}O_4.H_2O$).[30,59-62] The effect is also observed in CdS nanoclusters.[63]

1.6 THESIS OVERVIEW

The discovery of new organic-inorganic nanocomposites, and evaluation of their novel properties, attracts a wide range of scientists. In this thesis, the goal is to develop new synthetic strategies, and to prepare nanocomposites with new hosts.

In Chapter 2, studies on the melt intercalation of poly(ethylene oxide) into MoO_3 and MPS_3(M=Mn,Cd) will be described. Before this study, melt intercalation had been reported only with clay materials. The kinetics of intercalation was investigated for these new reactions.

Chapter 3 describes the preparation of polymer-containing nanocomposites with a layered titanate. This is the first time that polymers and titanates were combined to form ordered nanocomposites. The method employed is adapted from the exfoliation-adsorption technique investigated previously.[26,44-50] Ultrasonic processing is introduced to facilitate the exfoliation reaction.

Chapter 4 investigates the dispersion and exfoliation behavior of a layered titanate by ultrasonic processing. Reaction conditions were optimized to increase the rate and yield of desired products.

The work described in chapter 5 involves the use of ultrasonic processing to obtain long-chain alkylammonium intercalation compounds of tetratitanate and nanocomposites with several polymers. The dispersion behavior using ultrasound in the presence of tetrabutylammonium hydroxide is also investigated.

1.7 REFERENCES

1. SciFinder Scholar 2000 (accessed July 2001) Search term = Nanocomposites.

2. Roy, R. *Mat. Res. Soc. Symp. Proc.* **1993**, *286*, 241-250.

3. Lerf, A. Intercalation Compounds in Layered Host Lattices: Supramolecular Chemistry in Nanodimensions. In Handbook of Nanostructured Materials and Nanotechnology, Vol. 5; Nalwa, H., Ed.; Acad. Press: New York, 2000; pp 1-166.

4. Oriakhi, C. O. *J. Chem. Ed.* **2000**, *77*, 1138.

5. Ishii, T.; Nozawa, H.; Tamamura, T. *Appl. Phys. Lett.* **1997**, *70*, 1110.

6. Ishii, T.; Shibata, T.; Nozawa, H.; Tamamura, T. *AIP Conf. Proc.* **1998**, *442*, 494.

7. Gonsalves, K. E.; Merhari, L.; Wu, H.; Hu, Y. *Adv. Mater.* **2001**, *13*, 703.

8. Dawson, A; Kamat, P. V. *J. Phys. Chem. B* **2001**, *105*, 960.

9. Schöllhorn, R. Inclusion Comopounds Vol. 1: Structural Aspects of Inclusion Compounds Formed by Inorganic and Organometallic Host Lattices, Atwood; J. L.; Davies, J. E.; MacNicol, D. D. Eds. Academic Press: London, 1984, Chapter 7.

10. Haushalter, R. C.; Mundi, L. A. *Chem. Mater.* **1992**, *4*, 31.

11. Soghomonian, V.; Chen, Q.; Haushalter, R. C.; Zubieta, J.; O'Connor C. J. *Science*, **1993**, *259*, 1596.

12. Fischer, J. E. *Chem. Innovation* **2000**, *30*, 21.

13. Ajayan, P. M. *Chem. Rev.* **1999**, *99*, 1787.

14. Lawton, G. *Chem. Ind.* **2001**, *6*, 174.

15. Biswas, M.; Sinha Ray, S. *Adv. Polym. Sci.* **2001**, *155*, 167.

16. Vaia, R. A.; Giannelis, E. P. *Macromolecules* **1997**, *30*, 8000.

17. Lee, J.; Takekoshi, T.; Giannelis, E. P. *Mat. Res. Soc. Symp. Proc.* **1997**, *457*, 513.

18. Enzel, P.; Bein, T. *J. Chem. Soc., Chem. Commun.* **1989**, 1326.

19. Enzel, P.; Bein, T. *J. Phys. Chem.* **1989**, *93*, 6270.

20. Enzel, P.; Bein, T. *Chem. Mater.* **1992**, *4*, 819.

21. Julien, C.; Khelfa, A.; Guesdon, J. P.; Gorenstein, A. *Appl. Phys. A* **1994**, *59*, 173.

22. Elder, S. H.; Cot, F. M.; Su, Y.; Heald, S. M.; Tyryshkin, A. M.; Bowman, M. K.; Gao, Y.; Joly, A. G.; Balmer, M. L.; Kolwaite, A. C.; Magrini, K. A.; Blake, D. M. *J. Am. Chem. Soc.* **2000**, *122*, 5138.

23. Schöllhorn, R.; Kuhlmann, R. *Mater. Res. Bull.* **1976**, *11*, 83.

24. Brec, R. *Solid State Ionics* **1986**, *22*, 3.

25. Yang, D.; Frindt, R. F. *J. Mater. Res.* **2000**, *15*, 2408.

26. Lagadic, I.; Léaustic, A.; Clément, R. *J. Chem. Soc. Chem. Commun.* **1992**, 1396.

27. Sasaki, T.; Watanabe, M.; Michiue, Y.; Komatsu, Y.; Izumi, F.; Takenouchi, S. *Chem. Mater.* **1995**, *7*, 1001.

28. Nakano, S.; Sasaki, T.; Takemura, K.; Watanabe, M. *Chem. Mater.* **1998**, *10*, 2044.

29. Sasaki, T.; Watanabe, M.; Hashizume, H.; Yamada, H.; Nakazawa, H. *Chem. Commun.*, **1996**, 229.

30. Sasaki, T.; Watanabe, M. *J. Am. Chem. Soc.* **1998**, *120*, 4682.

31. Sasaki, T.; Komatsu, Y.; Fujiki, Y. *Inorg. Chem.* **1989**, *28*, 2776.

32. Sasaki, T.; Watanabe, M.; Komatsu, Y.; Fujiki, Y. *Inorg. Chem.* **1985**, *24*, 2265.

33. Ogawa, M.; Takizawa, Y. *Mol. Cryst. Liq. Cryst.* **2000**, *341*, 357.

34. Okawa, M.; Takizawa, Y. *Chem. Mater.* **1999**, *11*, 30.

35. Choy, J.-H.; Han, Y.-S.; Park, N.-G.; Kim, H.; Kim, S.-W. *Synth. Met.* **1995**, *71*, 2053.

36. Pomogailo, A. D. *Rus. Chem. Rev.*, **2000**, *69*, 53.

37. Sanchez, C.; Ribot, F.; Lebeau, B. *J. Mater. Chem.* **1999**, *9*, 35.

38. Oriakhi, C. O. Ph.D. Thesis, Oregon State University, Corvallis, OR, April, 1996.

39. Jacobson, J. A. Solid State Chemistry: Compounds, Cheetham, A. K.; Day, P., Eds.; Clarendon, oxford, 1992, 234.

40. Hazen, R. M. *Science* **1983**, *219*, 1065.

41. Hazen, R. M.; Finger, L. W. *J. Appl. Phys.* **1984**, *56*, 1838.

42. Moller, K.; Bein, T. *Chem. Mater.* **1998**, *10*, 2950.

43. Wu, J.; Lerner, M. M. *Chem. Mater.* **1993**, *5*, 835.

44. Vaia, R. A.; Vasudevan, S.; Krawiec, W.; Scanlon, L. G.; Giannelis, E. P. *Adv. Mater.* **1995**, *7*, 154.

45. Lemmon, J. P.; Lerner, M. M. *Chem. Mater.* **1994**, *6*, 207.

46. Lemmon, J. P.; Lerner, M. M. *Solid State Commun.* **1995**, *94*, 533.

47. Aranda, P.; Ruiz-Hitzky, E. *Chem. Mater.* **1992**, *4*, 1395.

48. Nazar, L. F.; Wu, H.; Power, W. P. *J. Mater. Chem.* **1995**, *5*, 1985.

49. Liu, Y. J.; DeGroot, D. C.; Schindler, J. L.; Kannewurf, C. R.; Kanatzidis, M. G. *Chem. Mater.* **1991**, *3*, 992.

50. Tsai, H. L.; Schindler, J. L.; Kannewurf, C. R.; Kanatzidis, M. G. *Chem. Mater.* **1997**, *9*, 875.

51. Mason, T. J. Practical Sonochemistry: User's Guide to Applications in Chemistry and Chemical Engineering, Ellis Horwood Limited: West Sussex, England, 1991, Chapter 1.

52. Suslick, K. S.; Casadonte, D. J.; Green, M. L. H.; Thompson, M. E. *Ultrasonics* **1987**, *25*, 56.

53. Chatakonda, K.; Green, M. L. H.; Thompson, M. E.; Suslick, K. S. *J. Chem. Soc., Chem. Commun.* **1987**, 900.

54. Tagaya, H.; Takeshi, K.; Ara, K.; Kadokawa, J.-I.; Karasu, M.; Chiba, K. *Mater. Res. Bull.* **1995**, *30*, 1161.

55. Wold, A.; Dwight, K. Solid State Chemistry: Synthesis, structure, and properties of selected oxides and sulfides, Chapman & Hall, Inc., New York, 1993, Chapter 2.

56. Ingle, J. D.; Crouch, S. R. Spectrochemical Analysis, Prentice-Hall, Inc., New Jersey, 1988.

57. Komori, Y.; Sugahara, Y.; Kuroda, K. *Chem. Mater.* **1999**, *11*, 3.

58. Fegler, S. L.; Heckman, Jr., J. W.; Klomparens, K. L. Scanning and Transmission Electron Microscopy: An Introduction, W. H. Freeman and Company: New York, 1993, Chapter 5.

59. Shinada, M.; Sugano, S. *J. Phys. Soc. Japan* **1966**, *21*, 1936.

60. Sandroff, C. J.; Hwang, D. M.; Chung, W. M. *Phys. Rev. B* **1986**, *33*, 5953.

61. Sasaki, T.; Watanabe, M. *J. Phys. Chem. B* **1997**, *101*, 10159.

62. Kavan, L.; Stoto, T.; Grätzel, M. *J. Phys. Chem.* **1993**, *97*, 9493.

63. Vossmeyer, T.; Katsikas, L.; Giersig, M.; Popovic, I. G.; Diesner, K.; Chemseddine, A.; Eychmüller, A.; Weller, H. *J. Phys. Chem.* **1994**, *98*, 7665.

CHAPTER 2

PREPARATION OF LAYERED NANOCOMPOSITES OF PEO WITH $MnPS_3$, $CdPS_3$ AND MoO_3 BY MELT INTERCALATION

Nipaka Sukpirom, Christopher O. Oriakhi, and Michael M. Lerner

Department of Chemistry and Center for Advanced Materials Research,

Oregon State University,

Corvallis, OR 97331-4003, USA

Mater. Res. Bull. **2000**, *35*, 325-331.

2.1 ABSTRACT

Intercalated nanocomposites comprised of polyethylene oxide (PEO) and MPS_3 (M = Mn, Cd) or MoO_3 are prepared by the direct heating of the alkali-metal intercalated host with PEO. This process, known as melt intercalation, has previously been applied to polymers with layered silicates. Reaction rates and yields are low below the melting temperature for PEO, but at 125°C a significant or quantitative conversion to the ordered nanocomposite can be achieved in 5–30 h. Intercalated nanocomposite yields are followed by powder X-ray diffraction to provide relative reaction rates at 50, 75, and 125°C for PEO with $M_w = 1 \times 10^5$ and 5×10^6.

KEYWORDS: A. layered compounds, A. composites, A. nanostructures, B. intercalation reactions, C. X-ray diffraction

2.2 INTRODUCTION

Layered nanocomposites, comprised generally of an organic polymer incorporated between layers of an inorganic host, have received much attention as they have been proposed and determined to have novel, and technologically useful, properties [1]. Accordingly, much research has been devoted to the preparation of these materials [2]. Nanocomposites may contain ordered domains with polymer intercalated between host layers, and/or disordered assemblies of polymer with exfoliated host layers. Several general synthetic strategies are known, including the *in situ* polymerization of intercalated monomers, an exfoliation/adsorption process, and template syntheses. Perhaps the most attractive for industrial application is the direct heating of layered host and polymer, known as the melt intercalation, described by Giannelis and coworkers [3-7]. This process simply entails the direct heating of a mixture of polymer and layered host (or chemically-modified host) at a temperature that provides for a significant rate of polymer self-diffusion. Using this method, the incorporation of a number of polymers into layered silicas, including polystyrene [4,5], poly(ethylene oxide) (PEO) [6], a co-polymer of isobutylene with p-bromomethylestyrene [7] and nylon 6 [8] have been reported.

In this report, we extend the melt intercalation process to other layered hosts, describing the preparation of nanocomposites of PEO with layered MoO_3 or MPS_3 hosts by direct heating of the polymer with an alkali-metal intercalation compound of the host.

2.3 EXPERIMENTAL

2.3.1 Synthesis of host materials

Li_xMoO_3 was prepared by reaction of MoO_3 (Aldrich, 99.5%) with $Na_2S_2O_4$ (Fisher, laboratory grade) to afford Na_xMoO_3, followed by ion exchange in aqu. LiCl (LiCl, Mallinckrodt, 99.8%) using a literature method [9]. MPS_3 (M = Cd, Mn) was prepared by heating CdS (Aldrich, 99.995%) or Mn (Aldrich, 99.9%) with a stoichiometric amount of red phosphorus (Johnson Matthey, 99%) and sulfur (Mallinckrodt, 99.9%) in a vacuum-sealed quartz tube at 650 or 750 °C for 2 weeks [10-12]. The formation and purity of the MPS_3 phase was confirmed by powder X-ray diffraction (PXRD), which showed no crystalline impurities. The potassium hydrate intercalation compounds, $K_xM_{1-x/2}PS_3{\cdot}\delta H_2O$, were formed by reaction of MPS_3 with 2 M KCl (KCl, Mallinckrodt, 99.5%) [13]. The products were filtered and washed with de-ionized water, then air-dried. Subsequently, PXRD showed only the ion-exchanged product to be present. For $CdPS_3$, this reaction was carried out in the presence of 0.1 M EDTA ($C_{10}H_{14}O_8N_2Na_2{\cdot}2H_2O$, Mallinckrodt, 100.6%) in an $NaHCO_3$ (Mallinckrodt, 100.2%)/Na_2CO_3 (Mallinckrodt, 99.62%) buffer solution according to a literature procedure [13].

2.3.2 Synthesis and characterization of nanocomposites

The host material and low or high molecular weight poly(ethylene oxide) (PEO) (Aldrich, $M_w = 1 \times 10^5$ or 5×10^6) were mixed, ground, and approximately 30 mg of the mixture pelletized into a cylinder of 3 mm radius at 2 tons pressure. The reactant ratios are reported below in g polymer/g layered host (g/g). The pellets were heated in air at the allotted temperature and time. The product structure was periodically examined by PXRD (2–60° 2θ, 0.02° 2θ sec^{-1}, Cu K_α radiation). An intercalated nancomposite yield, χ(t), was evaluated by comparing the relative contents of intercalated nanocomposite and layered host phases from each PXRD pattern:

$$\chi(t) = \frac{I(001p) + I(002p)}{I(001r) + I(001p) + I(002p)} \quad (1)$$

where I (*001*p) and I (*002*p) are the integrated intensities of the corresponding reflections of the intercalated nanocomposite product, and I (*001*r) is the integrated intensity of that reflection from the starting layered host reactant. This form of χ was chosen in order to utilize the strongest reflections in each pattern and also to minimize the angular difference in reactant and product reflections, since the average diffraction angle for (*001*) and (*002*) of the nanocomposite was in each case close to that of (*001*) of the host.

2.4 RESULTS AND DISCUSSION

At 75 and 125°C, nanocomposite formation was evident from the decrease of the (*001*) reflection of the starting layered host structure, and simultaneous appearance of new peaks indexed as (*001*) and (*002*) of an ordered nanocomposite phase. Fig. 2.1 shows a sequence of PXRD patterns for the pellet containing PEO and $LiMoO_3$. PXRD patterns of the pellets as formed and after heating at 125°C are shown in Fig. 2.2. The basal-repeat distances for starting materials were 9.3 ($LiMoO_3$), 9.2 ($K_xMn_{1-x/2}PS_3 \cdot \delta H_2O$) and 9.3Å ($K_xCd_{1-x/2}PS_3 \cdot \delta H_2O$), and for the nanocomposite products were 16.3, 15.2, and 15.5Å, respectively. The product basal-repeat distances in each case were 8–10 Å greater than the unintercalated host layer thickness, and agree therefore with values previously ascribed to a bilayer of PEO incorporated between host layers [14]. While ordered nanocomposites containing PEO monolayers with 4–5 Å increases in basal-repeat have been reported by other preparative methods [14], monolayer incorporation was not observed in the current experiments either as an intermediate product or at limiting polymer stoichiometries.

The ratio of PEO to $LiMoO_3$ was varied from 0.1–0.5 g/g in order to establish an approximate stoichiometry for the ordered nanocomposites. After heating for 4–6 hours at 125°C, the intercalated nanocomposite yields, χ, became relatively constant, and increased with higher polymer loading to $\chi = 0.9$ at 0.4 g/g. (Fig. 2.3) At a reactant ratio of 0.5 g/g, χ no longer increased, indicating the

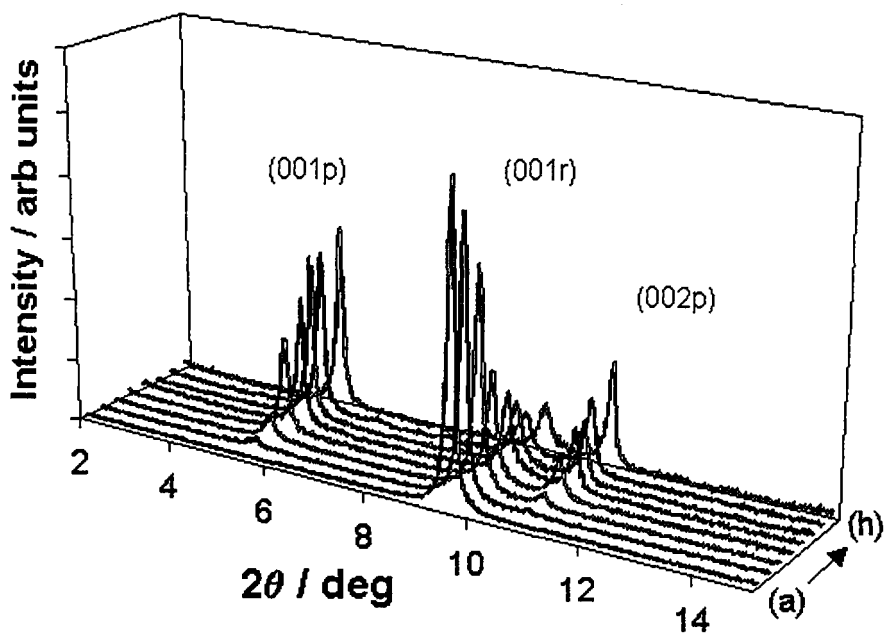

Figure 2.1 Stacking PXRD patterns for $LiMoO_3$ + PEO pellet heated at 125 °C. Heating times for samples (front pattern to back) were 0 (a), 1 (b), 3 (c), 9 (d), 18 (e), 27 (f), 35 (g), and 40 h (h).

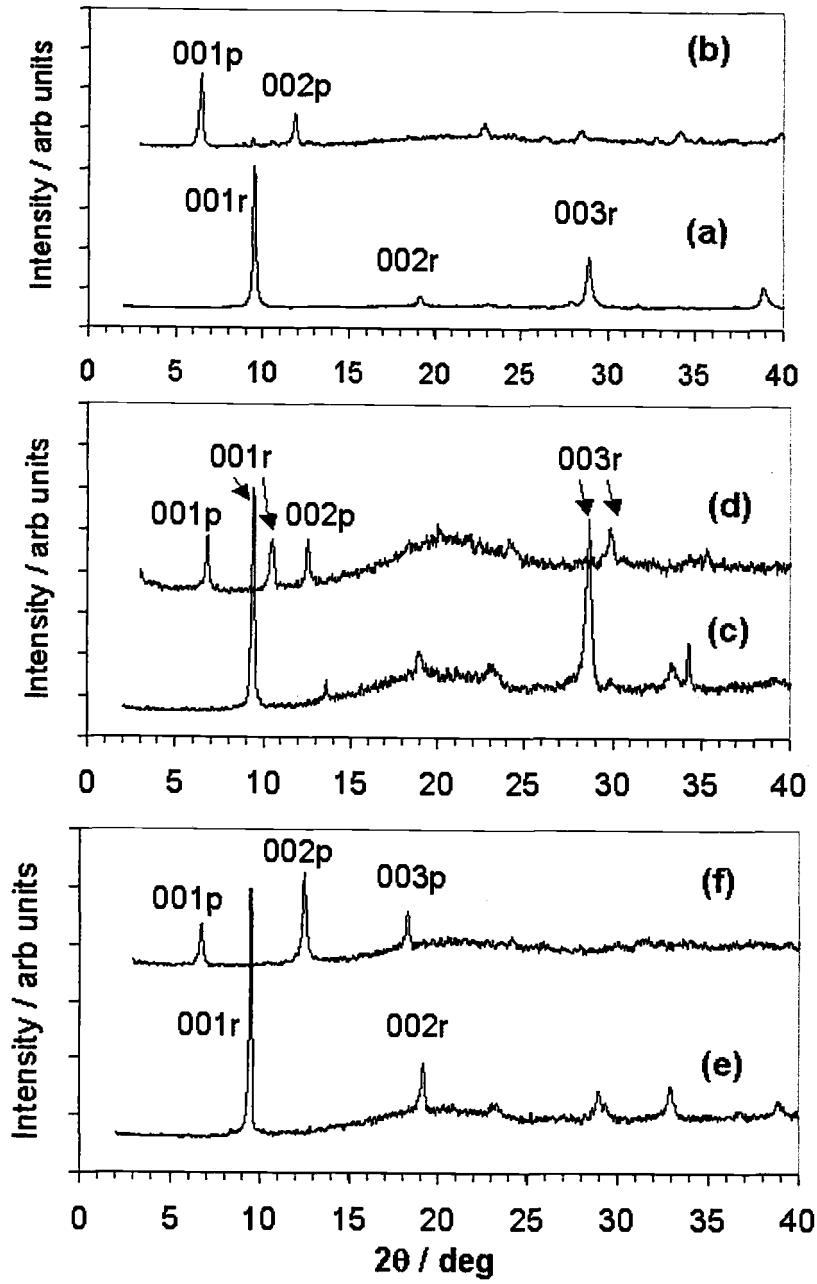

Figure 2.2 PXRD patterns for pellets before and after heating at 125°C; $LiMoO_3$ + PEO (a), heated for 4 h (b); $K_xMn_{1-x/2}PS_3$ + PEO (c), heated for 20 h (d); $K_xCd_{1-x/2}PS_3$ + PEO (e), and heated for 30 h (f). In each graph, the upper pattern is offset by 1° for clarity.

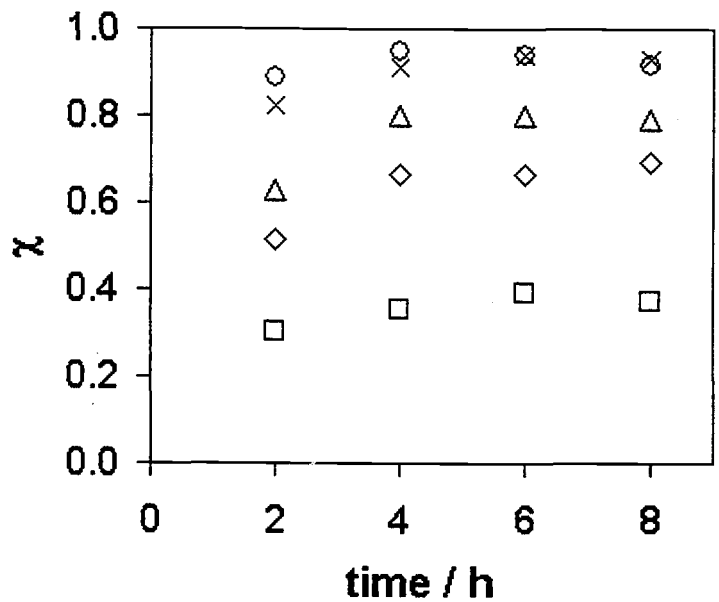

Figure 2.3 Intercalated nanocomposite yields, χ, for the following starting pellet compositions in g PEO / g $LiMoO_3$, 0.1 (□), 0.2 (◇), 0.3 (△), 0.4 (x), and 0.5 (o). Time indicates heating at 125°C.

ordered product stoichiometry is close to 0.4 g/g. Previously, a stoichiometry of approximately 0.3 g/g was determined for products obtained by the exfoliation / adsorption method. [15] Higher PEO loadings resulted in less crystalline products that showed weak sharp reflections and the evolution over time of a very broad diffraction intensity between 15 and 25 °. This was ascribed to the formation of an exfoliated, or disordered, nanocomposite structure, and subsequent reactions were therefore carried out at loadings of 0.4 g/g. Similarly, reactions carried out at 160°C with 0.4 g/g or higher polymer loading produced a primarily amorphous product ascribed to the exfoliated nanocomposite.

Intercalated nanocomposite yields, χ, determined during reactions of high and low molecular weight PEO with the hosts $LiMoO_3$, $K_xMn_{1-x/2}PS_3$ and $K_xCd_{1-x/2}PS_3$ at 50, 75 and 125 °C are provided in Figure 2.4, and χ values determined for each combination after 60 h reaction are reported in Table 2.1. Reaction temperature has a strong affect on rate in these direct syntheses. It has been noted already that polymer segmental motion can be the rate-limiting step in melt intercalation processing. [4] In these experiments, even prolonged interaction below the PEO melting temperature (60–65°C) results in little polymer incorporation, with $\chi < 0.2$ in all cases after 60 h. Reactions carried out above the melting transition had a significantly greater rate. Polymer molecular weight was important to the rate of reaction with $K_xMn_{1-x/2}PS_3$, on the other hand this had no measurable effect of molecular weight for $K_xCd_{1-x/2}PS_3$.

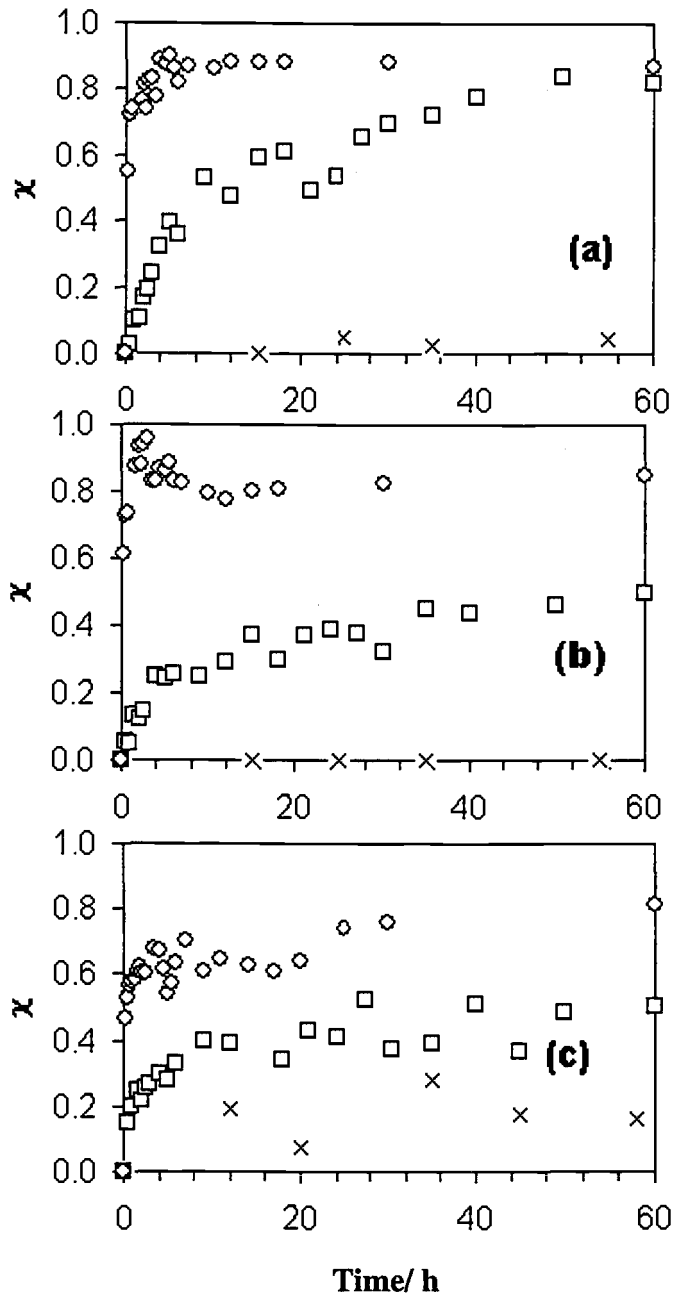

Figure 2.4 Intercalated nanocomposite yields, χ, for reactions at 50°C (x), 75°C (□), and 125°C (o); $LiMoO_3$ + 1 × 10^5 PEO (a), $LiMoO_3$ + 5 × 10^6 PEO (b), $K_xMn_{1-x/2}PS_3$ + 1 × 10^5 PEO (c).

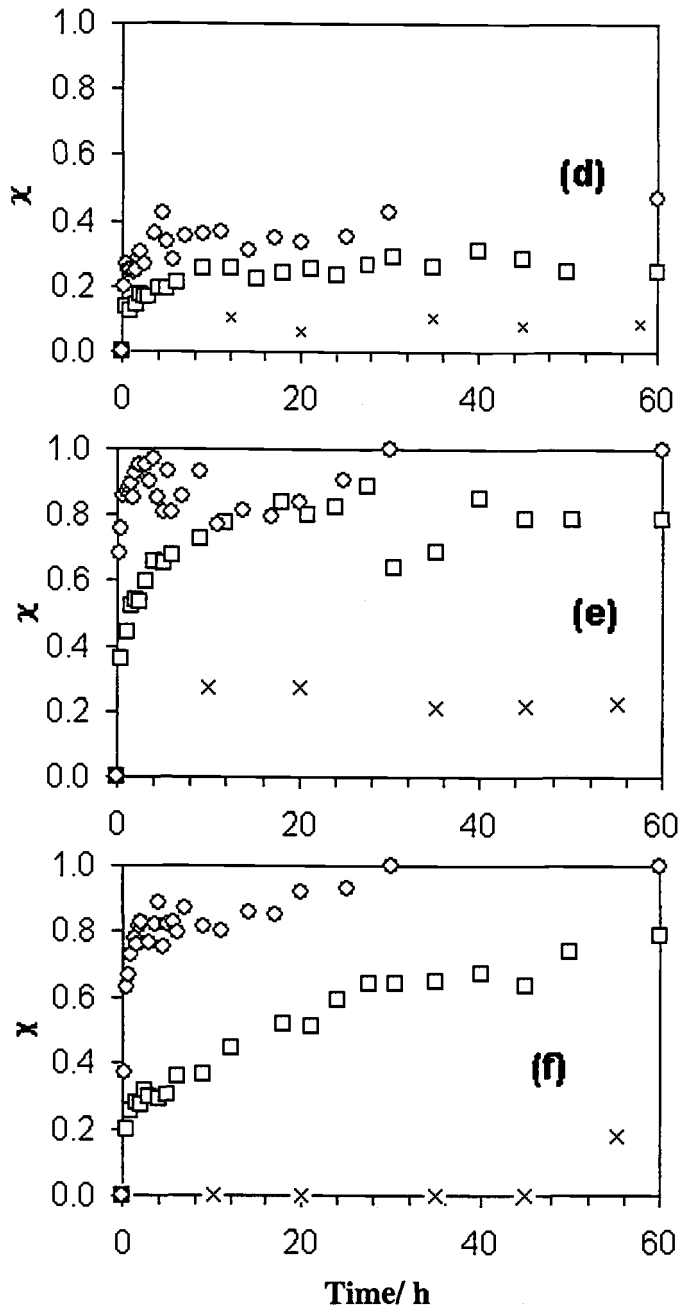

Figure 2.4 (continued) Intercalated nanocomposite yields, χ, for reactions at 50°C (x), 75°C (□), and 125°C (o); $K_xMn_{1-x/2}PS_3 + 5 \times 10^6$ PEO (d), $K_xCd_{1-x/2}PS_3 + 1 \times 10^5$ PEO (e), and $K_xCd_{1-x/2}PS_3 + 5 \times 10^6$ PEO (f).

Table 2.1 Intercalated nanocomposite yields, χ, after heating pellets for 60 h at 50, 75, or 125°C.

Host	Temperature (°C)	χ	
		PEO (1×10^5)	PEO (5×10^6)
$LiMoO_3$	50	0.04	0.06
	75	0.82	0.50
	125	0.87	0.85
$K_xMn_{1-x/2}PS_3$	50	0.16	0.09
	75	0.50	0.25
	125	0.81	0.47
$K_xCd_{1-x/2}PS_3$	50	0.20	0.18
	75	0.79	0.79
	125	1.0	1.0

The intercalated nanocomposite yields with $K_xMn_{1-x/2}PS_3$ were significantly lower than for the other layered hosts. In these products, however, all peak intensities were markedly reduced, suggesting that the formation of an amorphous, exfoliated, nanocomposite was significant in this case. Again, the appearance of a broad diffraction intensity around 15–25 °2θ is consistent with the above interpretation. Despite the similarity in the host MPS_3 structures for M = Mn and Cd, the extent of potassium exchange, and therefore the layer charge densities, can be different, which may explain the preference for intercalated vs. exfoliated structures in these reactions.

2.5 ACKNOWLEDGMENT

The authors gratefully acknowledge support from NSF grant DMR-9900390.

2.6 REFERENCES

1. Lerner, M.; Oriakhi, C. in *Handbook of Nanophase Materials*, Ed. A. Goldstein, Marcel Dekker: New York, 1997, pp. 199–219.

2. Giannelis, E. *Appl Organometal Chem* **1998**, *12*, 675.

3. Giannelis, E. *Adv Mater* **1996**, *8*, 29.

4. Vaia, R.; Jandt, K.; Kramer, E.; Giannelis, E. *Macromolecules* **1995**, *28*, 8080.

5. Vaia, R.; Jandt, K.; Kramer, E.; Giannelis E. *Chem Mater* **1996**, *8*, 2628.

6. Vaia, R.; Vasudevan, S.; Krawiec, W.; Scanlon, L.; Giannelis E. *Adv Mater* **1995**, *7*, 154.

7. Burnside, S.; Wang, H.; Giannelis E. *Chem Mater* **1999**, *11*, 1055.

8. Liu, L.; Qi, Z.; Zhu X. *J Applied Polym Sci* **1999**, *71*, 1133.

9. Thomas, D.; McCarron, E. *Mater Res Bull.* **1986**, *21*, 945.

10. Tayler, B.; Steger, J.; Wold A. *J Solid State Chem* **1973**, *7*, 461.

11. Klingen, V.; Ott, R.; Hahn, H. *Z Anorg Allg Chem* **1973**, *396*, 271.

12. Oriakhi, C.; Lerner, M. *Chem Mater* **1996**, *8*, 2106.

13. Clement, R.; Garnier, O.; Jegoudez J. *Inorg Chem* **1986**, *25*, 1404.

14. Oriakhi, C.; Nafshun, R.; Lerner M. *Mater Res Bull* **1996**, *31*, 1513.

15. Lemmon, J.; Wu, J.; Oriakhi, C.; Lerner M. *Electrochim Acta*, **1995**, *40*, 2245.

CHAPTER 3

PREPARATION OF ORGANIC-INORGANIC NANOCOMPOSITES WITH A LAYERED TITANATE

Nipaka Sukpirom and Michael M. Lerner

Department of Chemistry and Center for Advanced Materials Research,

Oregon State University,

Corvallis, OR 97331-4003, USA.

Chem. Mater. **2001**, *13*, 2179-2185

3.1 ABSTRACT

Layered nanocomposites with poly(ethylene oxide), PEO, and poly(vinylpyrrolidone), PVP, incorporated between $H_xTi_{2-x/4}\square_{x/4}O_4$ ($\square$=Ti vacancy) titanate layers, are synthesized from a colloidal titanate suspension obtained by exfoliation in aqueous tetrabutylammonium hydroxide and subsequent acidification. Products are characterized by powder X-ray diffraction, thermal analyses, FTIR spectroscopy, scanning electron microscopy and elemental analysis. Interlayer expansions for the vacuum-dried nanocomposites are 0.81 and 2.2 nm for the PEO and PVP-containing products, respectively. Both nanocomposites are comprised of 10-100 μm diameter platelets, much larger than those of 0.1-1 μm for the starting titanate. FTIR spectra indicate the presence of the polymers, and suggest decreased water interaction with titanate sheet surfaces for the polymer-containing products. Thermal analyses of nanocomposites show intercalate water loss below 200°C, polymer degradation and structure decomposition between 200-450°C, and a titanate phase change above 450°C. Elemental analyses give empirical formulas of $H_{0.7}Ti_{1.83}O_4(C_2H_4O)_{1.54}(H_2O)_{1.28}$ and $H_{0.7}Ti_{1.83}O_4(C_{16}H_{36}N)_{0.05}(C_6H_9NO)_{1.22}(H_2O)_{0.92}$ for the PEO and PVP nanocomposites, respectively. These results are compared with those obtained for other layered nanocomposites.

3.2 INTRODUCTION

A wide range of polymers and hosts have been combined to form nanocomposite structures, and nanostructured materials have been shown to exhibit novel, and technologically useful, mechanical, optical, electrical, and barrier properties.[1-3] Layered nanocomposites are materials generally comprised of an organic polymer incorporated between sheets of an inorganic host. Much research has been devoted to developing new synthetic methods for these materials: layered nanocomposites have been prepared by the *in situ* polymerization of intercalated monomers, the exfoliation of a layered host and subsequent adsorption of polymer and reaggregation, template syntheses of host structures in polymer-containing solutions, and direct melt intercalation of polymers into hosts.[4-6]

Table 3.1 provides a selected summary indicating the range of different hosts that have been studied in layered nanocomposites. By far, the most work has concentrated on the aluminosilicate smectite clays such as montmorillonite and hectorite. These hosts have a number of advantages in this application. Firstly, they spontaneously delaminate in appropriate aqueous conditions, and are also amenable to melt intercalation,[5] greatly facilitating the preparation of nanocomposites. Aluminosilicate clays are also inexpensive, non-toxic, refractory, and can be surface modified. Clay-based nanocomposites have therefore shown properties that indicate commercial potential as structural materials,[2,29-31] uv barrier coatings,[31] gas barrier coatings,[31,32] and fire retardants.[33]

Table 3.1 Selected list of inorganic hosts studied in layered nanocomposites with poly(ethyleneoxide), PEO, and poly(vinylpyrrolidone), PVP.

Host	**Polymer**	**Reference**
smectite clays	PEO	5,7-9
	PVP	10-13
MoO_3	PEO	14-17
	PVP	16
V_2O_5	PEO	18
MoS_2	PEO	19-21
$NbSe_2$	PEO	22
	PVP	22
MPS_3	PEO	14,23-25
	PVP	23
$RuCl_3$	PEO	26
	PVP	26
graphite oxide	PEO	27,28

Nanostructures based on TiO_2 are a very attractive prospect due to the low cost, environmental acceptability, chemical stability, and photochemical properties of TiO_2 and many titanates. As with other inorganic solids, the optical properties of TiO_2 have been modified by preparing nanoparticles.[34-36] Composite materials comprising nanostructured TiO_2 have also been examined, a polyimide matrix with nanostructured titania has been reported and proposed for use in waveguides.[37] A TiO_2 nanocomposite with PVP was prepared by a sol-gel method via hydrolysis of a titanium alkoxide.[38] This method produced a disordered titania network homogeneously dispersed in PVP.

Hervieu and Raveau originally reported a series of nonstoichiometric layered titanates, $A_xTi_{2-x/4}\square_{x/4}O_4.H_2O$ (A=Li-Cs or H, x=0.67–0.73, $\square$ indicates vacant Ti sites) with a lepidocrocite-like structure.[39] In the past few years, Sasaki and coworkers have prepared and characterized protonated and exfoliated forms of these materials.[36,40-44] A mixed-metal sheet structure with Li substitution in the Ti sites, $A_xTi_{2-x/3}Li_{x/3}O_4$ (A=K-Cs or H, x=0.7-0.8), has also been reported by the same group.[45] The proton-exchanged form of the first structure, $H_{0.7}Ti_{1.83}\square_{0.17}O_4.0.7H_2O$ (H-Ti), swells and then delaminates in aqueous solutions containing tetrabutylammonium (TBA) cations.[41-44] Detailed XRD and optical characterization of the resulting colloidal suspensions have clearly demonstrated that when the mole ratio of TBA to protons in H-Ti (TBA/H) exceeds 0.5, the titania sheet galleries swell with water to the extent that a majority or all of the titanate layers become exfoliated into individually suspended sheets in the

solution.[42-44] The complete exfoliation process occurs simply by stirring in the TBA-containing aqueous solution and requires several days, the reaction is most favorable when high (5/1) TBA/H ratios are used.[41,44]

Recent work by Sasaki et. al. has demonstrated that multilayer thin films of titania nanosheets can be prepared a layer-by-layer self-assembly approach.[46] Repeated immersions of a substrate in solutions of the colloidal titania suspension followed by poly(dimethyldiallyl ammonium chloride) (PDDACl) resulted in the deposition of thin films containing 0.65 nm PDDA layers between individual titania layers.

We here report the application of the colloidal suspensions of exfoliated titania sheets as precursors to form lamellar titania nanocomposites with PEO and PVP, and the structural and compositional characterization of these new materials by XRD, TGA, DSC, FTIR and elemental analyses.

3.3 EXPERIMENTAL

3.3.1 Materials

Tetrabutylammonium hydroxide (Aldrich, 40% in water), TiO_2 (Aldrich, anatase form, 99.9+%), Cs_2CO_3 (Aldrich, 99.9%), poly(ethylene oxide) (PEO, Aldrich, M_n=100,000) and poly(vinylpyrrolidone) (PVP, Aldrich, M_n=40,000) were

used as received. $Cs_xTi_{2-x/4}\square_{x/4}O_4 \cdot yH_2O$, abbreviated Cs-Ti, was prepared according to a literature method.[39] Anatase TiO_2 (4.23 g) and Cs_2CO_3 (3.26 g) were ground together and heating briefly at 800°C in an alumina crucible to eliminate CO_2. The mixture was reground and reheated at 800°C twice for 20 h. The proton-exchanged material, $H_xTi_{2-x/4}\square_{x/4}O_4 \cdot yH_2O$ ($x \approx 0.7$, $y \approx 1$), abbreviated H-Ti, was prepared by stirring Cs-Ti powder in 100 ml of 1M HCl for 48 h, with the solution replaced after 24h. Powder X-ray diffraction (XRD) indicated that the proton exchange reaction was complete, and both solid products matched those described previously.[40,47]

3.3.2 H-Ti exfoliation

H-Ti (0.25 g) was added to an aqueous solution of tetrabutylammonium (TBA) hydroxide (50 ml) in a 100 ml glass bottle, maintaining a 0.5 mol/mol ratio of TBA to protons in H-Ti. The sample was prepared using a GE600 ultrasonic processor with titanium alloy probe (13 mm dia.) for 20 minutes at settings of 600 W / 30% amplitude. After ultrasonication, the exfoliated H-Ti layers are suspended in the solution, and no solid can be isolated by filtration on 11 μm pore dia. paper (Whatman #1). The reaggregated colloid was obtained by freeze-drying the solution for 24 h (Virtis Research Equipment freeze dryer) and has composition $H_xTBA_{1-x}Ti_{2-x/4}\square_{x/4}O_4 \cdot yH_2O$ ($x \approx 0.7, y \approx 1$), abbreviated as TBA/H-Ti.

3.3.3 Preparation of PEO/H-Ti, and PVP/H-Ti

PEO/H-Ti and PVP/H-Ti nanocomposites were prepared by adding aqueous polymer solutions to stirred suspensions of the exfoliated H-Ti described above. In both cases, a 3 mol/mol ratio of polymer formula unit to protons in H-Ti was used to ensure that the polymer was present in excess. The solutions were acidified by adding aqueous HCl until gel formation was observed, and stirred for an additional 2 minutes. The gels were filtered, washed copiously with DI water, and dried under vacuum for 24 h. Alternately, the PVP/H-Ti gel was cast on a glass substrate and dried in air for 24 h to obtain a thin film.

3.3.4 Characterization

Powder X-ray diffraction (XRD) of all materials were obtained using a Siemens D5000 diffractometer and CuK_α radiation (0.15418 nm) from 2-60°2θ in 0.02° steps. Thermal analyses were performed at 10°C/min under flowing N_2 (20 ml/min) using a Shimadzu TGA-50 and DSC-50. Infrared spectra were recorded on samples pressed into KBr disks using Nicolet 510P FTIR spectrometer (resolution=1 cm^{-1}, 64 scans averaged). Elemental (C/H/N/Ti) analyses were performed by Desert Analytics Laboratory (Tucson, AZ) and converted to the compositions $H_xTi_{2-x/4}O_4(TBA)_m(polymer)_n(H_2O)_p$ by setting x=0.7 and assuming

residual mass is due to oxygen. Microstructures were observed for samples coated with 60/40 Au/Pd using an Amray SEM operated at an accelerating voltage of 10.0 kV.

3.4 RESULTS AND DISCUSSION

As described previously, the layered titanate $H_xTi_{2-x/4}\square_{x/4}O_4 \cdot yH_2O$ ($x \approx 0.7$), H-Ti, is readily obtained by proton exchange from the Cs intercalate, and slowly delaminates on stirring with excess aqueous tetrabutylammonium (TBA).[44] The long processing time to obtain the stable colloidal suspension is inconvenient when using the exfoliated H-Ti as a precursor, but the suspension can be obtained from H-Ti within minutes by use of ultrasonic processing. These details will be reported separately.[48] In this work, a stable suspension of exfoliated H-Ti was obtained by ultrasonication of H-Ti in aqueous solution with TBA/H=0.5 for 20 min.

When aqueous solutions of poly(ethylene oxide), PEO, or poly(vinylpyrrolidone), PVP, are added to a suspension of exfoliated H-Ti, and the solution acidified to pH=2, gels rapidly form and a solid precipitate can be obtained by filtration. These observations suggest the spontaneous aggregation of titanate sheets and polymer. Strong attractive coulombic forces should arise between the negative titanate sheets and polymer in solution, since PVP is positively-charged at pH<3.0-3.5,[49] and PEO forms complexes with cations in aqueous solution.

Powder XRD patterns for the solid products obtained and the starting H-Ti phase are shown in Figure 3.1, and the derived basal repeat and stacking domain lengths are listed in Table 3.2. Due to preferred orientation of the platy particles, strong lines in these patterns are due to basal repeat reflections. H-Ti shows a basal repeat dimension of 0.93 nm, which indicates a monolayer of water intercalated along with protons between titania sheets.[40] After heating to 100°C for 0.5 h, intercalate water is removed and the layer thickness for H-Ti can be obtained directly from the broadened peak at 0.68 nm in Fig. 1(b). This agrees well with the value obtained by considering the crystallographic data for the parent titanate:[47] the distance between surface O atoms (0.42 nm) plus the diameter of an oxide (0.28 nm) gives a single sheet thickness of about 0.70 nm. When the colloidal suspension is freeze-dried to obtain the solid product TBA/H-Ti, the stacking repeat dimension increases to 1.75 nm. This expansion of about 1.1 nm is consistent with intercalation of TBA between titanate sheets, and matches the lamellar, turbostratic structure (repeat=1.75 nm) previously obtained after long-term stirring and solid reaggregation in aqueous TBA solution.[44]

After reaction with the polymer-containing solutions, neither the starting H-Ti phase nor the TBA/H-Ti phase described above are observed in XRD of the solid precipitates. New stacking repeat lengths of 1.49 and 2.88 nm for PEO/H-Ti and PVP/H-Ti, respectively, indicate galleries with expanded dimensions relative to H-Ti. The intercalate layer dimension for PEO/H-Ti is 1.49-0.68=0.81 nm. For several layered hosts, the incorporation of a PEO bilayer has been shown to result

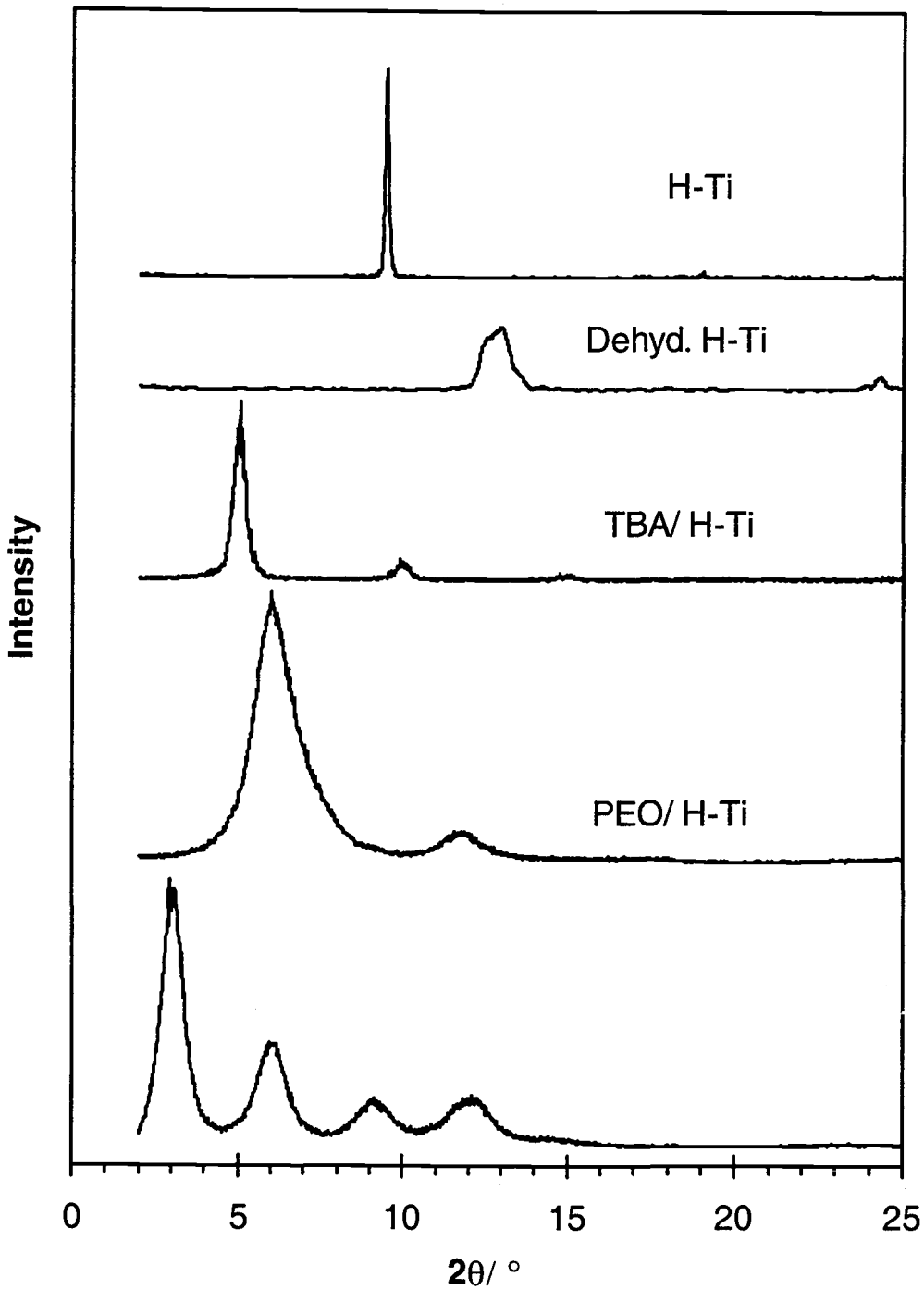

Figure 3.1 Powder X-ray diffraction patterns from samples.

Table 3.2 Basal repeat and stacking domain lengths for H-Ti, TBA/H-Ti, PEO/H-Ti, and PVP/H-Ti from powder XRD data.

sample	basal repeat / nm	stacking domain length* / nm
H-Ti	0.93	80
TBA/H-Ti	1.75	20
PEO/H-Ti	1.49	6
PVP/H-Ti	2.88	8

* determined using the Scherrer relation [50]

in gallery dimensions of 0.8-0.9 nm.[9,18,24] A simple bilayer scheme for the PEO/H-Ti structure with PEO bilayer is presented in Figure 3.2. PVP/H-Ti has a polymer gallery dimension of approximately 2.2 nm. With such a large dimension and limited structural information, the polymer arrangement cannot be deduced in this case. Wang, et. al. reported an expansion of 3.2 nm for PVP incorporated between MoO_3 layers,[16] and 2.3 nm for PVP galleries within $RuCl_3$ layers.[26] Kathleen, et. al. reported an expansion of 0.39-1.33 nm depending on the amount of PVP incorporated into PVP/hectorite nanocomposites.[10] Other studies [12,13] showed expanions of 1.34 and 1.38 nm for PVP incorporated into mica and montmorillonite.

SEM images of particle microstructures for H-Ti, PEO/H-Ti, and PVP/H-Ti are shown in Figure 3.3. The H-Ti has a platy morphology with platelet diameters of 0.1-1 μm. PEO/H-Ti and PVP/H-Ti consist of much larger aggregates, with particle diameters in the range of 10-100 μm. The formation of a gel and subsequent drying process appears to generate these larger particles.

The presence of PEO and PVP in the nanocomposites was confirmed by FTIR. Spectra from H-Ti, TBA/H-Ti, PEO/H-Ti, PVP/H-Ti, as well as the starting polymers are shown in Figure 3.4, and a summary of peak positions and assignments is provided in Table 3.3. H-Ti has a broad peak with a maximum at 3425 cm^{-1}, with a shoulder at 3220 cm^{-1}. The broad peak can be ascribed to an O-H stretching vibration either for H_2O (or H_3O^+) that is strongly associated with the layer surface; the peak position for H_2O without strong hydrogen bonding should

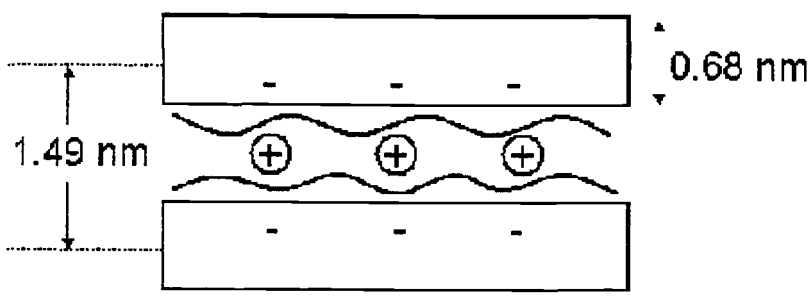

Figure 3.2 Structure scheme for PEO/H-Ti.

(a)

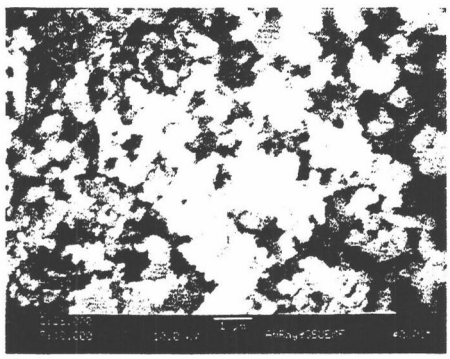

(b)

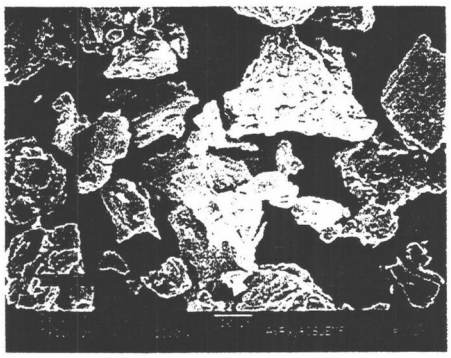

(c)

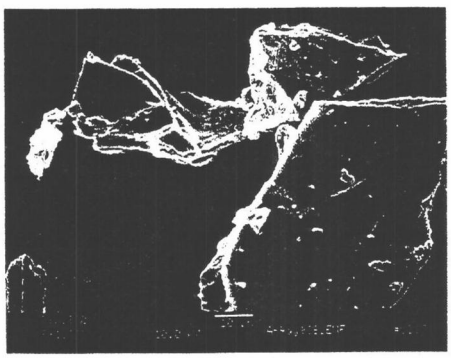

Figure 3.3 SEM images of (a) H-Ti, (b) PEO/H-Ti, and (c) PVP/H-Ti.

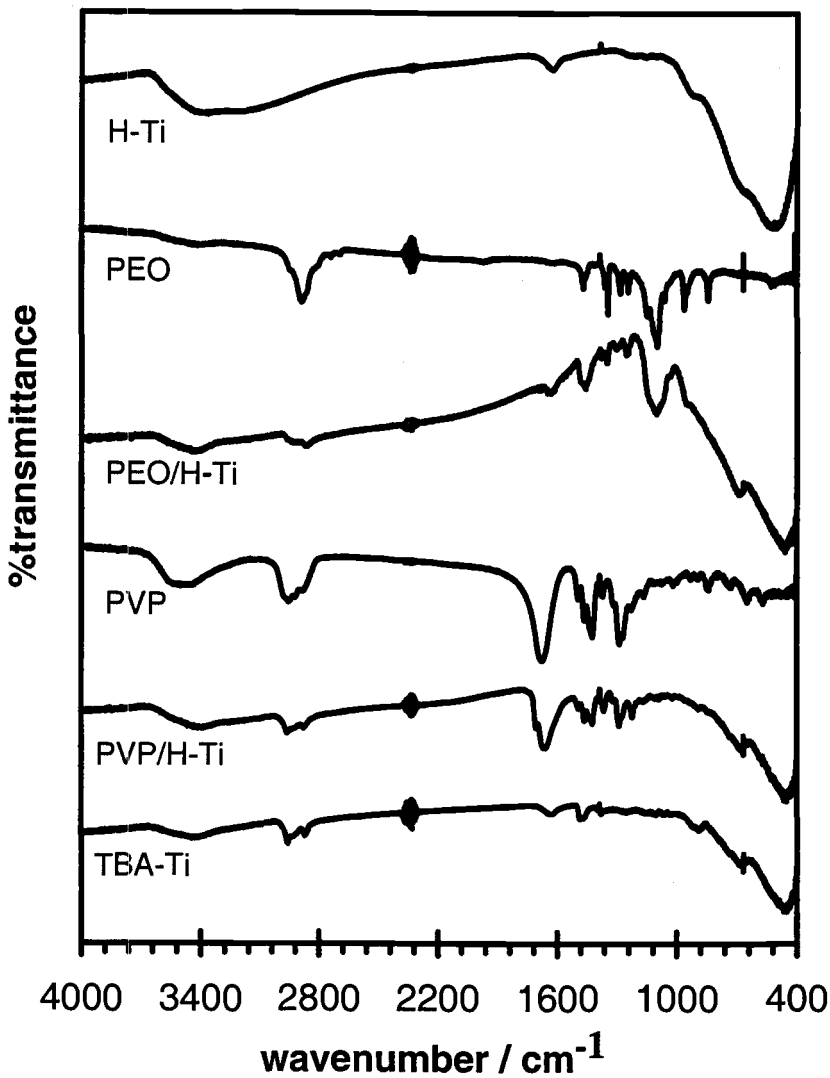

Figure 3.4 FTIR spectra for powder samples in KBr pellets. Peak positions are summarized in Table 3.3.

Table 3.3 FTIR peak positions and assignments for H-Ti, PEO/H-Ti, PVP/H-Ti, and starting polymers (s=strong, w=weak, b=broad, h=shoulder).

H-Ti	PEO *	PEO/ H-Ti	PVP *	PVP/ H-Ti	TBA/ H-Ti	assignment
3423 bs	3421 b	3437 b	3512 b	3419 b	3455 b	O-H str
3217 bs						
1628 b		1653 w			1654 bw	OH_2 bend
921 h					902 bw	Ti=O str
676 h		693 h		684 b	693 b	
535 bs		447 bs		466 bs	485 bs	Ti-O str
	2950 h	2942 b	2955 b	2965	2962	C-H str
			2939 h			"
	2888 s	2873	2896 h	2880 w	2878 w	"
			1495	1494 w	1488 w	CH_2 bend
	1472	1457	1463	1463	1468 w	"
			1423 s	1424		CH_2 def
	1342	1350 w	1375	1365		"
	1296	1306 w				C-C str
	1227	1254 w	1250 h	1225		"
	1104 s	1111 s				C-O str
		1049 w				
	963					C-C str
	843		849			"
	529 bw					
			1683 s	1675 s		C=O str
			1289 s	1289		C-N str
			1168 w		1156 w	
			739 w			
			651			
			572			

* PEO assignments from ref [51], PVP assignments from ref [52,53]

lie above 3600 cm^{-1}.[54] The shoulder at 3220 cm^{-1} can be ascribed to an overtone of the H_2O bending mode at about 1630 cm^{-1}. In TBA/H-Ti, PEO/H-Ti, and PVP/H-Ti, the broad O-H peak appears at reduced intensity, indicating a decreased water content in the solid. The O-H peak positions for these three samples (at 3455, 3437, 3512 cm^{-1}, respectively) indicate strong water association with the layer surfaces.

H-Ti has a strong, broad vibration at 535 cm^{-1}, which shifts to lower wavenumbers in TBA/H-Ti, PEO/H-Ti, and PVP/H-Ti. This absorption peak can be ascribed to the Ti-O (bridging) vibration, which gives rise to a strong broad peak centered around 600 cm^{-1} in anatase TiO_2. The shifted position for this vibration may be related to a decrease in hydrogen-bonding at the titanate surface as a result of the gallery expansion after intercalation of TBA, PEO, or PVP. The Ti=O (apical) stretching mode is tentatively assigned to the shoulder observed near 920 cm^{-1}. For comparison, this mode occurs near 1000 cm^{-1} in layered vanadates.[55] The mode is not clearly seen in the nanocomposites prepared.

The FTIR spectrum for PEO/H-Ti exhibits the CH_2 stretching, bending, and other deformation modes present in PEO at 2942, 2987, 1457, and 1350 cm^{-1}. The shifted peak positions relative to those for the neat polymer could suggest a more anisotropic conformation for the PEO intercalate,[26,56] although the greater peak widths and lower peak intensities in the nanocomposites probably do not support any detailed analysis in this case. A strong absorption due to the C-O stretching vibration is observed at 1111 cm^{-1} in PEO/H-Ti. PVP/H-Ti shows absorbances

from alkyl groups, as well as prominent carbonyl and C-N stretching vibrations at 1675 and 1289 cm^{-1}. These peaks are at similar positions to those for PVP itself.

Figure 3.5 and Table 3.4 present the TGA and DSC traces and data for the solid products obtained. In agreement with previous results,[40] H-Ti loses approximately 10 wt% from ambient to 120°C, and a further 5 wt% after heating to high temperature. The losses correspond to endothermic and slightly exothermic events, respectively, and have been ascribed to loss of intercalate water (with retention of a protonated layer structure), followed by water loss (with sheet degradation) to form a disordered product. The disordered structure rearranges to form anatase above 450°C. The thermal degradation is summarized by the following reaction steps:

$$H_xTi_{2-x/4}\square_{x/4}O_4 \cdot yH_2O \rightarrow H_xTi_{2-x/4}\square_{x/4}O_4 + y\,H_2O \quad (1a)$$

$$H_xTi_{2-x/4}\square_{x/4}O_4 \rightarrow (2-x/4)\,TiO_2\ (amorphous) + x/2\,H_2O \quad (1b)$$

$$TiO_2\ (amorphous) \rightarrow TiO_2\ (anatase) \quad (1c)$$

The mass losses provide an approximate composition of $H_{0.6}Ti_{1.85}O_4 \cdot 1.03H_2O$, which indicates a intercalate water monolayer, and a proton content similar to that expected.

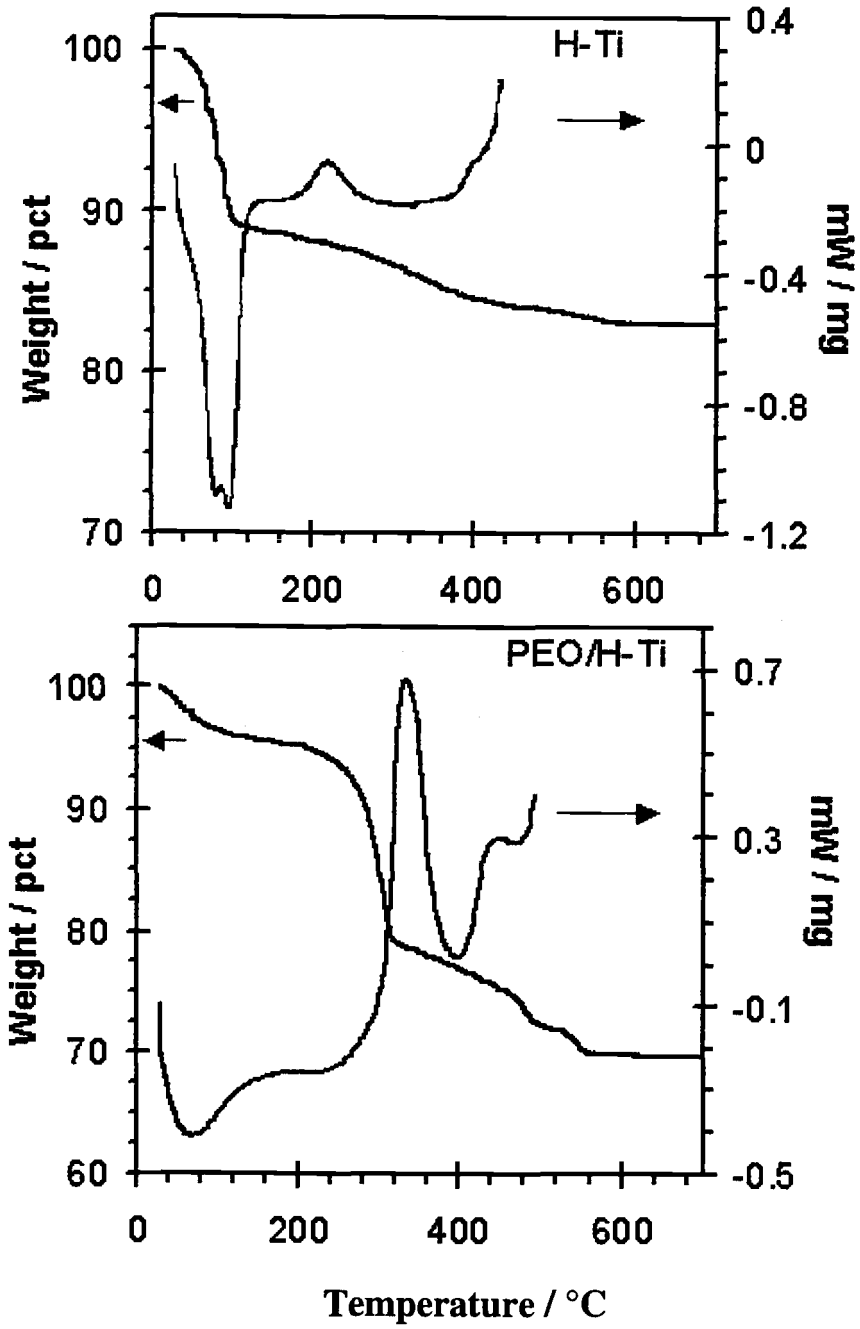

Figure 3.5 TGA and DSC traces obtained at 10°C/min under flowing N_2.

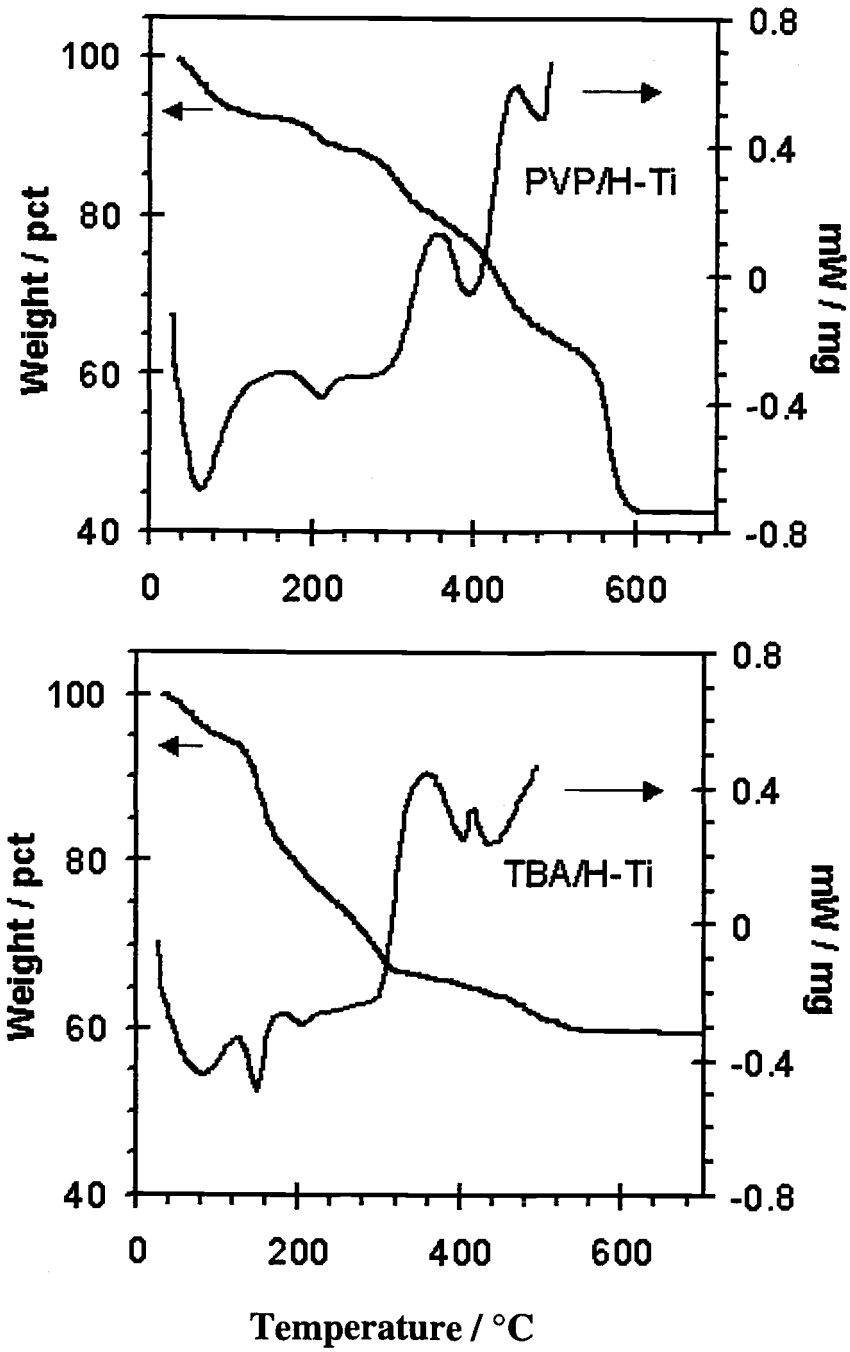

Figure 3.5 (continued) TGA and DSC traces obtained at 10°C/min under flowing N_2.

Table 3.4 Thermal analysis data for H-Ti, PEO/H-Ti, PVP/H-Ti, and TBA/H-Ti.

	Temp / °C	Mass Loss / pct	DSC peak
H-Ti	40-120	10.8	endo, vs
	160-400	3.9	exo, m (160-
300°C)			
			exo, m (350-
400°C)			
	400-600	1.5	exo, s
PEO/H-Ti	30-150	4.4	endo, m
	220-320	15.7	exo, vs (220-
400°C)			
	400-470	4.7	exo, m
	500-570	2.2	exo
PVP/H-Ti	30-160	7.4	endo, s
	175-240	3.5	endo, w
	270-400	7.1	exo, s
	400-485	15.8	exo, vs
	540-610	19.4	exo
TBA/H-Ti	30-130	6.0	endo, s
	130-180	12.1	endo, m
	185-230	4.8	endo, w
	230-320	9.6	exo, vs (230-
405°C)			
	330-440	2.5	exo, w (405-
440°C)			
	440-560	4.5	exo

PEO/H-Ti shows an endothermic loss of approximately 4 wt% below 120°C, again ascribed to intercalate water loss. A strong exotherm and mass loss from 220-320°C is ascribed predominantly to polymer decomposition, although the titania sheets may also degrade in this temperature range. The sum of polymer and water contents determined by elemental analyses is 38 wt% (see below), which is somewhat larger than that obtained by gravimetry to 900°C (31 wt%).

The TGA trace for H-Ti/PVP is similar to that reported for the TiO_2/PVP nanocomposite prepared by Zheng et al.[38] Losses below 250°C can be ascribed to intercalate water loss. Above 250°C, a complex series of exothermic degradation steps ensues. For comparison, decomposition of pure PVP begins about 340°C. The total weight loss to 900°C (58 wt%) is consistent with the sum of TBA, polymer, and water contents determined by elemental analyses (54 wt%).

Elemental (C/H/N/Ti) analyses are indicated in Table 3.5 and give compositions of $H_{0.7}Ti_{1.83}O_4(C_2H_4O)_{1.54}(H_2O)_{1.28}$ for PEO/H-Ti and $H_{0.7}Ti_{1.83}O_4(C_{16}H_{36}N)_{0.05}(C_6H_9NO)_{1.22}(H_2O)_{0.92}$ for PVP/H-Ti. The TBA contents in the polymer-containing samples were very low compared with that for TBA/H-Ti, which contains 31 wt% TBA. The XRD data indicate that no TBA/H-Ti phase is present, and these analytical results further indicate that little TBA is present in the polymer-occupied galleries. The intercalated water content indicates that the water/proton mole ratio increases only a small amount relative to that in H-Ti, so that most of the intercalated water could be associated with intercalate protons to make hydronium cations, as is the case in H-Ti.

Table 3.5 Compositional analyses for H-Ti, PEO/H-Ti, PVP/H-Ti, and TBA/H-Ti.

Sample		Wt Pct							
		C	H	N	Ti	TBA	Polymer	H_2O	Empirical Formula
PEO/H-Ti	obs	15.32	3.09	0.71	35.88				
	calc	15.86	4.01	0.06	35.60	1.0	27.6	9.4	$H_{0.7}Ti_{1.83}O_4(C_{16}H_{36}N)_{0.01}(C_2H_4O)_{1.54}(H_2O)_{1.28}$
PVP/H-Ti	obs	30.82	4.80	5.59	27.67				
	calc	30.77	4.86	5.63	27.65	3.6	43.0	5.2	$H_{0.7}Ti_{1.83}O_4(C_{16}H_{36}N)_{0.05}(C_6H_9NO)_{1.22}(H_2O)_{0.92}$
TBA/H-Ti*	obs	24.5	5.1	1.6	36.5				
	calc	24.3	5.5	1.8	36.8	30.6	-	5.3	$H_{0.7}Ti_{1.83}O_4(C_{16}H_{36}N)_{0.3}(H_2O)_{0.7}$

* data from ref [41]

3.5 CONCLUSION

PEO and PVP/titanate layered nancomposites can be prepared by (1) exfoliating layered titanates in aqueous TBA solutions, and (2) acidifying to form a gel. Structural characterization indicates that the PEO nanocomposites have polymer bilayers within titanate galleries. FTIR and thermal analyses indicate a reduced TBA and water content relative to the intercalation compounds formed without polymer.

3.6 ACKNOWLEDGMENT

The authors gratefully acknowledge support from NSF grant DMR-9900390 and helpful advice from Dr. Takayoshi Sasaki at NIRIM and Dr. Christopher Oriakhi at Hewlett-Packard. NS acknowledges support from the Royal Thai Government.

3.7 REFERENCES

1. Lerf, A. Intercalation Compounds in Layered Host Lattices: Supramolecular Chemistry in Nanodimensions. In *Handbook of Nanostructured Materials and Nanotechnology, Vol. 5*; Nalwa, H., Ed.; Acad. Press: New York, 2000; pp 1-166.

2. LeBaron, P.; Wang, Z.; Pinnavaia, T. *Appl. Clay Sci.* **1999**, *15*, 11.

3. Sanchez, C.; Ribot, F.; Lebeau, B. *J. Mater. Chem.* **1999**, *9*, 35.

4. Lerner, M.; Oriakhi, C. Polymers in Ordered Nanocomposites. In *Handbook of Nanophase Materials*, Goldstein, A., Ed.; Marcel Dekker: New York, 1997; pp 199-219.

5. Gianellis, E.P. *Adv. Mater.* **1996**, *8*, 29.

6. Oriakhi, C. *J. Chem. Ed.* **2000**, *77*, 1138.

7. Bujdak, J.; Hackett, E.; Giannelis, E.P. *Chem. Mater.* **2000**, *12(8)*, 2168.

8. Aranda, P.; Ruiz-Hitzky, E. *Appl. Clay. Sci.* **1999**, *15*, 119.

9. Lemmon, J.P.; Wu, J.; Oriakhi, C.O.; Lerner, M.M. *Electrochim. Acta* **1995**, *13/14*, 2245.

10. Carrado, K.A.; Xu, L. *Chem. Mater.* **1998**, *10(5)*, 1440.

11. Hild, A.; Séquaris J.-H.; Narres H.-D.; Schwuger, M. *Colloids surf. A: Physicochem. Eng. Aspects* **1997**, *123-124*, pp 515-522.

12. Ogawa, M.; Inagaki, M.; Kodama, N.; Kuroda, K.; Kato, C. *J. Phys. Chem.* **1993**, *97*, pp 3819-3823.

13. Miyata, H.; Sugahara, Y.; Kuroda, K.; Kato, C. *J. Chem. Soc., Faraday Trans. I* **1987**, *83*, pp 1851-1858.

14. Sukpirom, N.; Oriakhi, C.O.; Lerner, M.M. *Mater. Res. Bull.* **2000**, *3*, 325.

15. Kerr, T. A.; Wu, H.; Nazar, L. F. *Chem. Mater.* **1996**, *8*, 2005.

16. Wang, L.; Schindler, J.; Kannewurf, C.R.; Kanatzidis, M.G. *J. Mater. Chem.* **1997**, *7(7)*, 1277.

17. Nazar, L. F.; Wu, H.; Power, W. P. *J. Mater. Chem.* **1995**, *5*, pp 1985-93.

18. Liu, Y.-J.; Schindler, J.L.; DeGroot, D.C.; Kannewurf, C.R.; Hirpo, W.; Kanatzidis, M.G. *Chem. Mater.* **1996**, *8(2)*, 525.

19. Oriakhi, C.O.; Nafshun, R.L.; Lerner, M.M. *Mater. Res. Bull.* **1996**, *12*, 1513.

20. Gonzalez, G.; Santa Ana, M.A.; Benavente, E. *J. Phys. Chem. Solids* **1997**, *58*, 1457.

21. Bissessur, R.; Kanatzidis, M. G.; Schindler, J. L.; Kannewurf, C. R. *J. Chem. Soc., Chem. Commun.* **1993**, pp 1582-1585.

22. Tsai, H.-L.; Schindler, J.L.; Kannewurf, C.R.; Kanatzidis, M.G. *Chem. Mater.* **1997**, *9(4)*, 875.

23. Yang, D.; Frindt, R.F. *J. Mater. Res.* **2000**, *11*, 2408.

24. Oriakhi, C.O.; Lerner, M. *Chem. Mater.* **1996**, *8*, 2016.

25. Jeevanandam, P.; Vasudevan, S. *Chem. Mater.* **1998**, *10*, pp 1276-1285.

26. Wang, L.; Rocci-Lane, M.; Brazis, P.; Kannewurf, C.R.; Kim, Y. I.; Lee, W.; Choy, J.H.; Kanatzidis, M.G. *J. Am. Chem. Soc.* **2000**, *28*, 6629.

27. Matsuo, Y.; Tahara, K.; Sugie, Y. *Carbon* **1997**, *1*, 113.

28. Matsuo, Y.; Tahara, K.; Sugie, Y. *Carbon* **1996**, *5*, 672.

29. Kojima, Y.; Usuki, A.; Kawasumi, M.; Okada, A.; Fukushima, Y.; Kurauchi, T.; Kamigaito, O. *J. Mater. Res.* **1993**, *8*, 1185.

30. Fischer, H.R.; Gielgens, L.H.; Koster, T.P.M. *Acta Polym.* **1999**, *50*, 122.

31. Manolis, L. A Little Goes A Long Way. *Plastics Technol.* **1999**, *45(6)*, pp 52-57.

32. Lan, T.; Kaviratna, P.D.; Pinnavaia, T.J. *Chem. Mater.* **1994**, *6*, 573.

33. Gilman, J.W. *Appl. Clay Sci.* **1999**, *15*, 31.

34. Serpone, N.; Lawless, D.; Khairutdinov, R.; Pelizzetti, Ezio *J. Phys. Chem.* **1995**, *99*, 16655.

35. Kocher, M.; Daubler, T. K.; Harth, E.; Scherf, U.; Gugel, A.; Neher, D. *Appl. Phys. Lett.* **1998**, *72(6)*, 650.

36. Sasaki, T.; Watanabe, M. *J. Phys. Chem. B* **1997**, *101*, 10159.

37. Yoshida, M.; Lal, M.; Kumar, N. Deepak; Prasad, P.N *J. Mater. Sci.* **1997**, *32(15)*, 4047.

38. Zheng, M.-P.; Jin, Y.-P.; Jin, G.-L.; Gu, M.-Y. *J. Mater. Sci. Lett.* **2000**, *19*, 433.

39. Hervieu, M.; Raveau, B. *Rev. Chim. Miner.* **1981**, *18*, 642.

40. Sasaki, T.; Watanabe, M. Michiue, Y.; Komatsu, Y.; Izumi, F.; Takenouchi, S. *Chem. Mater.* **1995**, *7*, 1001.

41. Sasaki, T.; Nakano, S.; Yamauchi, S.; Watanabe, M. *Chem. Mater.* **1997**, *9*, 602.

42. Sasaki, T.; Watanabe, M.; Hashizume, H.; Yamada, H.; Nakazawa, H. *J. Am. Chem. Soc.* **1996**, *118*, 8329.

43. Sasaki, T.; Watanabe, M. *Mol. Cryst. Liq. Cryst.* **1998**, *311*, 417.

44. Sasaki, T.; Watanabe, M. *J. Am. Chem. Soc.* **1998**, *120*, 4682.

45. Sasaki, T.; Kooli, F.; Iida, M.; Michiue, Y.; Takenouchi, S.; Yajima, Y.; Izumi, F.; Chakoumakos, B.C.; Watanabe, M. *Chem. Mater.* **1998**, *10*, 4123.

46. Sasaki, T.; Ebina, Y.; Watanabe, M.; Decher, G. *Chem. Commun.* **2000**, 2163.

47. Grey, I.E.; Li, C.; Madsen, I.C.; Watts, J.A. *J. Sol. St. Chem.* **1987**, *66*, 7.

48. Sukpirom, N.; Lerner, M. *Mater. Chem. Eng., A* **2001**, in press.

49. Frank, H.P. *J. Poly. Sci.* **1954**, *12*, 565.

50. Cullity, B.D. *Elements of X-ray Diffraction, 2nd Ed.*; Addison-Wesley: Reading, MA, 1978.

51. Yoshihara, T.; Tadokoro, H.; Murahashi, S. *J. Chem. Phys.* **1964**, *41*, 2902.

52. The Infrared Spectra Atlas of Monomers and Polymers; Sadler Research Laboratories, 1980.

53. Cohen Stuart, M.A.; Fleer, G.J.; Bijsterbosch, B.H. *J. Coll. Interface Sci.* **1982**, *90(2)*, 321.

54. The Infrared Spectra of Minerals; Farmer, V.C., Ed.; Mineralogical Society: London, 1974.

55. Huguenin, F.; Gambardella, M.; Torresi, R.; Torresi, S.; Butty, D. *J. Electrochem. Soc.* **2000**, *147*, 2437.

56. Montarges, E.; Michot, L.J.; Lhote, F.; Frabien, T.; Villieras, F. *Clays Clay Miner.* **1995**, *43(4)*, 417.

CHAPTER 4

RAPID EXFOLIATION OF A LAYERED TITANATE BY ULTRASONIC PROCESSING

Nipaka Sukpirom and Michael M. Lerner

Department of Chemistry and Center for Advanced Materials Research,

Oregon State University,

Corvallis, OR 97331-4003, USA

Mater. Chem. Eng., A, **2001**, in press.

4.1 ABSTRACT

The application of ultrasound dramatically increases the rate of exfoliation of $H_xTi_{2-x/4}O_4 \cdot yH_2O$ (H-Ti) in the presence of aqueous tetrabutylammonium (TBA) hydroxide. The effect of ultrasonication power and processing time on particle size distributions are evaluated. Applied powers of 60-300 W and reaction times of 2-30 minutes effectively reduce the H-Ti particle size to <100 nm. Both particle size distribution analysis and UV/VIS spectroscopy were used to study the effect of ratio of TBA ion to exchangeable protons in H-Ti; a minimum ratio of TBA/H≥0.5 is required for rapid exfoliation.

4.2 INTRODUCTION

Following initial studies on layered titanates of composition $A_xTi_{2-x/4}\square_{x/4}O_4.H_2O$ (A=Li-Cs or H, x=0.67–0.73, □=Ti vacancy) with a lepidocrocite-like structure,[1] Sasaki and coworkers have reported the swelling and subsequent exfoliation of $H_xTi_{2-x/4}O_4 \cdot yH_2O$ (x=0.7, y≈1), abbreviated as H-Ti, in aqueous tetrabutylammonium (TBA) hydroxide.[2-7] When the mole ratio of TBA to exchangeable protons in H-Ti (abbreviated as TBA/H) exceeds 0.5, a stable colloidal form can be obtained after shaking the suspension for 1-2 weeks.[3,7] These stable colloids have been shown by optical[2] and structural[4,7] methods to be comprised primarily of titania sheets individually suspended in the aqueous solution. The most favorable reaction conditions employed a high ratio with TBA/H≥5.[3,6]

Exfoliated titania suspensions have been used as precursors to new titania meso-, micro- and nanostructures. Sasaki and coworkers have prepared multilayer thin films of titania nanosheets using sequential layer-by-layer self-assembly of poly(dimethyldiallyl ammonium chloride) and titania nanolayers.[9] In another study, thin (20-30 nm) flakes of TiO_2 were obtained by freeze-drying and subsequent thermal processing of suspensions.[3] A mesoporous alumina-pillared titanate, with a large basal spacing of 2.6 nm, was produced by the direct reaction of a titania suspension with a solution containing polyoxoaluminum cations.[8] Our group has studied the preparation of layered nanocomposites with poly(ethylene

oxide) or poly(vinylpyrrolidine) incorporated between titania sheets.[10] These lamellar structures are an interesting addition to those derived from other inorganic layers such as aluminosilicate clays, and the low cost, environmental acceptability, chemical stability, and photochemical properties of titania suggest that useful materials may be obtained by this approach.

A considerable drawback to the above synthetic approach lies in the process required for exfoliation of the titania sheets, which requires a relatively long time, a low solids content, and a high TBA concentration. These factors make the approach seem unfavorable for large-scale reactions and the production of low-cost materials. In this report, we describe the application of ultrasound to facilitate the production of exfoliated titania suspensions. The effects of time, power, and TBA/H ratios are investigated.

4.3 EXPERIMENTAL

4.3.1 Materials

Tetrabutylammonium hydroxide (Aldrich, 40% in water), TiO_2 (Aldrich, anatase form, 99.9+%), and Cs_2CO_3 (Aldrich, 99.9%) were used as received. $Cs_xTi_{2-x/4}O_4 \cdot yH_2O$ (Cs-Ti) was prepared according to a literature method.[11] Anatase TiO_2 (4.23 g) and Cs_2CO_3 (3.26 g) were ground together and heated briefly at 800°C in an alumina crucible to eliminate CO_2. The mixture was reground and

reheated twice at 800°C for 20 h. The proton-exchanged material, $H_xTi_{2-x/4}O_4 \cdot yH_2O$ (x=0.7, y≈1), abbreviated as H-Ti, was prepared by stirring Cs-Ti powder (1.0 g) in 1M HCl (100 ml) for 48 h, with the solution refreshed after 24 h. Powder X-ray diffraction (XRD) indicated that the proton exchange reaction was complete, and XRD patterns obtained for both Cs-Ti and H-Ti matched those described previously.[1,7]

4.3.2 Ultrasonic processing and characterization

H-Ti (0.25 g) was added to an aqueous solution of tetrabutylammonium (TBA) hydroxide in a 100 ml glass bottle, and then exposed to 20 kHz ultrasound using a GE600 ultrasonic processor with a 13 mm diameter Ti alloy probe. The sample volume was 50 mL for all reactions. The ultrasound power supplied, reaction time, and the mole ratio of TBA to exchangeable protons in H-Ti (TBA/H) were varied as described in the text. For longer sonication times or higher powers, the reaction vessel was placed in an ice bath to maintain the suspension temperature below 40°C.

Sample labels indicate the processing conditions as follows: Ti-180-20-1 refers to a sample exposed to 180 W ultrasound for 20 minutes with TBA/H=1. As controls, aqueous suspensions of H-Ti were also evaluated without ultrasonic

processing. For example, sample Ti-0-0-0 was added to de-ionized water without further processing, and Ti-0-3wk-0.5 was stirred for 3 weeks at a TBA/H=0.5.

Particle size distributions in the suspensions were obtained immediately following ultrasound processing with a Horiba CAPA-700 PDA . The particle size analysis is based on centrifugation followed by light absorption measurements, and has a minimum size discrimination of 100 nm. Particle sizes were determined using the sedimentation time and Stokes' equation:[12]

$$D = 18\,\eta_0 \ln(x_2/x_1) \;/\; (\rho - \rho_0)\omega^2 t \qquad (1)$$

where D is the particle diameter (cm), η_0 is the viscosity coefficient of the dispersion medium (P), x_1 and x_2 are the center of rotation to sedimentation plane and center of rotation to measuring plane distances (cm), ρ and ρ_0 are sample and dispersion medium densities (g/cm^3), ω is the rotational angular velocity (rad/s), and t is the sedimentation time (s). Equation (1) assumes spherical particles, and for platy particles with large aspect ratios:

$$D = (1.178\, w\, t)^{1/2} \qquad (2)$$

where w is the platelet width and t is the platelet thickness.[12]

The distribution at each size range was evaluated by light absorbance as:[13]

$$\log I_0 - \log I_i = K \sum_{i=1}^{n} k N_i D_i^2 \qquad (3)$$

where I_0 and I_i are incident and transmitted light intensities, K is the cell optical constant, k is the particle absorption coefficient (assumed invariant to particle dimension), N is the particle population, and D is the particle diameter.

Suspensions were diluted 1:10 in de-ionized water and analyzed using a Hewlett-Packard 8425A diode array UV/VIS spectrophotometer directly following sonication (delay time <10 min) and again after standing for 24 h. Powder X-ray diffraction (XRD) samples were obtained by casting films onto a glass substrate and air-drying for 24 h, data were obtained using a Siemens D5000 diffractometer with CuK_α radiation (1.5418 Å) from 2-60 °2θ in 0.02° steps.

4.4 RESULTS AND DISCUSSION

The effect of the applied ultrasound power was investigated first. The power applied is an important consideration - higher powers might lead to more rapid exfoliation, but also tend to heat the suspensions locally and cause structural changes other than exfoliation.

The particle size distributions for samples sonicated at 30–300 W for 30 min with TBA/H=1 are shown in Figure 4.1. As prepared, the H-Ti powder is comprised of aggregates containing 1-2 μm particles;[3,10] when a control sample (Ti-0-0-0) is dispersed into distilled water with no processing 60% of particles are in this size range, with no measurable content below 0.1 μm. All the sonicated samples in the series show a dramatic reduction in the 1-2 μm particle size content, to 0-6%, with the predominant particle size becoming <0.1 μm. These results indicate that ultrasound is effective at reducing the H-Ti particle sizes, although the resolution limitation of the centrifugation method does not directly show whether individual titania sheets are formed in the colloids. After low power sonication, Ti-30-30-1 also shows a significant component of particles larger than 3 μm. It may be that the TBA, aside from intercalating into the titania structure, also causes some initial particle aggregation. No evidence for such aggregates is seen following sonication at higher powers.

Sonication at 120 W was effective for particle size reduction, and did not present difficulty in maintaining low suspension temperatures at longer processing times, and was therefore chosen for further experiments. With TBA/H fixed at 1, the processing time was varied from 2-30 minutes. The results displayed in Figure 4.2 show that all samples gave similar size distributions under these conditions, with the largest content <0.1 μm in each case. For comparison, a distribution is also shown for a sample obtained after stirring for 3 weeks with TBA/H=5. At the longest processing time, sample Ti-120-30-1 contains a small component of 1-6 μm

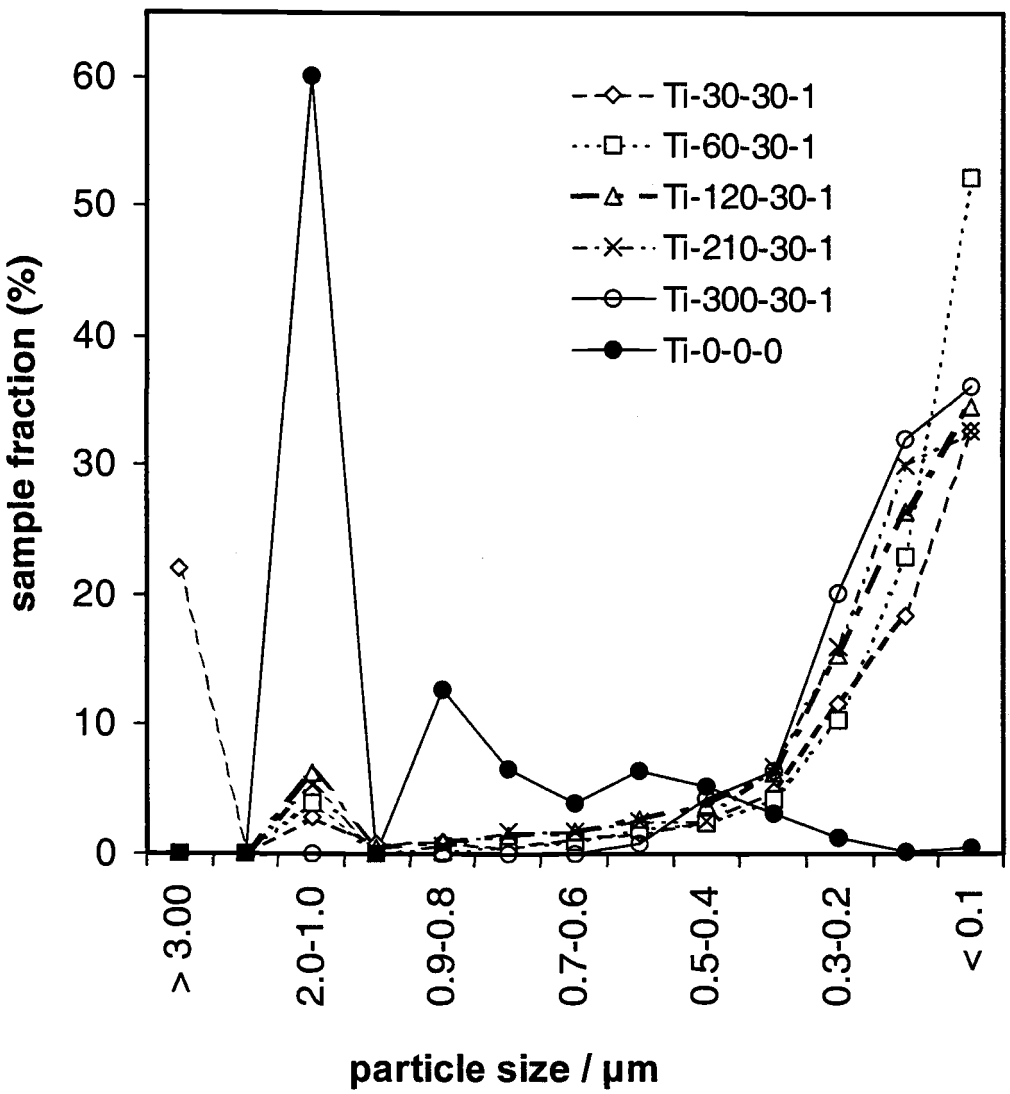

Figure 4.1 Particle size distributions for samples processed for 30, 60, 120, 210 and 300 W for 30 minutes with TBA/H=1, and for H-Ti dispersed in distilled water without sonication (sample Ti-0-0-0).

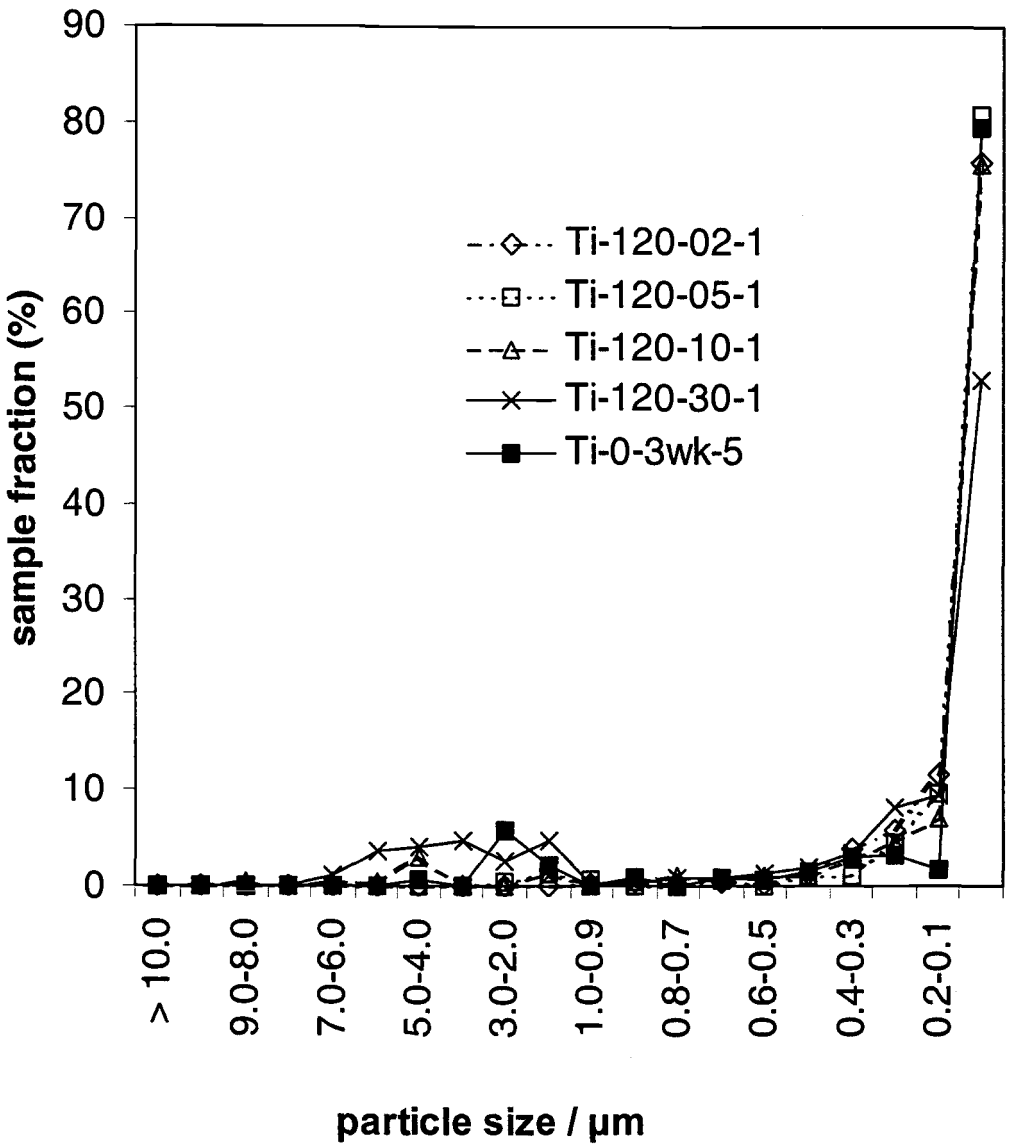

Figure 4.2 Particle size distributions for samples processed for 2, 5, 10 and 30 minutes at 120 W with TBA/H = 1 and for a sample with TBA/H=5 stirred for 3 weeks without sonication (Ti-0-3 wks-5).

particles. The nature of these reaggregates will be discussed below. From the power and time studies, it is clear that particle size reduction can be rapidly achieved using ultrasound, but careful control over both processing power and time may be required to optimize the sample dispersion.

One concern is that sonication could degrade the titanate layer structure to form TiO_2 or other phases. This could potentially explain the larger particle size components observed in some suspensions. In order to investigate whether crystalline degradation products are present, powder XRD of air-dried samples were obtained on a series of products obtained by processing at 120 W for 2-120 minutes with TBA/H=1. Due to preferred orientation of the cast films, the XRD patterns obtained show only a series of 10 or more basal (*0k0*) reflections. These are all readily indexed according to a basal-repeat distance of the layered TBA-intercalated phase of 1.73 nm. This distance agrees well with that obtained previously and indicates the presence of both a TBA and water monolayer between titania sheets.[4-6] No other reflections are observed in any XRD patterns obtained in this manner. The domain sizes for the TBA-intercalated phases are indicated in Table 4.1. All the sonicated samples show smaller domain sizes than the sample stirred for three weeks.

Previous reports indicate that anatase TiO_2 is produced by thermolysis of TBA-intercalated phase. The strongest peak for oriented anatase is *(101)* and would appear at 25.3°2θ, which could be hidden beneath a strong (*050*) reflection from the TBA-intercalated phase at approx. 25°2θ.

Table 4.1 Basal repeat domain sizes for samples processed at 120 W and TBA/H=1 compared with stirred sample Ti-0-3wk-1.

sample	**domain size* / nm**
Ti-120-2-1	21
Ti-120-5-1	27
Ti-120-10-1	25
Ti-120-30-1	26
Ti-120-120-1	19
Ti-0-3wk-1	40

* domain sizes were determined using the Scherrer relation [16]

In order to eliminate the interference from the TBA-intercalated phase, dried thin-film samples were heated from 150-500°C for 1 h and the XRD patterns recollected. Figure 4.3 shows the patterns of Ti-120-10-1 following the heating at different temperatures. From 100-300°C, the layered titania structure is preserved but the sample loses intercalated water and the basal repeat dimension is reduced, with a corresponding shift in the *(0k0)* reflections to higher angle. The calculated basal repeat distances decrease to 1.46 nm (200°C), 1.08 nm (300°C), and 0.94 nm (400°C). The final value corresponds to the distance expected for the anhydrous form.[5] After heating to 400°C and above, the *(101)* anatase peak is evident in the patterns due to thermolysis of the intercalate structure. The associated shift in *(0k0)* reflections at 200°C can be used to eliminate the interference with the strongest anatase diffraction peak. All solid products processed at 120 W and TBA/H=1 were studied by XRD after heating to 200°C, and there was no evidence for anatase or any other crystalline phase content, even after sonication for 120 minutes. Comparing anatase samples with the XRD signal/noise resolution in this region indicates that the samples all contain <4% anatase content above 14 nm domain size. The reaggregated particles in some samples do not therefore appear to be associated with the formation of ordered phases.

Previous studies have determined that stable colloidal suspensions are not obtained by shaking when TBA/H<0.5.[4] Since the composition of the TBA-intercalated phase has TBA/H≈0.43, [3,6,10] below this ratio all TBA can be accommodated into the intercalate structure. At the lower reaction ratios, the

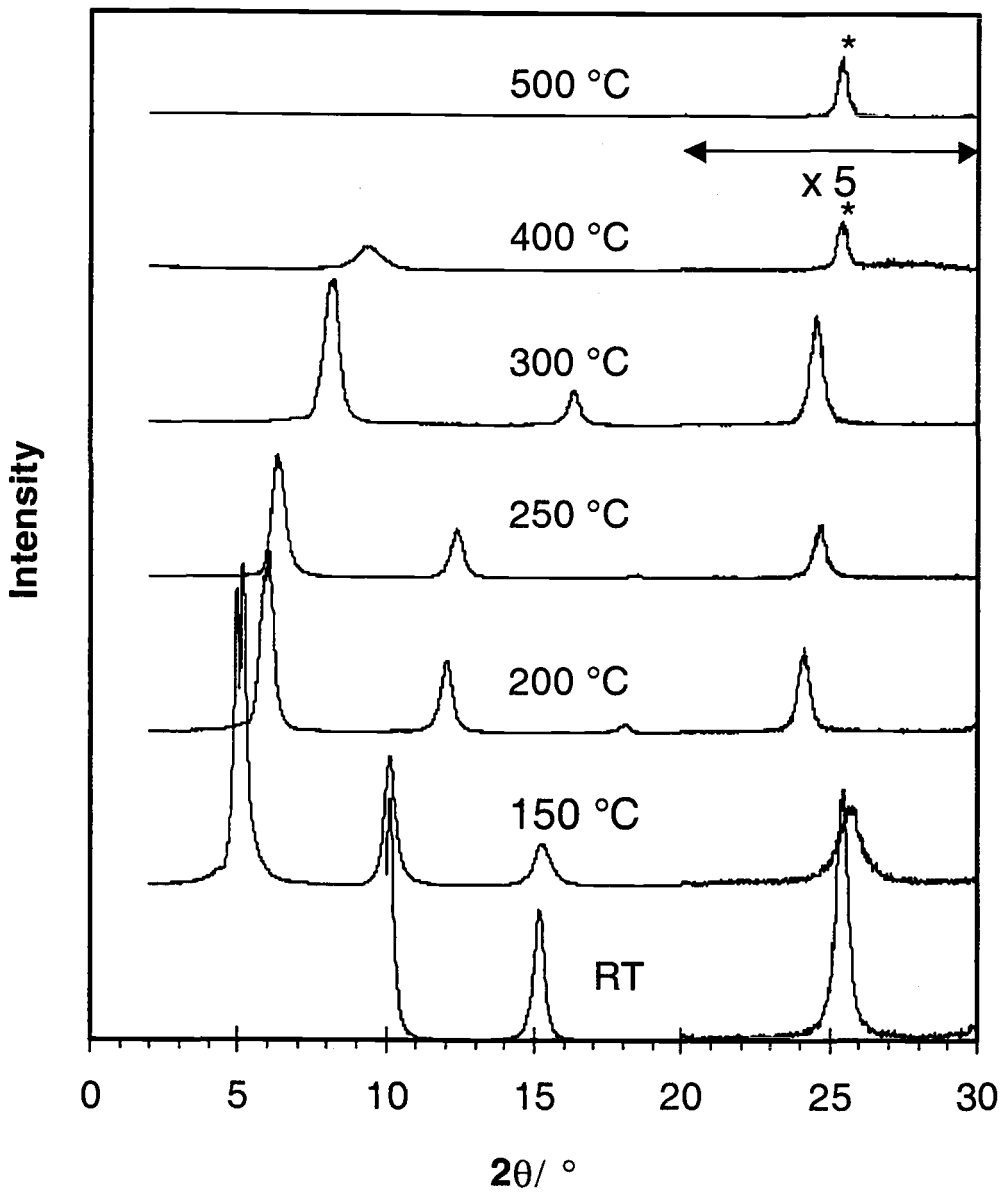

Figure 4.3 XRD patterns of Ti-120-10-1 at ambient temperature and after heating to 150-500°C for 1 h. Diffraction patterns intensities from 20-30°2θ are 5x. The asterisks indicate *(101)* anatase reflections.

solution concentration of TBA may be too low to stabilize the titania sheets. On the other hand, high TBA/H ratios, which are more effective in stabilizing the colloids, are problematic in further reaction steps (such as nanocomposite formation) and are also less likely to be practical for large-scale reactions.

In order to evaluate the effect of TBA/H ratios, samples were processed at 120 W for 30 minutes with TBA/H=0-1. Particle size distributions for three suspensions with TBA/H=0, 0.25, and 1 are shown in Figure 4.4. Without the addition of TBA, sample Ti-120-30-0 retains about 40% content of 1-2 μm particles. The lowest TBA concentration tested (in Ti-120-30-0.25) is effective at reducing particle dimensions, with the majority of particles reduced to 0.1-0.2 μm. The major size component for samples with TBA/H$\geq$0.5 is <0.1 μm.

In Figure 4.5, the sample fraction with particle size <0.1 μm, x_e, is plotted against TBA/H for several samples processed at 120 W for 30 minutes. The plot shows a steady with TBA/H ratio, with a break between TBA/H=0.25 and 0.5. This break may be related to the above discussion that the TBA-intercalated phase can accommodate up to TBA/H=0.4 within galleries. The presence of excess TBA in solution facilitates the particle size reduction under these conditions. For comparison, x_e is also indicated for samples stirred, but not sonicated, for 1 h with TBA/H=1 and for 3 weeks with TBA/H=5. The latter condition, although time consuming and requiring large quantities of TBA, produces the greatest particle size reduction.

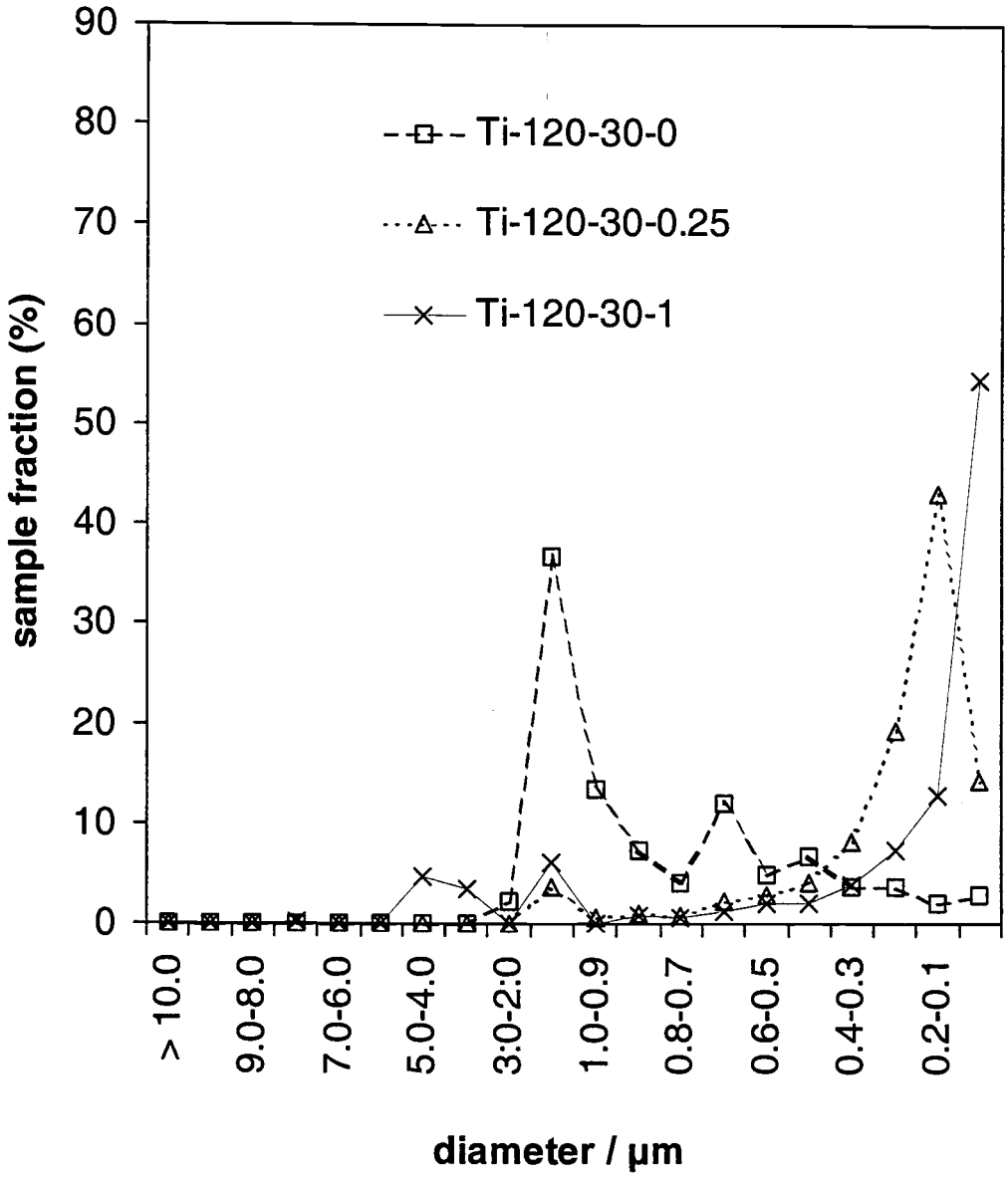

Figure 4.4 Particle size distributions for samples processed at 120 W for 30 minutes with TBA/H=0, 0.25 and 1.

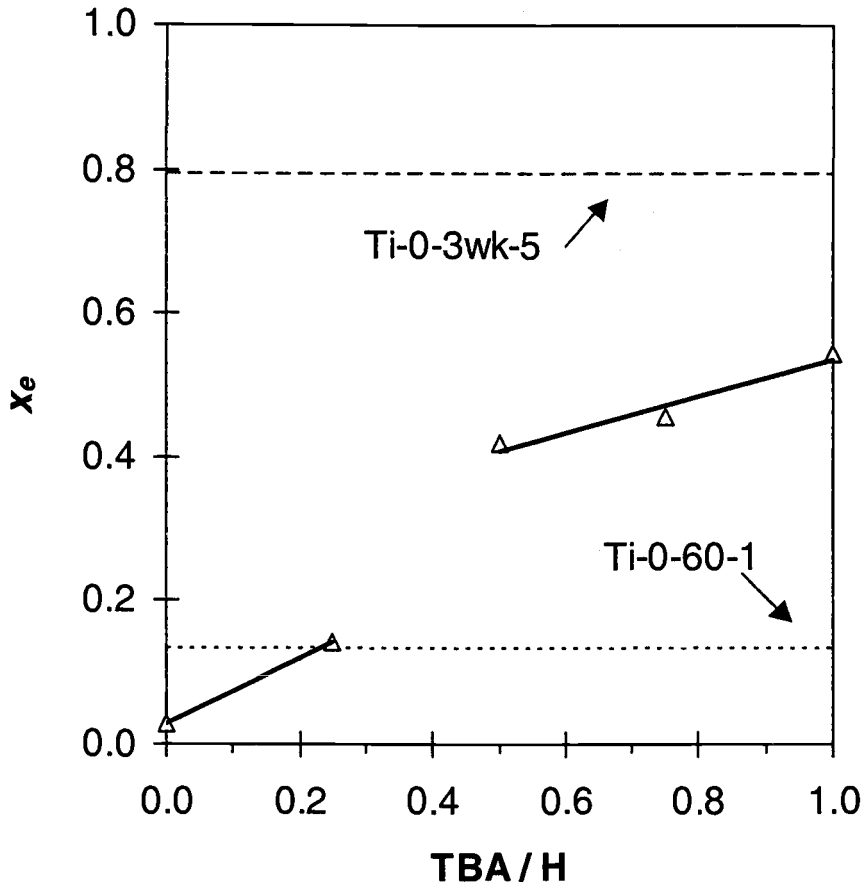

Figure 4.5 Reaction quotient, x_e, vs. TBA/H-Ti for samples processed at 120 W for 30 minutes. The dashed lines represent x_e for stirred samples Ti-0-3wk-5 and Ti-0-60-1.

The UV/VIS absorption spectra for samples Ti-0-0-0 (*Fig. 4.6a*) and Ti-120-30-0 (*Fig. 4.6b*) show a weak, very broad peak, and it is visually apparent that the large particles in these samples (predominantly 1-2 μm) are significantly sedimented from solution during the UV/VIS analysis. Analysis of the samples after 24 h (*Fig. 4.7a,b*) shows that the peaks are highly attenuated, which is due to further sedimentation. After processing with TBA/H=0.25 (*Fig. 4.6c*), the broad peak increases dramatically in intensity. The smaller particles present (mainly 0.1-0.2 μm) are more stable in colloidal suspension and the absorbance is only reduced by approximately 10% after standing for 24 h (*Fig. 4.7c*). These broad features are ascribed to light scattering from the relatively large titania particles in suspension. The larger number of smaller particles in the Ti-120-30-0.25 suspension scatter light more effectively, leading to the increased peak intensity.

In contrast, the suspensions processed with TBA/H$\geq$0.5 (*Fig. 4.6d-f*) show narrower absorbance features with peak maxima at 270 nm. These absorbance peaks can be ascribed to the excitonic electronic transition for the titania sheets.[2,14] The elimination of the broad scattering feature, and stability of the colloid for longer periods, (*Fig. 4.7d-f*) provide supporting evidence for the exfoliation of titanate layers into nanometer dimensions.[6,15]

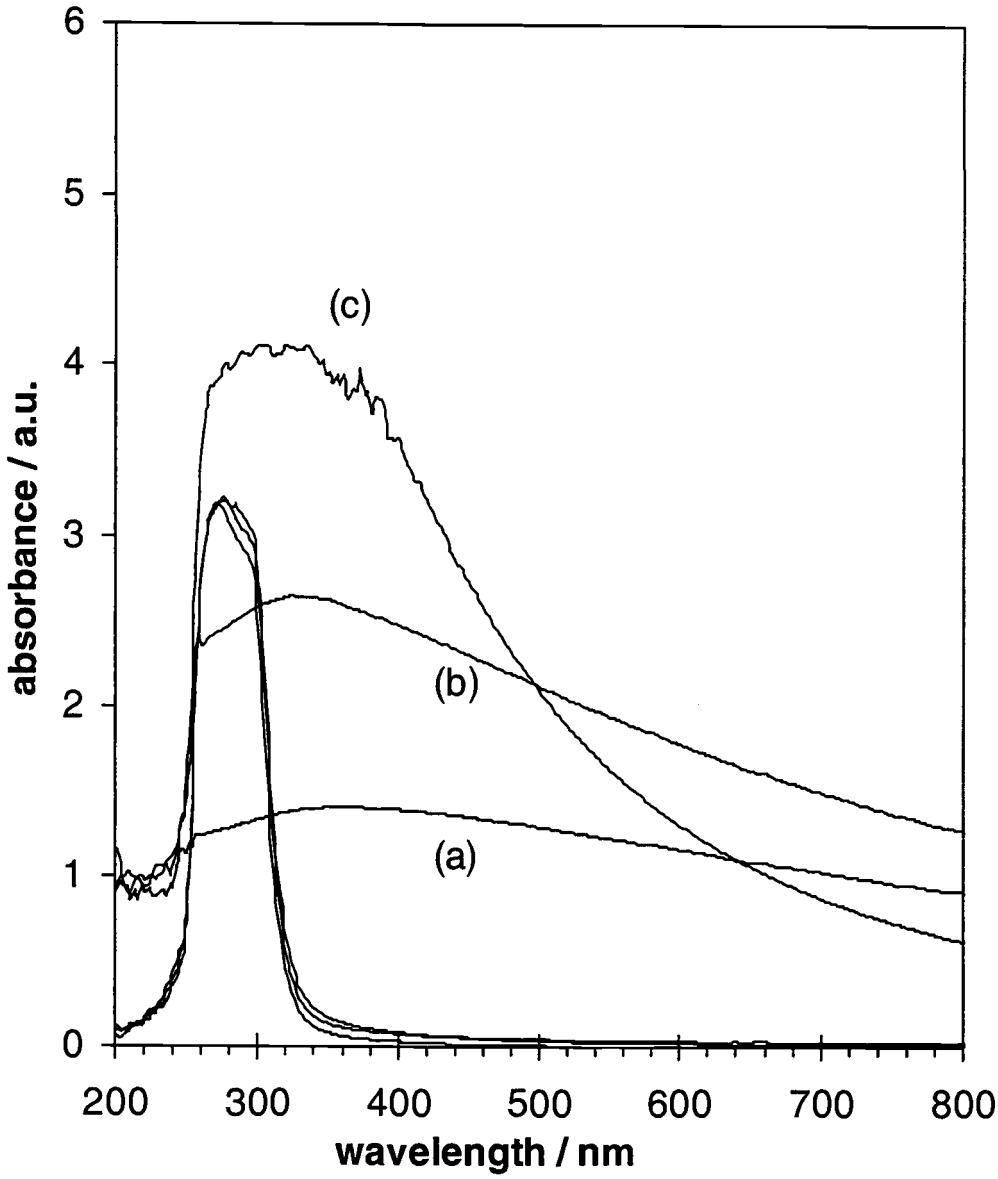

Figure 4.6 UV/VIS absorption spectra for samples Ti-0-0-0 (a), Ti-120-30-0 (b), Ti-120-30-0.25 (c), Ti-120-30-0.5 (d), Ti-120-30-0.75 (e), and Ti-120-30-1 (f).

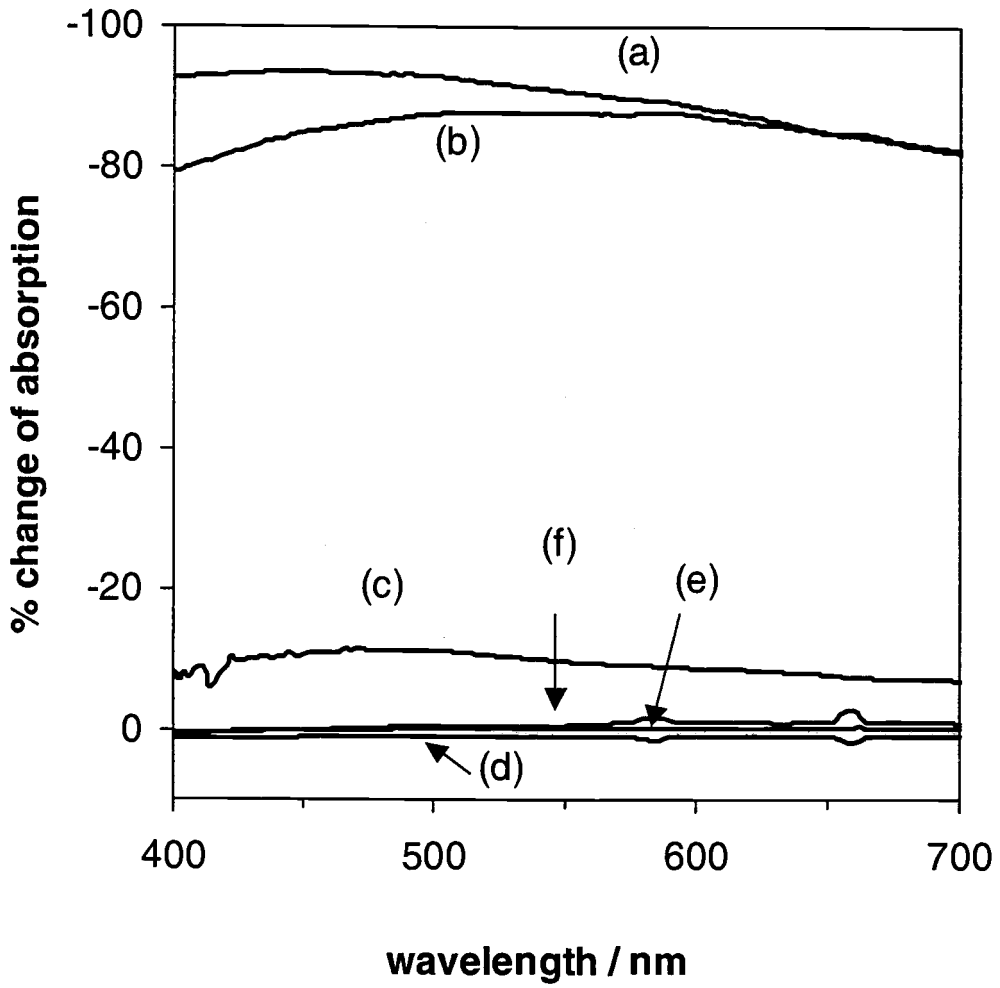

Figure 4.7 Changes in UV/VIS absorption after standing for 24 h for Ti-0-0-0 (a), Ti-120-30-0 (b), Ti-120-30-0.25 (c), Ti-120-30-0.5 (d), Ti-120-30-0.75 (e), and Ti-120-30-1 (f).

4.5 ACKNOWLEDGEMENT

The authors gratefully acknowledge support from NSF grant DMR-9900390 and helpful advice from Dr. Takayoshi Sasaki at NIRIM. NS acknowledges support from the Royal Thai Government.

4.6 REFERENCES

1. Sasaki, T.; Watanabe, M.; Michiue, Y.; Komatsu, Y.; Izumi, F.; Takenouchi, S. *Chem. Mater.* **1995**, *7*, 1001.

2. Sasaki, T.; Watanabe, M. *J. Phys. Chem. B* **1997**, *101*, 10159.

3. Sasaki, T.; Nakano, S.; Yamauchi, S.; Watanabe, M. *Chem. Mater.* **1997**, *9*, 602.

4. Sasaki, T.; Watanabe, M.; Hashizume, H.; Yamada, H.; Nakazawa, H. *J. Am. Chem. Soc.* **1996**, *118*, 8329.

5. Sasaki, T.; Watanabe, M. *Mol. Cryst. Liq. Cryst.* **1998**, *311*, 417.

6. Sasaki, T.; Watanabe, M. *J. Am. Chem. Soc.* **1998**, *120*, 4682.

7. Sasaki, T.; Kooli, F.; Iida, M.; Michiue, Y.; Takenouchi, S.; Yajima, Y.; Izumi, F.; Chakoumakos, B.C.; Watanabe, M. *Chem. Mater.* **1998**, *10*, 4123.

8. Kooli, F.; Sasaki, T; Rives, V.; Watanabe, M. *J. Mater. Chem.* **2000**, *10*, 497.

9. Sasaki, T.; Ebina, Y.; Watanabe, M.; Decher, G. *Chem. Commun.* **2000**, 2163.

10. Sukpirom, N.; Lerner, M. *Chem. Mater.* **2001**, *13*, 2179.

11. Grey, I.; Li, C.; Madsen, I.; Watts, J. *J. Solid State Chem.* **1987**, *66*, 7.

12. Bernhardt, C. *Particle Size Analysis:Classification and Sedimentation Methods*; Chapman & Hall: London, **1994**; Chapter 3.

13. The Society for Analytical Chemistry *The Determination pf Particle Size: I. A Critical Review of Sedimentation Methods*, W. Heffer & Sons Ltd, Cambridge, **1968**, p. 17.

14. Vossmeyer, T.; Katsikas, L.; Giersig, M.; Popovic, I.G.; Diesner, K.; Chemseddine, A.; Eychmüller, A.; Weller, H. *J. Phys. Chem.* **1994**, *98*, 7665.

15. Murray, C.B.; Norris, D.J.; Bawendi, M.G. *J. Am. Chem. Soc.* **1993**, *115*, 8706.

16. Cullity, B.D. *Elements of X-ray Diffraction, 2nd Ed.*; Addison-Wesley: Reading, MA, 1978.

CHAPTER 5

INTERCALATION AND NANOCOMPOSITES WITH LAYERED TETRATITANATE: RAPID SYNTHESES USING ULTRASOUND

Nipaka Sukpirom and Michael M. Lerner

Department of Chemistry and Center for Advanced Materials Research,

Oregon State University

Corvallis, OR 97331-4003, USA

Chem. Mater., submitted for publication, 2001.

5.1 ABSTRACT

Ultrasound is used to effect the rapid, direct intercalation of long-chain (C6-C18) alkylammonium ions between $Ti_4O_9^{2-}$ (tetratitanate) layers, and to prepare dispersions that react with polymer solutions to form the first nanocomposites with tetratitanate. Powder XRD on the isolated solids gives phase purity and basal spacings that suggest a relatively high kink concentration for the alkylammonium intercalation compounds. UV/Vis spectrometry and particle size distribution analyses are used to monitor changes in tetratitanate particle size as a function of ultrasonication time and concentration of tetrabutylammonium (TBA), which acts a dispersing agent. The dispersed tetratitanate suspension reacts with poly(ethyleneoxide), poly(vinylpyrrolidone), or poly(ethylenimine) to form layered nanocomposites, which are characterized by powder XRD, and elemental, thermal and SEM analyses.

5.2 INTRODUCTION

Nanocomposites can be defined as materials comprising two or more components with at least one having nanoscale dimensions, and have received significant academic and technological attention. Nanocomposites have been shown to display new or enhanced mechanical, catalytic, electronic, magnetic, and optical properties that cannot be obtained from either the individual components or from macro- or micro-dimensioned composites. Their novel properties are often related to confinement, quantum-size effects, and/or interfacial interactions. [1,2] Combinations of organic with inorganic components are especially interesting in that there is the potential to realize the distinctive characteristics of these components within a single material.

Two basic forms of organic-inorganic nanocomposites have been studied in detail. Disordered structures can be prepared by sol-gel methods. This case involves a modification of the conventional sol-gel chemistry, based on the hydrolysis and condensation of inorganic molecular precursors. An organic component, usually polymeric, is included prior to, or during, gelation. [3,4] A second major research area involves nanocomposites that include polymer guests within inorganic hosts. Several different synthetic strategies have been developed for layered hosts, such as the intercalation of polymers into a pre-formed host, or the templated nucleation and growth of the inorganic host in a solution containing an organic polymer. [2]

Most studies on layered nanocomposites have employed smectite aluminosilicate clays as the inorganic hosts. These clays have the advantage of low charge densities on the layer surfaces under typical processing conditions, which allows their spontaneous exfoliation in aqueous solution. They are also suitable for some direct (melt) polymer intercalation reactions at elevated temperatures. [5,6] The commercial potential of polymer-clay nanocomposites includes use in structural materials, [7-10] UV barrier coatings, [10] gas barrier coatings, [10,11] and fire retardants. [12] Other layered hosts such as MoO_3, [13-16] MPS_3 (M=Mn,Cd), [13,17,18] V_2O_5, [19] and MS_2 (M=Ti,Ta,Mo) [18,20,21] have also been studied in detail. With these hosts, nanocomposites have most often been prepared by either the *in situ* polymerization of monomer intercalates, or an exfoliation-adsorption method where the reduced host exfoliates into an aqueous solution.

TiO_2 and many titanates have unique and technologically important optical, electronic, and chemical properties. Some layered titanates have been shown to intercalate inorganic or organic cations. A recent example is $H_xTi_{2-x/4}O_4.H_2O$ (x~0.7), abbreviated as H-Ti, which has a lepidocrocite-type layer structure. [22] Edge-sharing TiO_6 octahedra form planar sheets, protons and hydronium ions are incorporated between sheets to maintain charge neutrality. H-Ti is prepared by proton exchange of the cesium form, which is itself obtained by the high temperature reaction of Cs_2CO_3 and TiO_2. In 1996, Sasaki and coworkers first described the exfoliation of H-Ti in an aqueous solution containing

tetrabutylammonium (TBA) cations. [22,23] Recently, we reported the use of aqueous H-Ti dispersions to synthesize ordered nanocomposites with a number of water-soluble polymers. [24] However, two drawbacks to the practical large-scale application of these nanocomposites are the high cost of producing H-Ti and the instability of this protonated form towards acidic solutions and/or long-term air exposure.

Another long-established layered form for titanates is the corrugated sheet seen in potassium tetratitanate ($K_2Ti_4O_9$). The $[Ti_4O_9]^{2-}$ sheets have TiO_6 octahedra linked by shared edges and vertices, with interlayer potassium ions. Proton exchange in aqueous acid preserves the tetratitanate layers to yield $H_2Ti_4O_9.xH_2O$, x~1.2, abbreviated H-Ti4. [25] H-Ti4 is easy and inexpensive to prepare, and has shown potentially useful ion exchange, semiconducting, and photocatalytic properties. [26] Figure 5.1 shows schematic representations for the H-Ti and H-Ti4 structures.

The intercalation or exfoliation of tetratitanate is expected to be more difficult than for the planar-sheet H-Ti lepidocrocite form, which has a lower interlayer electrostatic interaction. [22] Some intercalation compounds with inorganic or organic cations, especially alkylammonium cations, have been prepared. Choy et al. reported the intercalation of butylammonium cations at 60°C, but did not observe any direct solvo-intercalation of longer chain alkylammonium cations (C8-C18) into H-Ti4. However, these longer chain cations did exchange with a butylammonium intercalate after reaction for 24 h. They observed a linear fit

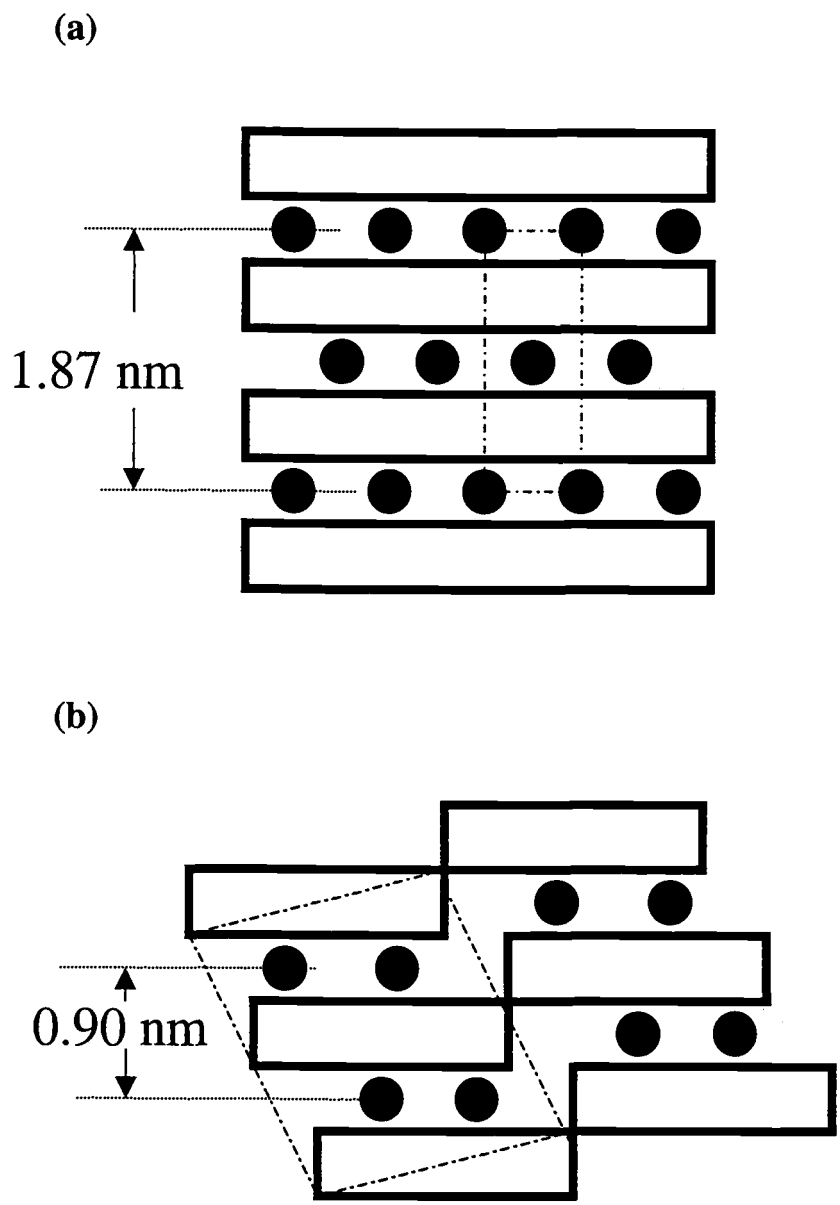

Figure 5.1 Schematic representations of (a) the planar-sheet lepidocrocite structure in H-Ti, and (b) the corrugated sheet structure in H-Ti4.

for the basal spacing with the number of carbon atoms in the intercalate. [27] Okawa and Takizawa [26,28] reported the intercalation of alkylammonium ions (C4-C18) into tetratitanate by reaction of H-Ti with the desired cation and 0.1 M [2.2.2]-cryptand in 1,4-dioxane at room temperature for 1 week. The alkylammonium salt reagents employed were present in the products obtained, but the intercalation compounds with longer-chain cations were not stable when washed to remove these residual salts.

We report here the application of ultrasonication to disperse $H_2Ti_4O_9$ in aqueous solution, allowing the rapid, direct intercalation of n-alkylammonium ions (C6-C18) and also providing a facile method to form the first nanocomposites containing polymers between tetratitanate layers.

5.3 EXPERIMENTAL

5.3.1 Materials

Hexylamine (Avocado Research Chemicals Ltd, 99%), dodecylamine (Aldrich, 98%), tetradecylamine (TCI America, Inc.), hexadecylamine (Aldrich, 98%), octadecylamine (Aldrich, 97%), tetrabutylammonium hydroxide, TBAOH, (Aesar, 55% w/w aqueous solution), PEO (Aldrich, M_v=1x10^5), PVP (Aldrich, M_w=4x10^4), and PEI (Aldrich, M_w=7.5x10^5, 50 wt% solution in water) were used

as received. $K_2Ti_4O_9$ was prepared according to a literature method [29] by grinding anatase TiO_2 (Aesar, 99.9%) and KNO_3 (Mallinckrodt, reagent) together in a 2 mol/mol ratio and then heating at 1000°C for 2 days. The proton-exchanged form was prepared by stirring $K_2Ti_4O_9$ (1.0 g) in 100 mL of 2M HCl for 3 h at 50°C. [30] The powder X-ray diffraction (XRD) pattern (basal spacing=0.90 nm) indicated complete proton exchange and matched that obtained previously for $H_2Ti_4O_9.xH_2O$ (H-Ti4) with x=1.2. [29,30] The dehydrated form (basal spacing=0.76 nm) was obtained by heating at 150°C. The reduction in basal spacing is consistent with a single layer of hydronium ions between titanate layers prior to dehydration.

5.3.2 Intercalation of alkylammonium ions

H-Ti4 (0.25 g) was added to an aqueous solution of hexylamine or a 100% ethanol solution of alkylamine (C12-C18) in a 100 mL glass bottle, with a 5 mol/mol ratio of amine to protons in $H_2Ti_4O_9$. Ultrasound was applied to the suspensions using a GE600 ultrasonic processor with Ti alloy probe (13 mm dia.) at 180 W for 0.25 h. The suspensions were collected by filtration then air-dried for 12 h. The nomenclature used for solid products indicates the reagent alkylammonium chain length, ex. C14/Ti4.

5.3.3 Dispersion of H-Ti4

H-Ti4 (0.10 g) was added to an aqueous solution of TBAOH in a 100 mL glass bottle, with mole ratios of TBA/H in H-Ti4 varied from 0-5, and ultrasonicated at 180 W for 0-120 minutes. Reactions longer than 120 minutes generate too much heat and cause degradation of H-Ti4. Samples are labeled to indicate processing conditions as follows: Ti4-10-5 refers to a tetratitanate suspension ultrasonicated for 10 min with a TBA/H mol ratio of 5. As controls, aqueous suspensions of H-Ti4 were also evaluated without ultrasonication. For example, sample Ti4-0-0 was added to DI water without further processing, and Ti4-stir60-0 was stirred for 60 minutes without any addition of TBAOH.

5.3.4 Formation of nanocomposites

H-Ti4 (0.25 g) was added to an aqueous solution of TBAOH in a 100 mL glass bottle, with TBA/H=5, and ultrasonicated at 180 W for 1 h. The suspension was filtered to remove large particles. Aqueous solutions of PEO, PVP, or PEI were stirred into the H-Ti4 suspensions with a 3 mol/mol ratio of polymer formula unit to protons in H-Ti4. Gelation occurred immediately upon addition of the PEI solution. After addition of PEO and PVP, the solutions were acidified with HCl

until gelation occurred (at pH=3 and 1, respectively). Gels were collected by filtration, washed copiously with DI water, and then dried under vacuum for 24 h.

5.3.5 Characterization

XRD patterns were obtained using a Siemens D5000 diffractometer and Ni-filtered CuK_α radiation (0.15418 nm) in 0.02° steps. Sample preparation for dispersed solids involved casting a thin film onto a glass substrate and air-drying for 24 h. UV/Vis spectra on solutions were obtained using a Hewlett-Packard 8425A diode array spectrophotometer. Particle size distributions were determined with a Horiba CAPA-700 analyzer. Solutions for UV/Vis and particle size analysis were diluted 1:10 with distilled water. Thermal analyses of nanocomposites were performed by heating at 10°C/min under flowing N_2 in a Shimadzu TGA-50 or DSC-50. SEM samples were coated with 60/40 Au/Pd alloy and examined with an Amray SEM at 8.0 kV accelerating voltage. Elemental (C/H/N/Ti) analyses were performed at Desert Analytics Laboratory (Tucson, AZ)

5.4 RESULTS AND DISCUSSION

5.4.1 Intercalation of alkylammonium ions

Alkylamines are protonated by reaction with H-Ti4 in water or ethanol. The alkylammonium ions intercalate into the tetratitanate layers after brief ultrasonication. XRD patterns of H-Ti4 and intercalation compounds are shown in Figure 5.2. Due to preferred orientation effects for the layered particles, only (*00l*) peaks are present. Table 5.1 lists the basal distances obtained from XRD, along with those reported previously. The XRD data indicate that the intercalation reactions are nearly complete, although small peaks that may be ascribed to H-Ti4 (or the dehydrated form) are present for the longer cations. By contrast with the present method, direct intercalation into H-Ti4 was not previously observed with chains longer than C8. [27]

The C6/Ti4 product obtained using ultrasound has a basal spacing of 2.16 nm, similar to that observed by Choy et al. Of the rest, all except C14/Ti4 have basal spacings that are significantly smaller than those reported previously. One possible explanation could lie in ultrasonic fragmentation of the alkylammonium ions; however, control experiments indicate that this does not occur under the conditions employed. [31]

Several groups have reported that products obtained at elevated temperatures can include significant concentrations of chain kinks. The lowest

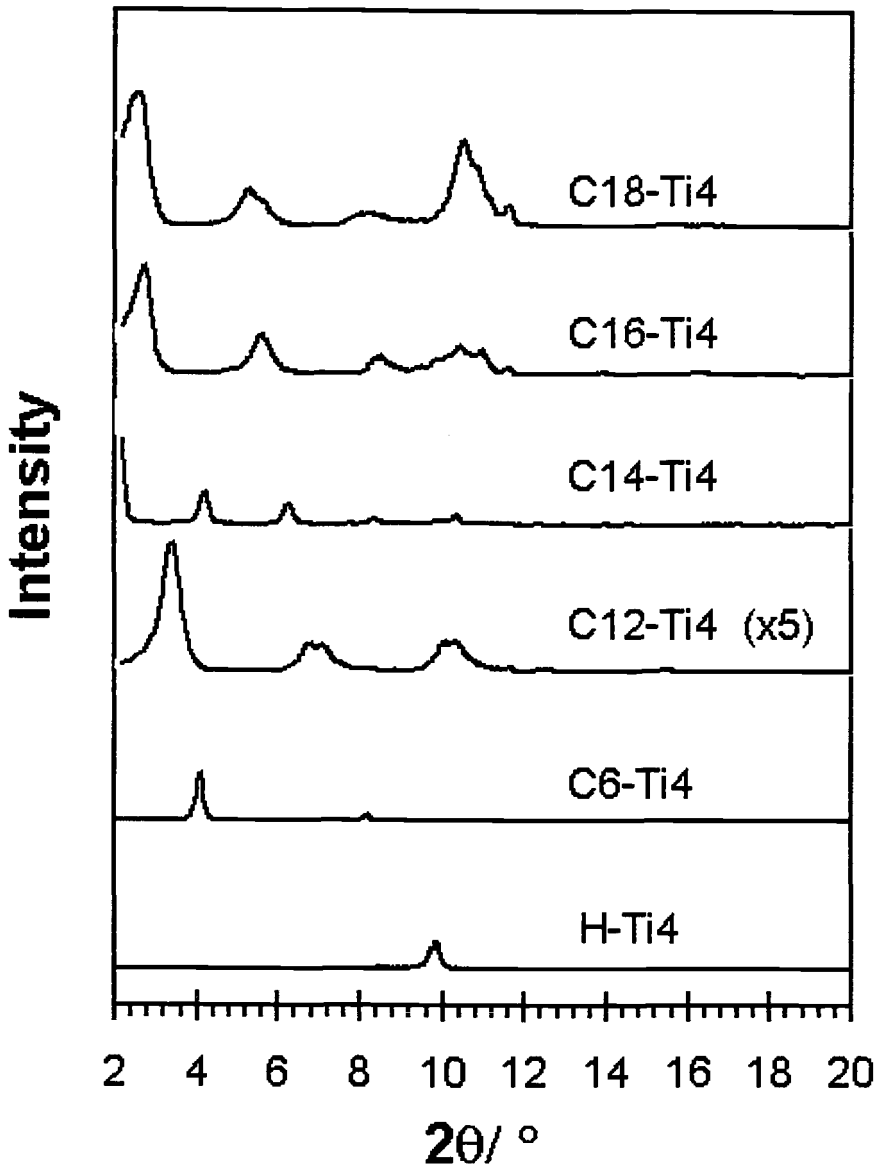

Figure 5.2 Powder XRD patterns of H-Ti4, and alkylammonium intercalates.

Table 5.1 Basal spacings for H-Ti4 and alkylammonium intercalation compounds.

	Basal spacing / nm		
	Sukpirom and Lerner	**Choy et al.**	**Okawa and Takizawa**
H-Ti4	0.90		
Dehydrated H-Ti4	0.76		
C6/Ti4	2.16	2.18	
C12/Ti4	2.65	3.60	3.85
C14/Ti4	4.31	4.07	4.29
C16/Ti4	3.27	4.55	4.72
C18/Ti4	3.34	5.02	5.04
reference	This study	[27]	[26]

energy state of alkylammonium chains in intercalation compounds generally contains all *trans* bonding. Kinks indicate the introduction of *gauche* bonds to form new rotational isomers of the hydrocarbon chains. Each change in conformation from *trans* to *gauche*, or kink, causes the alkyl chain length to decrease by approximately 0.13 nm. [32] Lagaly and Weiss studied kink conformation of long-chain alkylamines (C10-C18) intercalates in layer silicate, and found strong temperature dependence for the kink concentrations of each amine. [32] Chain disordering due to kink formation occurs with increasing temperature. Choy et al also described this effect for Cn/Ti4 ($n \geq 12$), such that the basal spacing of C18/Ti4 prepared at 75-100°C was reduced to 3.35 nm. [27] This basal spacing is similar to that obtained in the present study. The smaller gallery dimensions in the tetratinate intercalation compounds after ultrasonic processing is therefore consistent with relatively high kink concentrations.

5.4.2 Dispersion of H-Ti4

$H_xTi_{2-x/4}O_4.H_2O$ (x~0.7), abbreviated as H-Ti, is dispersed into individual lamella in the presence of tetrabutylammonium (TBA) ions after prolonged stirring. [33,34] Recently, we reported that ultrasonication led to a similar dispersion within 20 minutes. [35] The dispersions were then used as precursors for the facile production of nanocomposites by reaction with polymers in aqueous solution.

Using this model, we investigated the ultrasonic dispersion of H-Ti4 in the presence of TBA. UV/Vis spectra of the dispersions after different reaction times with TBA/H=5 (Figure 5.3A) show a strong, fairly sharp peak at 295-300 nm combined with a broad asymmetric feature ranging over 300-700 nm. The sharp peak is due to the excitonic electronic transition for isolated tetratitanate sheets, [33,36] while the broad feature results from scattering of large particles. [37] The change in relative intensities of these two features can be observed by plotting the ratio of absorbance at a wavelength outside of the sharp peak (375 nm was selected) to that at the peak, i.e. Abs(375)/Abs(300). This absorbance ratio decreases nearly linearly with the log of reaction time, until a value of approximately 0.8 is reached after 60 min (Figure 5.3B).

All XRD patterns on solids dried from the dispersion show a basal spacing of 1.81 nm, indicating that the tetratitanate sheets are intercalated with both TBA and water. For the planar-sheet H-Ti, the increase in basal spacing from dehydrated form to TBA intercalate (1.75-0.68=1.07 nm) [24,37] is similar to that observed here for H-Ti4 (1.81-0.76=1.05 nm).

The effect of TBA concentration on H-Ti4 dispersion was also examined. A reaction time of 1 h was chosen based on the results described above. UV/Vis spectra are shown in Figure 5.4A for TBA/H=0.1-5, and the ratio of absorbances, Abs(375)/Abs(300), is plotted against TBA/H ratio in 5.4B. A steep decrease in the relative degree of particle scattering is seen initially with increasing TBA/H, but

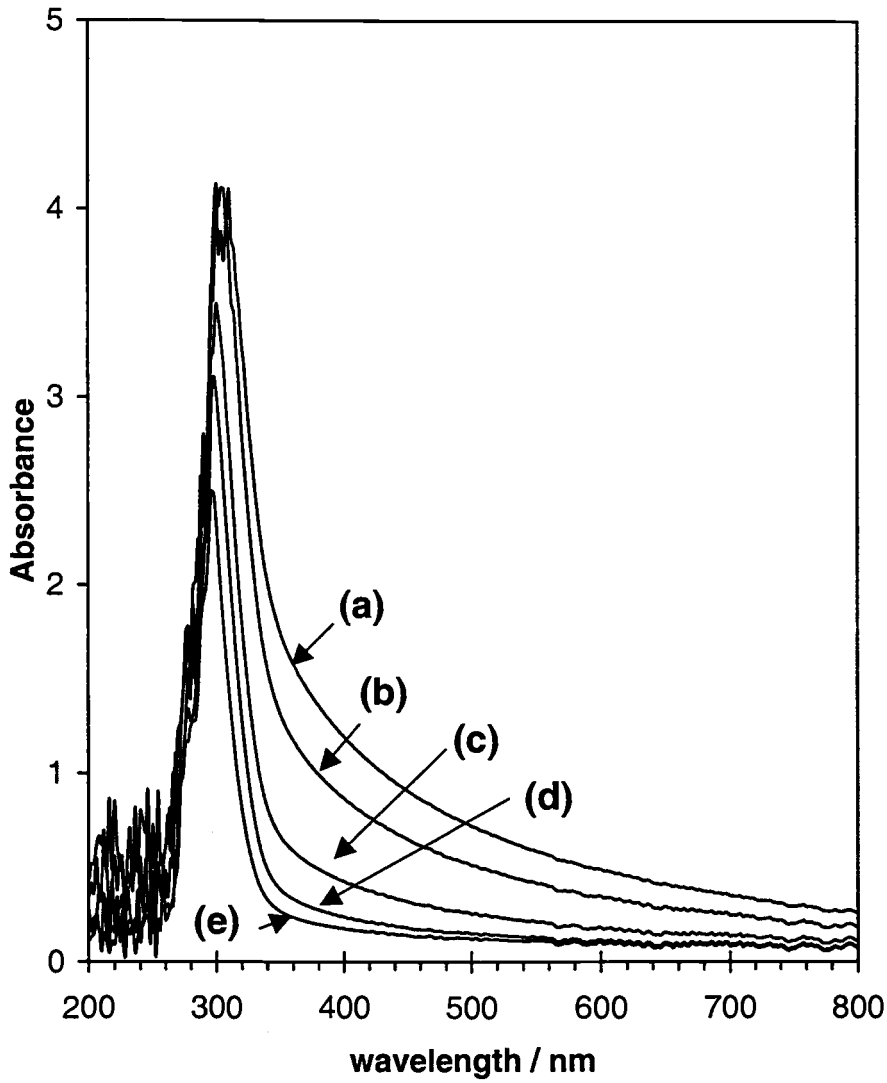

Figure 5.3A UV/Vis absorption spectra for H-Ti4 dispersed in aqueous solution, TBA/H=5, after ultrasonication at 180 W for (a) 5, (b) 10, (c) 30, (d) 60, and (e) 120 minutes.

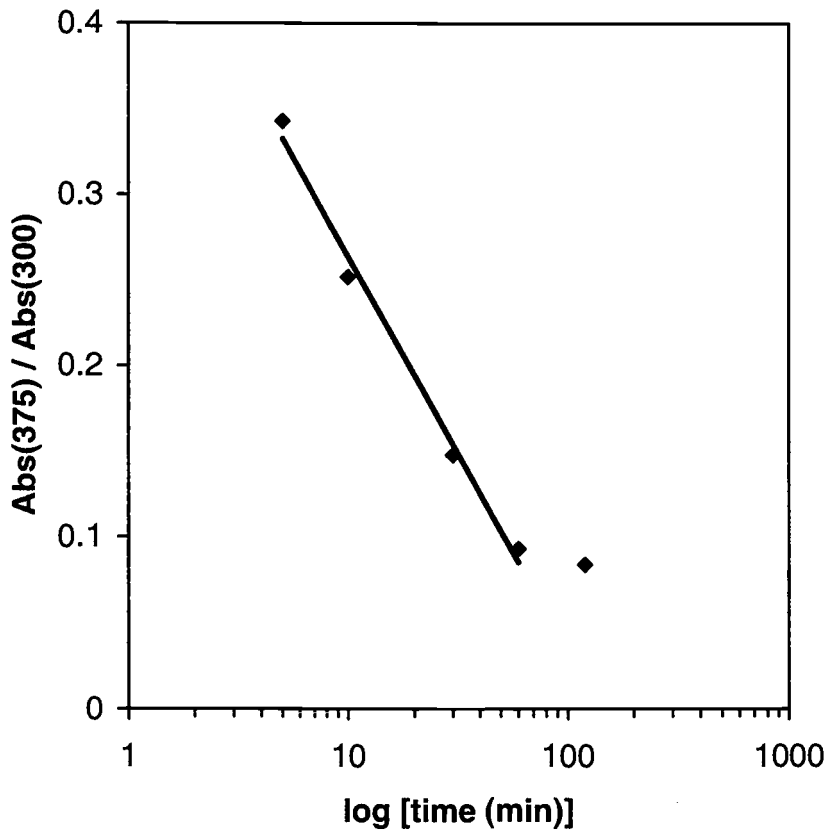

Figure 5.3B The ratio of absorptions at 375 nm to 300 nm as a function of ultrasonication time.

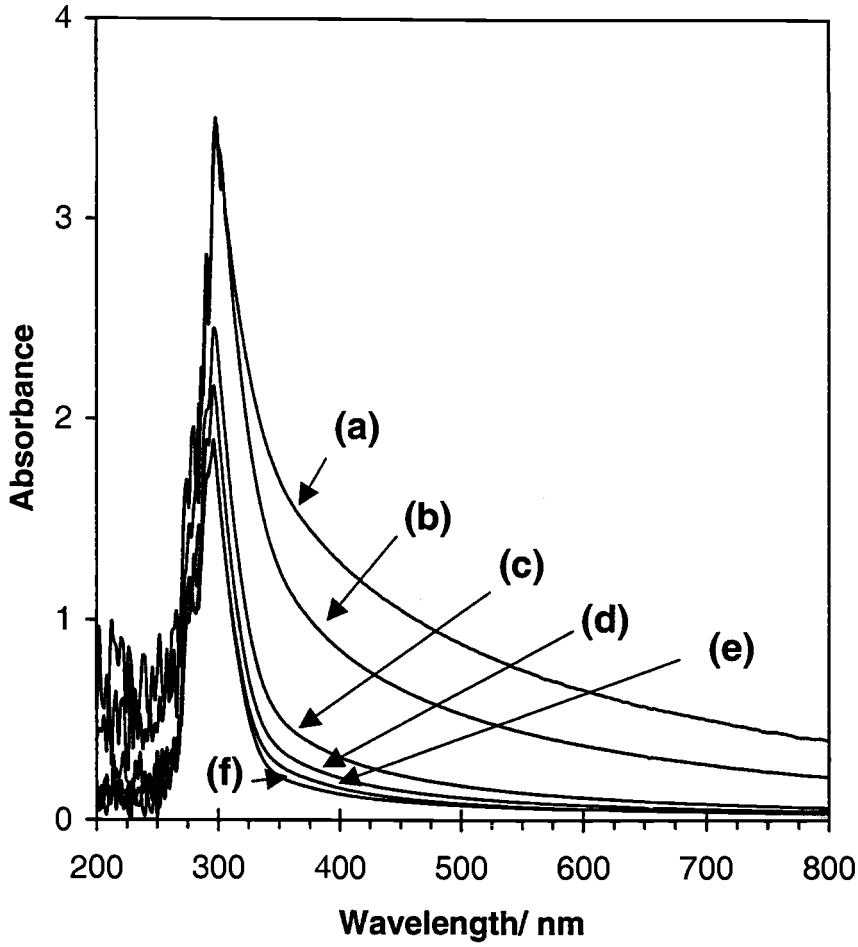

Figure 5.4A UV/Vis absorption spectra for H-Ti4 dispersed in aqueous solution, after ultrasonication at 180 W for 1 h with TBA/H = (a) 0.1, (b) 0.2, (c) 0.5, (d) 1.0, (e) 2.0, and (f) 5.0.

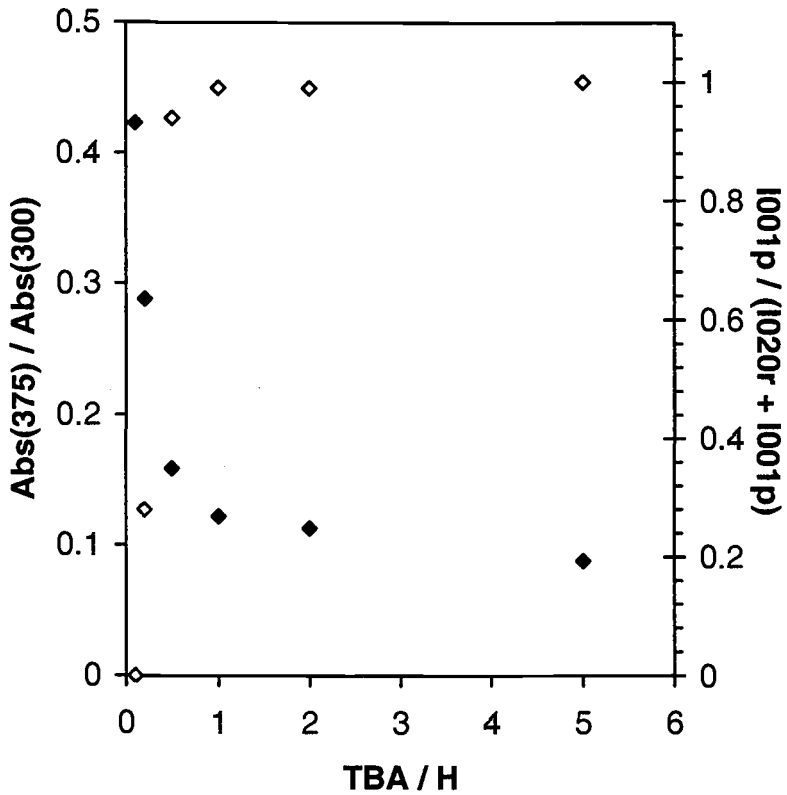

Figure 5.4B The ratio of absorptions at 375 nm to 300nm and the ratio of integrated XRD peak intensities, $I_{001p}/(I_{020r} + I_{001p})$, vs TBA/H ratio in solution.

there is little decrease in the absorbance ratio for TBA/H>1 and therefore the larger particle content seems to be near a minimum.

XRD patterns of cast solids (Figure 5.5) show the presence of two phases, the starting reagent H-Ti4 and the TBA-intercalation compound described above. The H-Ti4 content decreases with increasing TBA/H. The relative content of the two phases is evaluated as the ratio of integrated peak intensities, $I_{001p}/(I_{020r} + I_{001p})$ where I_{001p} and I_{020r} are the integrated intensities of the (001) diffraction peak for the TBA intercalation compound and the (020) peak for H-Ti4, respectively. This intensity ratio is plotted against TBA/H in Figure 5.4B. The intensity ratio is above 0.99 when TBA/H≥1, indicating that there is no significant content of H-Ti4 in these dispersed samples.

The particle size distributions obtained on the tetratitanate dispersions are shown in Figure 5.6. The starting reagent H-Ti4 contains mainly large particles (>10μm), with a very small content of submicron particles. Simply stirring in distilled water did reduce some larger particles to the 3-10 μm range, but did not generate additional submicron particles. Both dispersions rapidly settle in aqueous solution. A solution with TBA/H=0.1 and 60 min ultrasonication resulted in much more particle size reduction, with the major fraction at 1-3 μm and about 1/3 with submicron dimensions. (Figure 6c) At TBA/H=5, the smallest particle sizes are obtained and the very fines content (<0.1 μm) is now measurable. By comparison, ultrasonication of H-Ti with TBA/H=0.5 for 0.5 h resulted in over 40% of <0.1μm particles. [35] Significant dispersion, to form a stable colloidal suspension, occurs

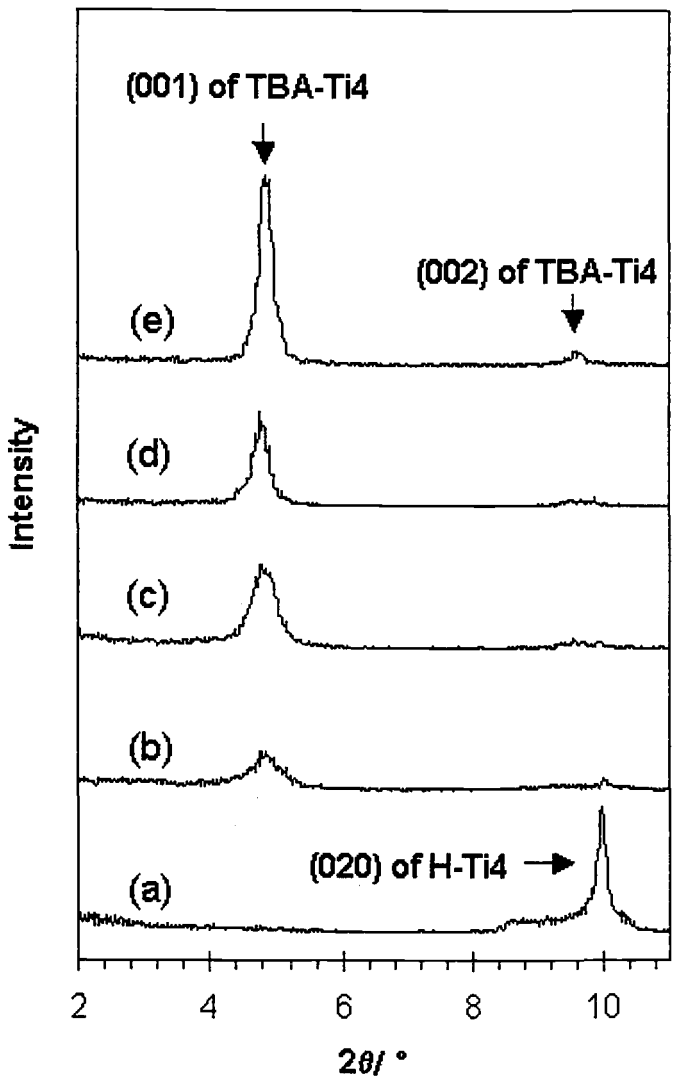

Figure 5.5 Powder XRD patterns of cast and dried samples of H-Ti4 after ultrasonication for 1 h at TBA/H = (a) 0.1, (b) 0.5, (c) 1.0, (d) 2.0, and (e) 5.0.

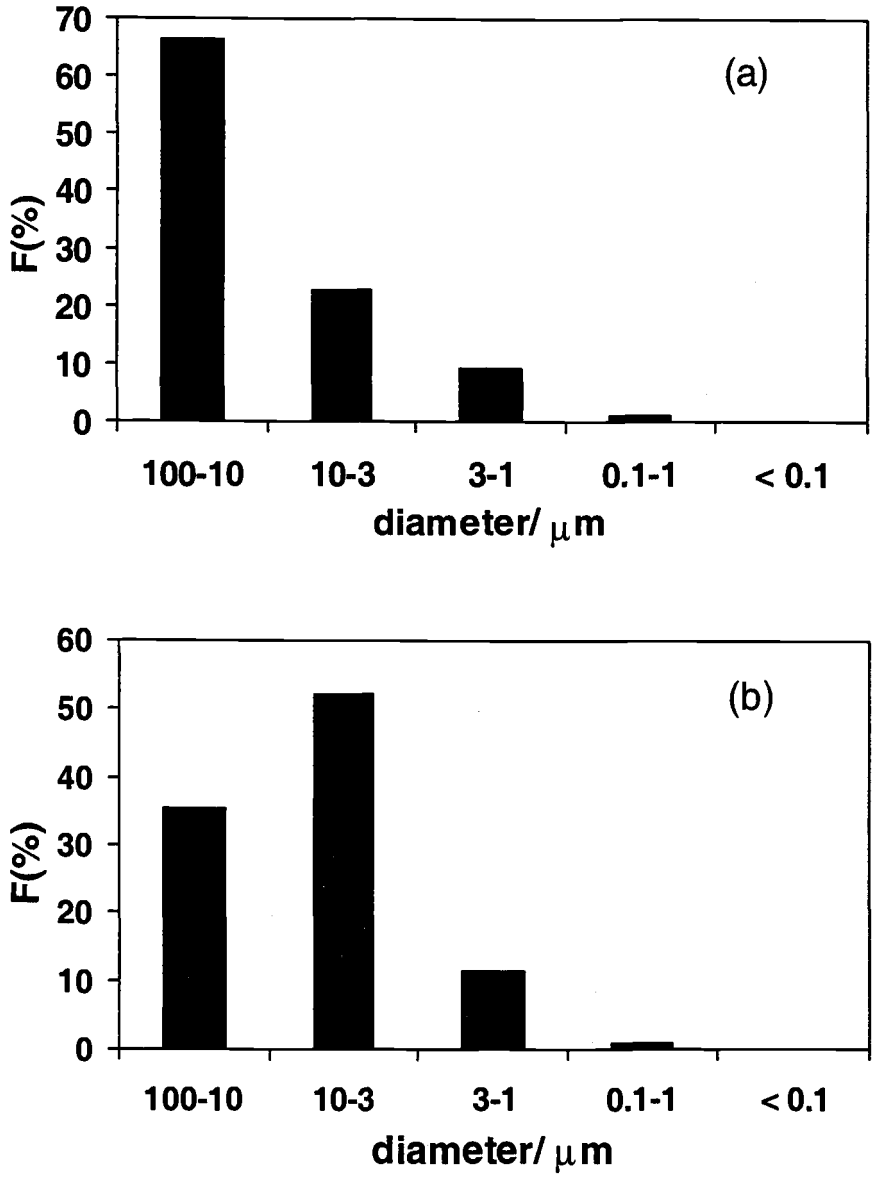

Figure 5.6 Particle size distributions of H-Ti4 samples after various reaction conditions, (a) H-Ti4 in distilled water with no further treatment, (b) after stirring for 60 minutes.

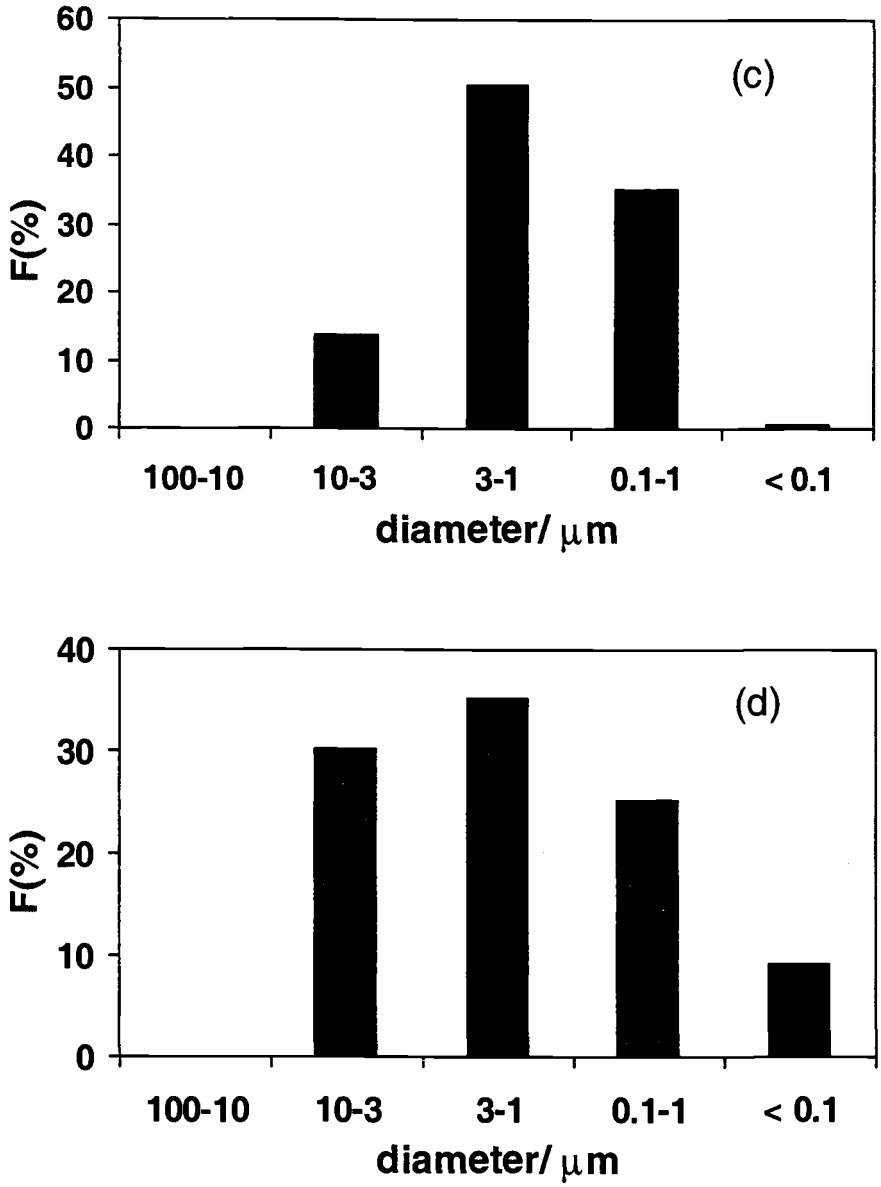

Figure 5.6 (continued) Particle size distributions of H-Ti4 samples after ultrasonication for 60 min with (c) TBA/H=0.1 or (d) TBA/H=5.

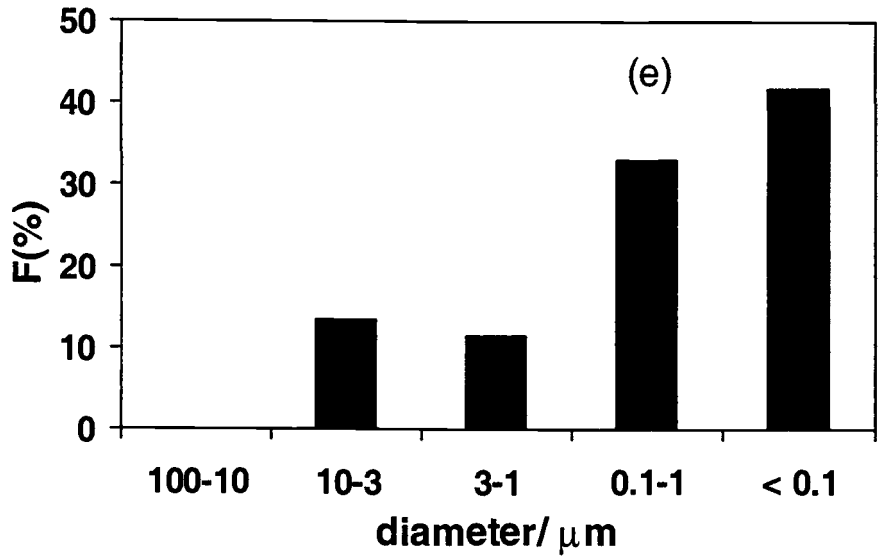

Figure 5.6 (continued) Particle size distributions of H-Ti after ultrasonication for 30 min with TBA/H=0.5. Data for (e) are from reference [24].

under appropriate conditions, but H-Ti4 does not appear to exfoliate to form individual lamella to the extent that has been shown for H-Ti. [35]

5.4.3 Polymer/H-Ti4 nanocomposites

When an aqueous solution of PEI is added to dispersed H-Ti4, a gel forms immediately. Gels also form after solutions of PEO and PVP are added to dispersed H-Ti4 and the suspensions acidified to pH = 3 and 1, respectively. Figure 5.7 shows XRD patterns of the dried solids for PEI/H-Ti4, PEO/H-Ti4, and PVP/H-Ti4. Only one, two, or three broad (00*l*) diffraction peaks are seen for the nanocomposites, indicating a decrease in stacking coherence relative to H-Ti4, but the absence of other ordered phases is significant and the peaks can be indexed to give basal distances of 2.30 nm (PEI/H-Ti4), 1.30 nm (PEO/H-Ti4), and 3.09 nm (PVP/H-Ti4).

The difference between basal distance for dehydrated H-Ti4 and the polymer-containing nanocomposites indicates the expansion due to polymer incorporation. This interlayer distance is 0.54 nm in PEO/H-Ti4, which agrees with values obtained for a monolayer PEO gallery in other layered hosts (reported expansions include 0.4-0.5 nm for PEO monolayers in montmorillonite and MPS_3 [17,20], 0.6 nm in MoO_3 [15], and 0.4 nm in kaolinite [38]). PVP becomes positively charged at pH<3.0-3.5, [39] so after acidification the polymer attracts the

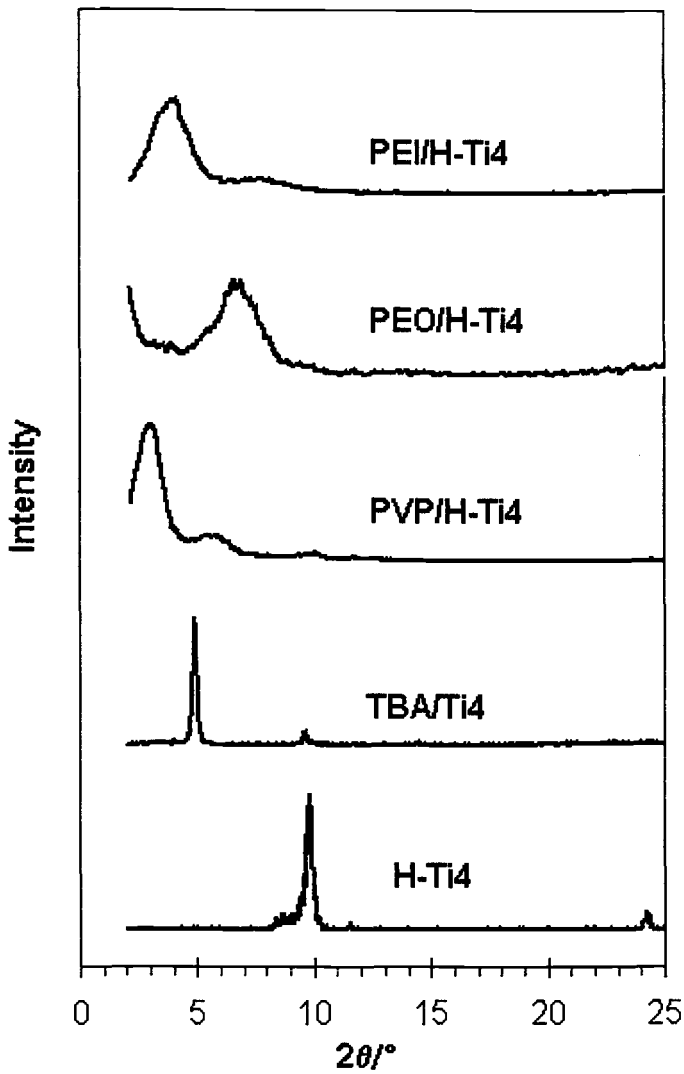

Figure 5.7 Powder XRD patterns of H-Ti4, TBA/Ti4, PEO/H-Ti4, PVP/H-Ti4, and PEI/H-Ti4.

negative tetratitanate sheets and precipitates. The interlayer distance for PVP/H-TI4 is similar to that in previous reports, including 2.2 nm for PVP intercalated in H-Ti, [24] 2.3 nm in $RuCl_3$, [40] and 2.24 nm in V_2O_5.[41] With such a large expansion and limited structural information, the polymer arrangement cannot be deduced in these galleries. Elemental analysis (discussed subsequently) shows a large TBA content for these materials, which may account for some of the gallery expansion.

Interlayer distances for layered nanocomposites containing PEI have been reported in the range of 0.36-0.47 nm for a range of hosts, including $RuCl_3$, Na-montmorillonite, MS_2, MoO_3, and MPS_3, [18,40] These dimensions are consistent with a polymer monolayer adsorbed between host sheets. [18] In contrast, PEI/H-Ti4 has an interlayer distance of 1.54 nm. One possibility is the co-insertion of TBA into the expanded galleries, since the TBA dimension of approximately 1.1 nm correlates well with the additional expansion observed. However, elemental analyses indicate a relatively small amount of TBA in the product.

Yin et al reported multiple phase changes and thermal events on heating H-Ti4, [42] including the loss of intercalated water (<200°C), and the formation of $H_2Ti_8O_{17}$ (200-250°C), monoclinic TiO_2 (250-300°C), and anatase (650-1000°C). These changes cause a continuous weight loss on heating H-Ti4 from ambient to 600°C. The calculated weight loss is 5.34% assuming complete conversion of $H_2Ti_4O_9$ to TiO_2; a similar value of 5.29% was obtained by heating dehydrated H-Ti4 to 800°C.

Thermal analyses of PEO/H-Ti4 and PVP/H-Ti4 using TGA and DSC are shown in Figure 5.8. Weight losses below 200°C can be ascribed to the loss of intercalated water. Above 200°C, multiple weight loss events occur, corresponding to polymer degradation and titanate phase changes. However, since the final stable residual consists solely of TiO_2, the tetratitanate mass is known from the gravimetric relationship between the phases described above. Therefore, the total polymer content can be determined using TGA. The results obtained correlate well with those from elemental analyses (see Table 5.2).

Final compositions obtained using elemental (C/H/N/Ti) analyses are $(C_{16}H_{36}N)_{0.07}Ti_4O_9(C_2H_4O)_{0.6}(H_2O)_{2.8}$ for PEO/H-Ti4, $(C_{16}H_{36}N)_{0.23}Ti_4O_9(C_6H_9NO)_{2.1}(H_2O)_{6.5}$ for PVP/H-Ti4, and $(C_{16}H_{36}N)_{0.07}Ti_4O_9(C_2H_5N)_{6.1}(H_2O)_{6.0}$ for PEI/H-Ti4. The water contents obtained are 10-15 wt%, which agrees with the low temperature losses in TGA data.

SEM images of particle microstructures for H-Ti4, PVP/H-Ti4, PEO/H-Ti4, and PEI/H-Ti4 are shown in Figure 5.9. H-Ti4 consists of rectangular needles with dimensions of approximately (0.1x0.5) and at least 3 μm in length. In contrast, the nanocomposites are larger, amorphous aggregates, with particle diameters in the range of 10-100 μm. This type of aggregation has been previously reported for polymer/H-Ti nanocomposites, and was ascribed to the gel processing method. [24]

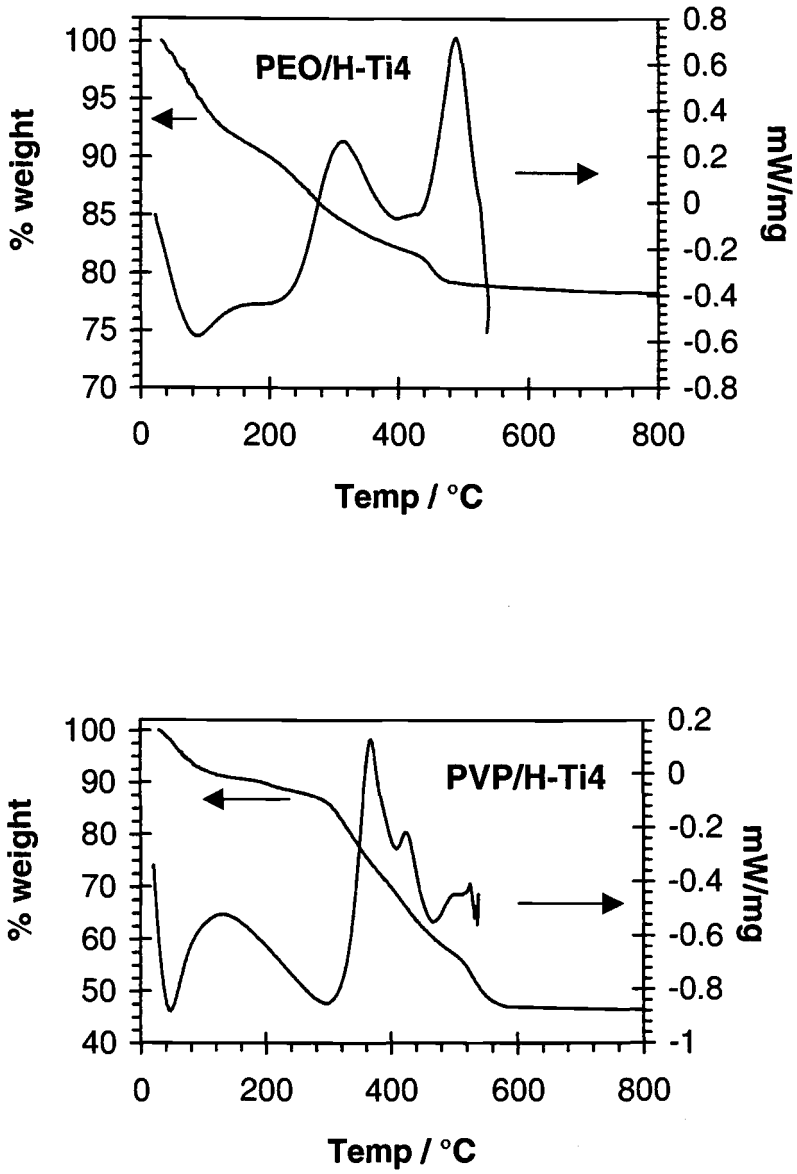

Figure 5.8 Thermal analyses of PEO/H-Ti4 and PVP/H-Ti4.

Table 5.2 Compositional analyses for PEO/H-Ti4, PVP/H-Ti4, and PEI/H-Ti4.

	Weight % Obs (calc)		
	PEO/H-Ti4	**PVP/H-Ti4**	**PEI/H-Ti4**
C	6.5 (6.5)	26.9 (26.8)	22.3 (22.4)
H	2.2 (2.5)	4.6 (5.5)	5.8 (6.3)
N	0.23 (0.22)	4.5 (4.5)	12.1 (12.1)
Ti	44.8 (44.8)	26.0 (26.0)	26.7 (26.7)
TBA	(4.0)	(7.6)	(2.4)
Polymer	(6.1)	(32.1)	(36.8)
H_2O	(11.7)	(15.8)	(14.6)
Total intercalate from e.a.	(21.8)	(55.4)	(53.8)
Total intercalate from TGA	17.9	51.6	50.1

(a)

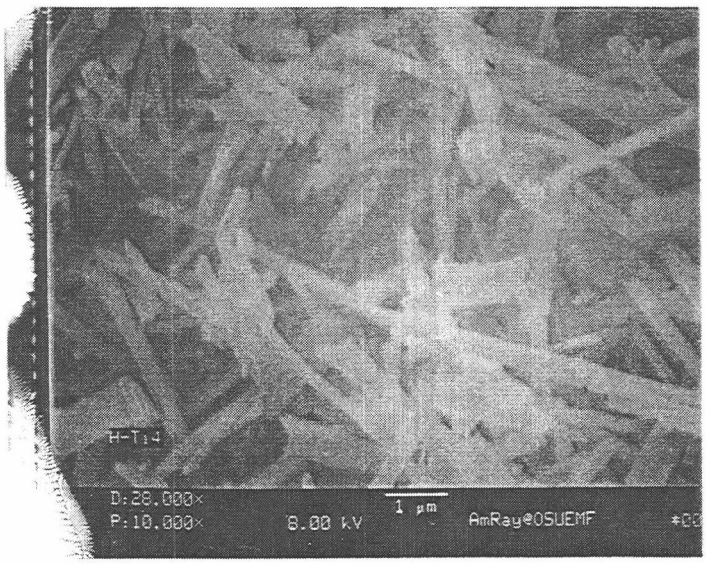

(b)

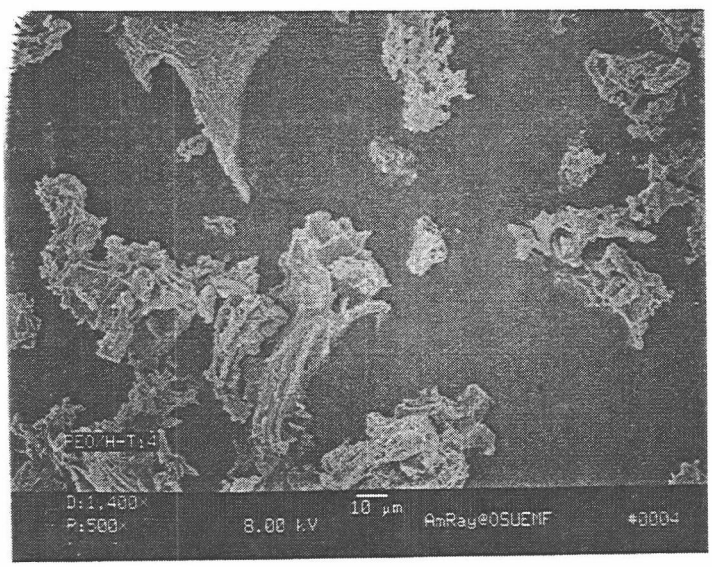

Figure 5.9 SEM images of (a) H-Ti4, (b) PEO/H-Ti4.

(c)

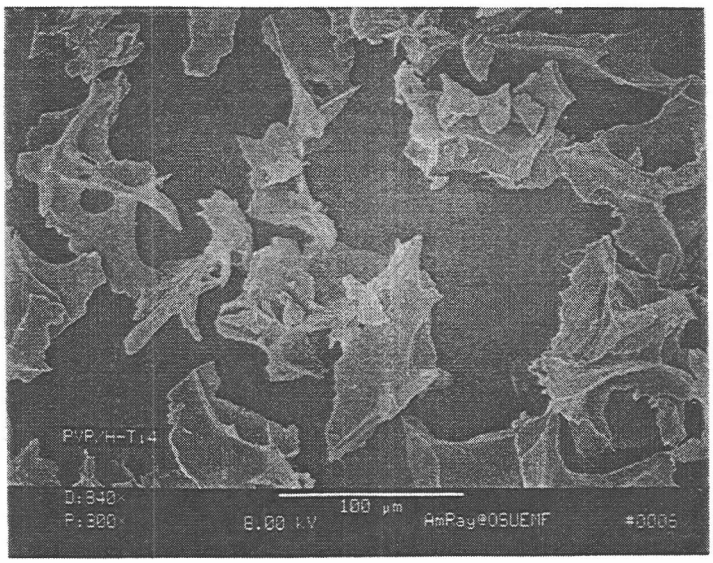

(d)

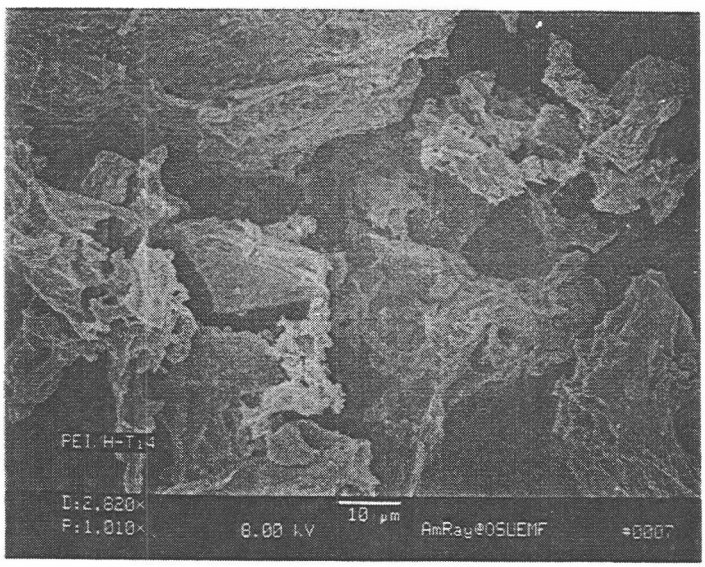

Figure 5.9 (continued) SEM images of (c) PVP/H-Ti4, and (d) PEI/H-Ti4.

5.5 ACKNOWLEDGMENT

The authors gratefully acknowledge support from NSF grant number DMR-9900390. N.S. acknowledges support from the Royal Thai Government.

5.6 REFERENCES

1. Lerf, A. Intercalation Compounds in Layered Host Lattices: Supramolecular Chemistry in Nanodimensions. In *Handbook of Nanostructured Materials and Nanotechnology, Vol. 5*; Nalwa, H., Ed.; Acad. Press: New York, 2000; pp 1-166.

2. Oriakhi, C. O. *J. Chem. Ed.* **2000**, *77*, 1138.

3. Sanchez, C.; Ribot, F.; Lebeau, B. *J. Mater. Chem.* **1999**, *9*, 35.

4. Pomogailo, A. D. *Russ. Chem. Rev.* **2000**, *69*, 53.

5. Giannelis, E. P. *Adv. Mater.* **1996**, *8*, 29.

6. Vaia, R. A.; Vasudevan, S.; Krawiec, W.; Scanlon, L. G.; Giannelis, E. P. *Adv. Mater.* **1995**, *7*, 154.

7. LeBaron, P.; Wang, Z.; Pinnavaia, T. *Appl. Clay Sci.* **1999**, *15*, 11.

8. Kojima, Y.; Usuki, A.; Kawasumi, M.; Okada, A.; Fukushima, Y.; Kurauchi, T.; Kamigaito, O. *J. Mater. Res.* **1993**, *8*, 1185.

9. Fischer, H. R.; Gielgens, L. H., Koster, T. P. M. *Acta Polym.* **1999**, *50*, 122.

10. Manolos, L.; *Plastics Technol.* **1999**, *45*, 52.

11. Lan, T.; Kaviratna, P. D.; Pinnavaia, T. J. *Chem. Mater.* **1994**, *6*, 573.

12. Gilman, J. W. *Appl. Clay Sci.* **1999**, *15*, 31.

13. Sukpirom, N.; Oriakhi, C. O.; Lerner, M. M. *Mater. Res. Bull.* **2000**, *35*, 325.

14. Ker, T. A.; Wu, H.; Nazar, L. F. *Chem. Mater.* **1996**, *8*, 2005.

15. Nazar, L. F.; Wu, H.; Power, W. P. *J. Mater. Chem.* **1995**, *5*, 1985.

16. Wang, L.; Schindler, J.; Kannewurf, C.R.; Kanatzidis, M.G. *J. Mater. Chem.* **1997**, *7(7)*, 1277.

17. Oriakhi, C. O.; Lerner, M. M. *Chem. Mater.* **1996**, *8*, 2016.

18. Oriakhi, C. O.; Nafshun, R. L.; Lerner, M. M. *Mater. Res. Bull.* **1996**, *31*, 1513.

19. Liu, Y.-J.; Schindler, J. L.; Degroot, D. C.; Kannewurf, C. R.; Herpo, W.; Kanatzidis, M. G. *Chem. Mater.* **1996**, *8*, 525.

20. Lemmon, J. P.; Wu, J.; Lerner, M. M. *Mater. Res. Soc. Symp. Proc.* **1994**, *351*, 83.

21. Lemmon, J. P.; Wu, J.; Oriakhi, C. O.; Lerner, M. M. *Electrochim. Acta* **1995**, *13/14*, 2245.

22. Sasaki, T.; Watanabe, M.; Hashizume, H.; Yamada, H.; Nakazawa, H. *J. Am. Chem. Soc.* **1996**, *118*, 8329.

23. Sasaki, T.; Watanabe, M.; Hashizume, H.; Yamada, H.; Nakazawa, H. *Chem. Commun.* **1996**, 229.

24. Sukpirom, N.; Lerner, M. *Chem. Mater.* **2001**, 13, 2179.

25. Sasaki, T.; Watanabe, M.; Komatsu, Y.; Fujiki, Y. *Inorg. Chem.* **1985**, *24*, 2265.

26. Ogawa, M.; Takizawa, Y. *Mol. Cryst. Liq. Cryst.* **2000**, *341*, 357.

27. Choy, J.-H.; Han, Y.-S.; Park, N.-G.; Kim, H.; Kim, S.-W. *Synth. Met.* **1995**, *71*, 2053.

28. Okawa, M.; Takizawa, Y. *Chem. Mater.* **1999**, *11*, 30.

29. Marchand, R.; Brohan, L.; Tournoux, M. *Mater. Res. Bull.* **1980**, *15*, 1129.

30. Sasaki, T.; Watanabe, M.; Komatsu, Y.; Fujiki, Y. *Inorg. Chem.* **1989**, *28*, 2776.

31. Solutions of octadecylamine in ethanol were examined by FAB/MS before and after ultrasonication at 180 W for 15 minutes. Both samples gave patterns with the primary peak at 270.3 M/z (100%), corresponding to the molecular weight of octadecylammonium ions, and two minor peaks at 268.3 M/z (15-20%), and 85.1 M/z (2-3%).

32. Lagaly, G.; Weiss, A. *Angew. Chem. Internat. Edit.* **1971**, *10*, 558.

33. Sasaki, T.; Watanabe, M. *J. Phys. Chem. B* **1997**, *101*, 10159.

34. Sasaki, T.; Watanabe, M. *Mol. Cryst. Liq. Cryst.* **1998**, *311*, 417.

35. Sukpirom, N.; Lerner, M. M. *Mater. Chem. Eng. A*, submitted for publication, 2001.

36. Vossmeyer, T.; Katsikas, L.; Giersig, M.; Popovic, I.G.; Diesner, K.; Chemseddine, A.; Eychmüller, A.; Weller, H. *J. Phys. Chem.* **1994**, *98*, 7665.

37. Sasaki, T.; Watanabe, M. *J. Am. Chem. Soc.* **1998**, *120*, 4682.

38. Gardolinski, J. E.; Carrera, C. M. *J. Mater. Sci.* **2000**, *35*, 3113.

39. Frank, H.P. *J. Poly. Sci.* **1954**, *12*, 565.

40. Wang, L.; Rocci-Lane, M.; Brazis, P.; Kannewurf, C. R.; Kim, Y.-I.; Lee, W.; Choy, J.-H.; Kanazidis, M. G. *J. Am. Chem. Soc.* **2000**, *122*, 6629.

41. Liu, Y.-J.; Degroot, D. C.; Schindler, J. L.; Kannewurf, C. R.; and Kanatzidis, M. G. *Adv. Mater.* **1993**, *5*, 369.

42. Yin, S.; Uchida, S.; Fujishiro, Y.; Aki, M.; Sato, T. *J. Mater. Chem.* **1999**, *9*, 1191.

CHAPTER 6

CONCLUSION

In this thesis, the conventional synthetic method for polymer-clay nanocomposites, melt intercalation, is successfully employed to other layered host such as MoO_3, $MnPS_3$, and $CdPS_3$. And, the exfoliation/adsorption method is modified and investigated to obtain new polymer-layered titanate nanocomposites.

Melt intercalation is attractive for industrial applications because the method is simple (mix and heat) and low cost (no solvent). Also, samples may be processed with the existing machine, such as an extruder. However, melt intercalation has only been used to prepare nanocomposites of layered clay materials. For the first time, it is here used with other layered hosts. The intercalation of poly(ethylene oxide) (PEO) into MoO_3 or MPS_3 (M=Mn,Cd) gives high yields ($\chi > 0.8$) in 5-30 h at temperatures above melting temperature of PEO (60-65 °C).

Layered titanate ($H_xTi_{2-x/4}O_4.yH_2O$, H-Ti) and tetratitanate ($H_2Ti_4O_9.xH_2O$, H-Ti4) are of interest because they are low cost, environmentally safe, chemically stable, and possess photocatalytic properties. Because the surface of titanate layers has higher charge per area than MoO_3 and MPS_3, layered titanate compounds are not amenable for melt intercalation. General synthetic approaches include melt intercalation, *in situ* polymerization of monomeric precursors, and exfoliation/adsorption. Unlike other approaches, exfoliation/adsorption is not

limited by diffusion of polymer or monomeric precursors, allowing it to be employed with many kinds of layered compounds. The difficulty with this approach for new hosts has been to obtain exfoliated layers. Here, titanate layers are exfoliated using a dispersing reagent, tetrabutylammonium hydroxide (TBAOH) and ultrasound. H-Ti layers are exfoliated within 30 minutes of ultrasonication at 120 W. The ratio of TBA ions to protons in titanate (TBA/H) is optimized to 0.5 for this process. H-Ti4 is not exfoliated by the similar procedure; however, it is significantly swelled using TBA/H = 5 and ultrasound for 60 minutes at 180 W. Exfoliated H-Ti and expanded H-Ti4 are use as precursors to prepare polymer-containing nanocomposites. PEO, polyvinylpyrrolidone (PVP), and polyethylenimine (PEI) were added to these suspensions to form gels that dried to form nanocomposites: these are the first polymer-containing nanocomposites reported for layered titanates.

Ultrasound is also applied to the intercalation of long-chain alkylammonium ions ($C_nH_{2n+1}NH_3^+$, n = 6-18) into H-Ti4 by reaction in the aqueous or ethanoic solution of alkylamines under ultrasound at 180 W for 15 minutes. The preparation of long-chain alkylammonium intercalated H-Ti4 was already reported; however, the previous methods require long reaction times, pre-intercalation, and/or the aid of macromolecules. These materials have been reported as precursors for preparation of nano-sized TiO_2 and transition metal-pillared tetratitanate compounds.

BIBLIOGRAPHY

Ajayan, P. M. *Chem. Rev.* **1999**, *99*, 1787.

Aranda, P.; Ruiz-Hitzky, E. *Appl. Clay. Sci.* **1999**, *15*, 119.

Aranda, P.; Ruiz-Hitzky, E. *Chem. Mater.* **1992**, *4*, 1395.

Bernhardt, C. *Particle Size Analysis:Classification and Sedimentation Methods*; Chapman & Hall: London, **1994**; Chapter 3.

Bissessur, R.; Kanatzidis, M. G.; Schindler, J. L.; Kannewurf, C. R. *J. Chem. Soc., Chem. Commun.* **1993**, pp 1582-1585.

Biswas, M.; Sinha Ray, S. *Adv. Polym. Sci.* **2001**, *155*, 167.

Brec, R. *Solid State Ionics* **1986**, *22*, 3.

Bujdak, J.; Hackett, E.; Giannelis, E.P. *Chem. Mater.* **2000**, *12(8)*, 2168.

Burnside, S.; Wang, H.; Giannelis E. *Chem Mater* **1999**, *11*, 1055.

Carrado, K.A.; Xu, L. *Chem. Mater.* **1998**, *10(5)*, 1440.

Chatakonda, K.; Green, M. L. H.; Thompson, M. E.; Suslick, K. S. *J. Chem. Soc., Chem. Commun.* **1987**, 900.

Choy, J.-H.; Han, Y.-S.; Park, N.-G.; Kim, H.; Kim, S.-W. *Synth. Met.* **1995**, *71*, 2053.

Clement, R.; Garnier, O.; Jegoudez J. *Inorg Chem* **1986**, *25*, 1404.

Cohen Stuart, M.A.; Fleer, G.J.; Bijsterbosch, B.H. *J. Coll. Interface Sci.* **1982**, *90(2)*, 321.

Cullity, B.D. *Elements of X-ray Diffraction, 2nd Ed.*; Addison-Wesley: Reading, MA, 1978.

Dawson, A; Kamat, P. V. *J. Phys. Chem. B* **2001**, *105*, 960.

Elder, S. H.; Cot, F. M.; Su, Y.; Heald, S. M.; Tyryshkin, A. M.; Bowman, M. K.; Gao, Y.; Joly, A. G.; Balmer, M. L.; Kolwaite, A. C.; Magrini, K. A.; Blake, D. M. *J. Am. Chem. Soc.* **2000**, *122*, 5138.

Enzel, P.; Bein, T. *Chem. Mater.* **1992**, *4*, 819.

Enzel, P.; Bein, T. *J. Chem. Soc., Chem. Commun.* **1989**, 1326.

Enzel, P.; Bein, T. *J. Phys. Chem.* **1989**, *93*, 6270.

Fegler, S. L.; Heckman, Jr., J. W.; Klomparens, K. L. Scanning and Transmission Electron Microscopy: An Introduction, W. H. Freeman and Company: New York, 1993, Chapter 5.

Fischer, H.R.; Gielgens, L.H.; Koster, T.P.M. *Acta Polym.* **1999**, *50,* 122.

Fischer, J. E. *Chem. Innovation* **2000**, *30*, 21.

Frank, H.P. *J. Poly. Sci.* **1954**, *12*, 565.

Gardolinski, J. E.; Carrera, C. M. *J. Mater. Sci.* **2000**, *35*, 3113.

Gianellis, E.P. *Adv. Mater.* **1996**, *8*, 29.

Giannelis, E. *Appl Organometal Chem* **1998**, *12*, 675.

Gilman, J.W. *Appl. Clay Sci.* **1999**, *15*, 31.

Gonsalves, K. E.; Merhari, L.; Wu, H.; Hu, Y. *Adv. Mater.* **2001**, *13*, 703.

Gonzalez, G.; Santa Ana, M.A.; Benavente, E. *J. Phys. Chem. Solids* **1997**, *58*, 1457.

Grey, I.E.; Li, C.; Madsen, I.C.; Watts, J.A. *J. Sol. St. Chem.* **1987**, *66*, 7.

Haushalter, R. C.; Mundi, L. A. *Chem. Mater.* **1992**, *4*, 31.

Hazen, R. M. *Science* **1983**, *219*, 1065.

Hazen, R. M.; Finger, L. W. *J. Appl. Phys.* **1984**, *56*, 1838.

Hervieu, M.; Raveau, B. *Rev. Chim. Miner.* **1981**, *18*, 642.

Hild, A.; Séquaris J.-H.; Narres H.-D.; Schwuger, M. *Colloids surf. A: Physicochem. Eng. Aspects* **1997**, *123-124*, pp 515.

Huguenin, F.; Gambardella, M.; Torresi, R.; Torresi, S.; Butty, D. *J. Electrochem. Soc.* **2000**, *147*, 2437.

Ingle, J. D.; Crouch, S. R. Spectrochemical Analysis, Prentice-Hall, Inc., New Jersey, 1988.

Ishii, T.; Nozawa, H.; Tamamura, T. *Appl. Phys. Lett.* **1997**, *70*, 1110.

Ishii, T.; Shibata, T.; Nozawa, H.; Tamamura, T. *AIP Conf. Proc.* **1998**, *442*, 494.

Jacobson, J. A. Solid State Chemistry: Compounds, Cheetham, A. K.; Day, P., Eds.; Clarendon, oxford, 1992, 234.

Jeevanandam, P.; Vasudevan, S. *Chem. Mater.* **1998**, *10*, pp 1276-1285.

Julien, C.; Khelfa, A.; Guesdon, J. P.; Gorenstein, A. *Appl. Phys. A* **1994**, *59*, 173.

Kavan, L.; Stoto, T.; Grätzel, M. *J. Phys. Chem.* **1993**, *97*, 9493.

Kerr, T. A.; Wu, H.; Nazar, L. F. *Chem. Mater.* **1996**, *8*, 2005.

Klingen, V.; Ott, R.; Hahn, H. *Z Anorg Allg Chem* **1973**, *396*, 271.

Kocher, M.; Daubler, T. K.; Harth, E.; Scherf, U.; Gugel, A.; Neher, D. *Appl. Phys. Lett.* **1998**, *72(6)*, 650.

Kojima, Y.; Usuki, A.; Kawasumi, M.; Okada, A.; Fukushima, Y.; Kurauchi, T.; Kamigaito, O. *J. Mater. Res.* **1993**, *8*, 1185.

Komori, Y.; Sugahara, Y.; Kuroda, K. *Chem. Mater.* **1999**, *11*, 3.

Kooli, F.; Sasaki, T; Rives, V.; Watanabe, M. *J. Mater. Chem.* **2000**, *10*, 497.

Lagadic, I.; Léaustic, A.; Clément, R. *J. Chem. Soc. Chem. Commun.* **1992**, 1396.

Lagaly, G.; Weiss, A. *Angew. Chem. Internat. Edit.* **1971**, *10*, 558.

Lan, T.; Kaviratna, P. D.; Pinnavaia, T. J. *Chem. Mater.* **1994**, *6*, 573.

Lawton, G. *Chem. Ind.* **2001**, *6*, 174.

LeBaron, P.; Wang, Z.; Pinnavaia, T. *Appl. Clay Sci.* **1999**, *15*, 11.

Lee, J.; Takekoshi, T.; Giannelis, E. P. *Mat. Res. Soc. Symp. Proc.* **1997**, *457*, 513.

Lemmon, J. P.; Lerner, M. M. *Chem. Mater.* **1994**, *6*, 207.

Lemmon, J. P.; Lerner, M. M. *Solid State Commun.* **1995**, *94*, 533.

Lemmon, J. P.; Wu, J.; Lerner, M. M. *Mater. Res. Soc. Symp. Proc.* **1994**, *351*, 83.

Lemmon, J.; Wu, J.; Oriakhi, C.; Lerner M. *Electrochim. Acta*, **1995**, *40*, 2245.

Lerf, A. Intercalation Compounds in Layered Host Lattices: Supramolecular Chemistry in Nanodimensions. In Handbook of Nanostructured Materials and Nanotechnology, Vol. 5; Nalwa, H., Ed.; Acad. Press: New York, 2000; pp 1-166.

Lerner, M.; Oriakhi, C. in *Handbook of Nanophase Materials*, Ed. A. Goldstein, Marcel Dekker: New York, 1997, pp. 199–219.

Lerner, M.; Oriakhi, C. Polymers in Ordered Nanocomposites. In *Handbook of Nanophase Materials*, Goldstein, A., Ed.; Marcel Dekker: New York, 1997; pp 199-219.

Liu, L.; Qi, Z.; Zhu X. *J Applied Polym Sci* **1999**, *71*, 1133.

Liu, Y. J.; DeGroot, D. C.; Schindler, J. L.; Kannewurf, C. R.; Kanatzidis, M. G. *Chem. Mater.* **1991**, *3*, 992.

Liu, Y.-J.; Degroot, D. C.; Schindler, J. L.; Kannewurf, C. R.; and Kanatzidis, M. G. *Adv. Mater.* **1993**, *5*, 369.

Liu, Y.-J.; Schindler, J. L.; Degroot, D. C.; Kannewurf, C. R.; Herpo, W.; Kanatzidis, M. G. *Chem. Mater.* **1996**, *8*, 525.

Manolis, L. A Little Goes A Long Way. *Plastics Technol.* **1999**, *45(6),* pp 52-57.

Manolos, L.; *Plastics Technol.* **1999**, *45*, 52.

Marchand, R.; Brohan, L.; Tournoux, M. *Mater. Res. Bull.* **1980**, *15*, 1129.

Mason, T. J. Practical Sonochemistry: User's Guide to Applications in Chemistry and Chemical Engineering, Ellis Horwood Limited: West Sussex, England, 1991, Chapter 1.

Matsuo, Y.; Tahara, K.; Sugie, Y. *Carbon* **1996**, *5*, 672.

Matsuo, Y.; Tahara, K.; Sugie, Y. *Carbon* **1997**, *1*, 113.

Miyata, H.; Sugahara, Y.; Kuroda, K.; Kato, C. *J. Chem. Soc., Faraday Trans. I* **1987**, *83*, pp 1851.

Moller, K.; Bein, T. *Chem. Mater.* **1998**, *10*, 2950.

Montarges, E.; Michot, L.J.; Lhote, F.; Frabien, T.; Villieras, F. *Clays Clay Miner.* **1995**, *43(4)*, 417.

Murray, C.B.; Norris, D.J.; Bawendi, M.G. *J. Am. Chem. Soc.* **1993**, *115*, 8706.

Nakano, S.; Sasaki, T.; Takemura, K.; Watanabe, M. *Chem. Mater.* **1998**, *10*, 2044.

Nazar, L. F.; Wu, H.; Power, W. P. *J. Mater. Chem.* **1995**, *5*, 1985.

Ogawa, M.; Inagaki, M.; Kodama, N.; Kuroda, K.; Kato, C. *J. Phys. Chem.* **1993**, *97*, pp 3819

.

Ogawa, M.; Takizawa, Y. *Mol. Cryst. Liq. Cryst.* **2000**, *341*, 357.

Okawa, M.; Takizawa, Y. *Chem. Mater.* **1999**, *11*, 30.

Oriakhi, C. O. *J. Chem. Ed.* **2000**, *77*, 1138.

Oriakhi, C. O. Ph.D. Thesis, Oregon State University, Corvallis, OR, April, 1996.

Oriakhi, C. O.; Lerner, M. M. *Chem. Mater.* **1996**, *8*, 2016.

Oriakhi, C. O.; Nafshun, R. L.; Lerner, M. M. *Mater. Res. Bull.* **1996**, *31*, 1513.

Pomogailo, A. D. *Russ. Chem. Rev.* **2000**, *69*, 53.

Roy, R. *Mat. Res. Soc. Symp. Proc.* **1993**, *286*, 241-250.

Sanchez, C.; Ribot, F.; Lebeau, B. *J. Mater. Chem.* **1999**, *9*, 35.

Sandroff, C. J.; Hwang, D. M.; Chung, W. M. *Phys. Rev. B* **1986**, *33*, 5953.

Sasaki, T.; Ebina, Y.; Watanabe, M.; Decher, G. *Chem. Commun.* **2000**, 2163.

Sasaki, T.; Komatsu, Y.; Fujiki, Y. *Inorg. Chem.* **1989**, *28*, 2776.

Sasaki, T.; Kooli, F.; Iida, M.; Michiue, Y.; Takenouchi, S.; Yajima, Y.; Izumi, F.; Chakoumakos, B.C.; Watanabe, M. *Chem. Mater.* **1998**, *10*, 4123.

Sasaki, T.; Nakano, S.; Yamauchi, S.; Watanabe, M. *Chem. Mater.* **1997**, *9*, 602.

Sasaki, T.; Watanabe, M. *J. Am. Chem. Soc.* **1998**, *120*, 4682.

Sasaki, T.; Watanabe, M. *J. Phys. Chem. B* **1997**, *101*, 10159.

Sasaki, T.; Watanabe, M. Michiue, Y.; Komatsu, Y.; Izumi, F.; Takenouchi, S. *Chem. Mater.* **1995**, *7*, 1001.

Sasaki, T.; Watanabe, M. *Mol. Cryst. Liq. Cryst.* **1998**, *311*, 417.

Sasaki, T.; Watanabe, M.; Hashizume, H.; Yamada, H.; Nakazawa, H. *Chem. Commun.*, **1996**, 229.

Sasaki, T.; Watanabe, M.; Hashizume, H.; Yamada, H.; Nakazawa, H. *J. Am. Chem. Soc.* **1996**, *118*, 8329.

Sasaki, T.; Watanabe, M.; Komatsu, Y.; Fujiki, Y. *Inorg. Chem.* **1985**, *24*, 2265.

Sasaki, T.; Watanabe, M.; Komatsu, Y.; Fujiki, Y. *Inorg. Chem.* **1989**, *28*, 2776.

Sasaki, T.; Watanabe, M.; Michiue, Y.; Komatsu, Y.; Izumi, F.; Takenouchi, S. *Chem. Mater.* **1995**, *7*, 1001.

Schöllhorn, R. Inclusion Comopounds Vol. 1: Structural Aspects of Inclusion Compounds Formed by Inorganic and Organometallic Host Lattices, Atwood; J. L.; Davies, J. E.; MacNicol, D. D. Eds. Academic Press: London, 1984, Chapter 7.

Schöllhorn, R.; Kuhlmann, R. *Mater. Res. Bull.* **1976**, *11*, 83.

SciFinder Scholar 2000 (accessed July 2001) Search term = Nanocomposites.

Serpone, N.; Lawless, D.; Khairutdinov, R.; Pelizzetti, Ezio *J. Phys. Chem.* **1995**, *99*, 16655.

Shinada, M.; Sugano, S. *J. Phys. Soc. Japan* **1966**, *21*, 1936.

Soghomonian, V.; Chen, Q.; Haushalter, R. C.; Zubieta, J.; O'Connor C. J. *Science*, **1993**, *259*, 1596.

Solutions of octadecylamine in ethanol were examined by FAB/MS before and after ultrasonication at 180 W for 15 minutes. Both samples gave patterns with the primary peak at 270.3 M/z (100%), corresponding to the molecular weight of

octadecylammonium ions, and two minor peaks at 268.3 M/z (15-20%), and 85.1 M/z (2-3%).

Sukpirom, N.; Lerner, M. *Chem. Mater.* **2001**, 13, 2179.

Sukpirom, N.; Lerner, M. *Mater. Chem. Eng., A* **2001**, in press.

Sukpirom, N.; Oriakhi, C. O.; Lerner, M. M. *Mater. Res. Bull.* **2000**, *35*, 325.

Suslick, K. S.; Casadonte, D. J.; Green, M. L. H.; Thompson, M. E. *Ultrasonics* **1987**, *25*, 56.

Tagaya, H.; Takeshi, K.; Ara, K.; Kadokawa, J.-I.; Karasu, M.; Chiba, K. *Mater. Res. Bull.* **1995**, *30*, 1161.

Tayler, B.; Steger, J.; Wold A. *J Solid State Chem* **1973**, *7*, 461.

The Infrared Spectra Atlas of Monomers and Polymers; Sadler Research Laboratories, 1980.

The Infrared Spectra of Minerals; Farmer, V.C., Ed.; Mineralogical Society: London, 1974.

The Society for Analytical Chemistry *The Determination pf Particle Size: I. A Critical Review of Sedimentation Methods*, W. Heffer & Sons Ltd, Cambridge, **1968**, p. 17.

Thomas, D.; McCarron, E. *Mater Res Bull.* **1986**, *21*, 945.

Tsai, H. L.; Schindler, J. L.; Kannewurf, C. R.; Kanatzidis, M. G. *Chem. Mater.* **1997**, *9*, 875.

Vaia, R. A.; Giannelis, E. P. *Macromolecules* **1997**, *30*, 8000.

Vaia, R. A.; Vasudevan, S.; Krawiec, W.; Scanlon, L. G.; Giannelis, E. P. *Adv. Mater.* **1995**, *7*, 154.

Vaia, R.; Jandt, K.; Kramer, E.; Giannelis E. *Chem Mater* **1996**, *8*, 2628.

Vaia, R.; Jandt, K.; Kramer, E.; Giannelis, E. *Macromolecules* **1995**, *28*, 8080.

Vossmeyer, T.; Katsikas, L.; Giersig, M.; Popovic, I. G.; Diesner, K.; Chemseddine, A.; Eychmüller, A.; Weller, H. *J. Phys. Chem.* **1994**, *98*, 7665.

Wang, L.; Rocci-Lane, M.; Brazis, P.; Kannewurf, C. R.; Kim, Y.-I.; Lee, W.; Choy, J.-H.; Kanazidis, M. G. *J. Am. Chem. Soc.* **2000**, *122*, 6629.

Wang, L.; Schindler, J.; Kannewurf, C.R.; Kanatzidis, M.G. *J. Mater. Chem.* **1997**, *7(7)*, 1277.

Wold, A.; Dwight, K. Solid State Chemistry: Synthesis, structure, and properties of selected oxides and sulfides, Chapman & Hall, Inc., New York, 1993, Chapter 2.

Wu, J.; Lerner, M. M. *Chem. Mater.* **1993**, *5*, 835.

Yang, D.; Frindt, R. F. *J. Mater. Res.* **2000**, *15*, 2408.

Yin, S.; Uchida, S.; Fujishiro, Y.; Aki, M.; Sato, T. *J. Mater. Chem.* **1999**, *9*, 1191.

Yoshida, M.; Lal, M.; Kumar, N. Deepak; Prasad, P.N *J. Mater. Sci.* **1997**, *32(15)*, 4047.

Yoshihara, T.; Tadokoro, H.; Murahashi, S. *J. Chem. Phys.* **1964**, *41*, 2902.

Zheng, M.-P.; Jin, Y.-P.; Jin, G.-L.; Gu, M.-Y. *J. Mater. Sci. Lett.* **2000**, *19*, 433.